Current Step Generation and Measurement with Rise-time in the Range of Nanoseconds

Muhammad Ziaur Rehman

School of Electrical Engineering

Master's Thesis submitted in partial fulfilment of the requirement for the degree of Master of Science in Technology.
Espoo. 20 May, 2018

Thesis supervisor:

Professor Matti Lehtonen

Thesis instructors:

D.Sc. (Tech.) Jari Hällström
D.Sc. (Tech.) Petri Kärhä

Aalto University
School of Electrical
Engineering

Aalto University

School of Electrical Engineering

Master's Programme in Electrical Engineering

ABSTRACT OF THE MASTER'S THESIS

Author: Muhammad Ziaur Rehman

Title: Current Step Generation and Measurement with Rise-time in the Range of Nanoseconds

Number of pages: 64+9 **Date**: 20-05-2018 **Language**: English

Department: Electrical Engineering

Professorship: Power systems and High Voltage Engineering **Code**: 3024

Supervisor: Professor Matti Lehtonen

Instructors : D.Sc. (Tech.) Jari Hällström, D.Sc. (Tech.) Petri Kärhä

A current step generator based on a charged coaxial cable is designed and tested for characterizing impulse current shunts. This thesis has developed a traceable calibration infrastructure for fast shunts and other current sensors, defined measurement techniques for a current step and improved the test procedure and measurement capabilities. For calibration of shunts, current coil sensors are used in the measurement circuits.

Since no calibration services are currently available for impulse current measuring systems, a best circuit combination is proposed for current step generation with a rise time of less than 5 ns, along with a proposed reference shunt that aims to provide the best and most stable measurement results with negligible noise, oscillations, and droop in the measured current step.

Based on techniques found in the literature, current steps are generated, and different sensors were used to measure the generated steep front current steps. The generation system consists of a 110-m long, 50-Ω coaxial cable and a spark gap. Various spark gap switches, including the SF_6 spark gap, are used for generating current steps. With the coaxial cable charged from one end, a current step is generated after reflecting back from the open end with a step length of twice the cable transmission delay. The cable is than discharged to the shunt (or coil) through the spark gap.

The measurement system consists of shunts and coil current sensors, 5:1 and 6.6:1 attenuators based on the requirement of the sensors. The recording instrument is a 1-GHz, 8-bit, 1-GS/s digitizer. The proposed step generator can produce current steps with a stable current of up to 100 A. The rise time of the step varies from 1.6 ns to 15 ns, depending on the spark gap used for switching. The produced current is constant within 0.5% for a step length of 960 ns generated with a coaxial cable 110 m in length.

To improve the test procedure and measurement capabilities, the thesis also analyzed factors affecting current step measurement, such as the type of coaxial cable, type of connection, extra shielding, clearances, interference sources, media of the spark gap, and the spark gap electrode distance (arc length). It is found that the measurement system and the rise time of current step is affected by many factors, including the coaxiality of the connection, impedance mismatch, interference, clearances, stray capacitances, and stray inductances. These results will enable future standardization of impulse current sensors.

Keywords: Current step, Measurement techniques, Calibration services, Rise time, noise, droop, steep front, impedance mismatch, spark gap medium, SF_6

Preface

First of all, thanks and praises to Almighty Allah alone, who gave me strength and wisdom to complete and accomplish my thesis. Praises to the Holy Prophet Muhammad P.B.U.H, my role model, who provided me the messages of how to become a great and achievable man.

I consider this work as the biggest learning process in my life based on theoretical, practical and professional education that I learned from the personalities I have been in contact with for time duration of my thesis. This work would not have been possible without finest guidance of my spiritual father and advisor, D.Sc. (Tech) Jari Hällström (Research Team Leader and senior scientist, Electrical Metrology at Mikes, VTT Technical Research Centre of Finland Ltd.). His friendly behavior gave me confidence and independence to explore the work at hand. His time to time pointers helped me in learning new things and fixing my mistakes. I also owe a lot to my supervisor Prof. Matti Lehtonen for his supervision. I am thankful to D.Sc. (Tech) Petri Kärhä (Institute of Signal Processing and Acoustics, Aalto university) for guidance and believing in me by providing with an opportunity for exciting and future changing international project for European high voltage electrical power industry. I would like to thank Dr. Joni Klüss from Mississippi State University, USA, who guided me while proceeding with the project work. And last, but not the least, I would like to thank all my colleagues including Jussi Havunen, Mr. Esa-Pekka Suomalainen, Mr. Tapio Lehtonen and Mr. Arttu Ollikainen for always there to help me in setting up my testing environment in High Voltage Lab at VTT Mikes.

I would like to mention the funding of this project. The Thesis topic is a part of an international project " Metrology for the electrical power industry". This project (14IND08 ELPow) has received funding from the EMPIR programme co-financed by the participating states and from the European Union's Horizon 2020 *research and innovation programme*. The project is a joint work between research institutes of multiple European countries where I was in continuous contact with PTB, Germany and RISE (Research Institute of Sweden) Sweden, which always provided me with an excellent research environment. I am very thankful to all the relevant officials including Anders Bergman from RISE, Sweden and Stephen Passon from Germany for their support.

I dedicate this work to my parents, Tahir Shah Muhammad and Shams ul Duha, without whom life would have hopeless. I would also like to thank my siblings, Muhammad Inam ur Rehman, Muhammad Ahtisham ur Rehman and Ammara for their love and support. Special thanks to my uncle Zubair Shah, the only reason behind my success as an Engineer. Thanks to my aunt Shabana for her support along with my uncle to make my basics strong enough to succeed in my life. Special thanks to my fiancé Nazii for her love and care. I thank for the support of my entire family. I would further appreciate support and kindness of my teachers and friends, Mr. Imran Gilani, Ms. Robina, my friends Hagop, Adnan, Faisal and others whom I might have forgotten to mention.

Muhammad Ziaur Rehman

Espoo, May 2018

Table of Contents

List of Symbols and Abbreviations

0.1 Symbols

I_{load}	Load current
V	Voltage
R_{shunt}	Resistance of shunt
R	Resistance
L_s	Parasitic inductance
R_s	Series resistance
M	Mutual inductance
B	Magnetic flux
I_c	Current flowing through an area enclosed by curve C
μ_o	Permeability of free space
r	Radius
v	Induced voltage
N	Number of turns
A	Area
k	Integrating constant of integrator
T_t	Total duration of current step
T_d	Peak current duration of current step
BW	Bandwidth
T_a	Rise-time
Z	Impedance
U_o	Applied voltage of DC generator
$R1$	Charging resistance
Za	Impedance of connected load
l	Length of coaxial cable
L	Inductance
τ	Rise-time of current step generated with step generator
L_o	Characteristic inductance of coaxial cable
C_o	Characteristic Capacitance of coaxial cable
t	transmission delay of coaxial cable
$T1$	Coaxial transmission line
$P1$	Rogowski coil from Pearson electronics with nominal sensitivity of 0.1 V/A

P2 Rogowski coil from Pearson electronics with nominal sensitivity of 1 V/A
S1 Shunt from T&M Research Products with nominal resistance of 0.5 Ω
S2 Shunt from T&M Research Products with nominal resistance of 0.1 Ω
S3 Shunt from T&M Research Products with nominal resistance of 0.01 Ω
SH Shunt from HILO-TEST with nominal resistance of 0.05 Ω
S Switch

0.2 Abbreviations

EMPIR European Metrology Programme for innovation and Research
HVDC High voltage Direct current
AC Alternating current
DC Direct current
HV High voltage
NMI National Metrology Institute

Chapter 1

Introduction

In basic studies of electricity, it is well known that current is the number of electrons or to put it more simply, the amount of charge flowing per unit time through a circuit, while voltage is the force which makes this charge flow possible. Having determined the current flowing through the circuit and its voltage, we can calculate how much work can potentially be done by that circuit. The amount of work or performance expected from electrical equipment has certain necessary ratings to follow. Apart from the voltage, it is the current that can also damage the equipment if it exceeds the defined rating [1].Current monitoring is important to determine not only how much current is flowing, but whether it is excessive or at a fault condition. The later information is of more importance, especially when the current exceeds the safe limit, since this would require a signal to switch off the power supply. Most of these fault conditions can result from surge current. In order to mitigate this, impulse currents are used for testing various kinds of electrical equipment.

High-impulse current is required not only for testing equipment (e.g. fuses and surge arresters), but also for various technical applications, including lasers, thermonuclear fusion, and plasma devices. High-impulse currents occur in lightning discharge electrical arcs, post arc phenomenon studies with circuit breakers, and electrical discharge studies in plasma physics [2]. In power systems, it is very necessary to measure high currents which occur due to reasons, such as short circuits resulting from high current flow having a very small rise time. Similarly, various components of electrical circuits, such as cables, conductors, and circuit breakers require measurement of high current for conducting tests, such as heat run and temperature rise tests [3]. Large magnitudes of impulse and switching surge currents occurring during lightning discharges and switching transients require special measuring techniques at a high potential level [4]. However, the sensors and transducers used for measuring these currents need characterization, standardization, and calibration before they can be used for measurement. One promising approach for solving this issue would be to generate current steps that have a steep rise time followed by a stable current region. These current steps can then be used for calibration of sensors measuring the impulse currents.

1.1 Research Problem

In technical and scientific fields other than power systems, it is necessary to determine the waveform and amplitude of a rapidly varying high current. The range of current amplitude may vary from several amperes to hundreds of kilo amperes. The rise time of these currents are in the range of microseconds to a few nanoseconds, and the current rise rate for such currents can be as high as 10^6 to 10^{12} A/s. For such cases, the sensors or measuring devices should be capable of measuring the signal over a wide frequency range.

Currently, the areas of test procedures and measurement capabilities for such currents having a high rising rate and the rise time lack traceable calibration services at the National Metrology Institute (NMI) level in Europe. The current measuring methods commonly used include resistive shunts, magnetic potentiometers or probes, Faraday and Hall Effect devices. The accuracy of measurement for such methods vary from 1% to 10% [4], thereby an extended research is required to improve the accuracy of these measurement methods and dependent factors leading to such calibration results. Few methods have been described in the past for the generation of

current step, including Blumlein generator [6] and simple coaxial cable based generator [7]. The coaxial cable generator described in [7] has been used for testing the dynamic behavior of impulse resistive shunts.

A variety of standards have been presented for impulse current shapes, measuring techniques, tests to be carried out with measuring systems, and the testing of various protection components including surge protection devices, and lightning rods or connectors. For example, standard IEC 60076-4[8] explains lightning impulse and switching impulse, IEC 60060-2[9] applies to high voltage test techniques and measuring systems, and IEC 61312-1[10] presents the general principle of protection against lightning electromagnetic impulse. However, no specific standards have yet been proposed for current steps, and very little information is available about characterization of the measuring systems [7], though many of the standard tests have been carried out using high-current impulses associated with lightning impulse events. In September 2010, a new standard IEC 62475:2010, was introduced as a horizontal standard covering a high-current test and measurement techniques which sets the requirements for impulse current measurement systems [11]. The measurement circuits for such impulse currents and current steps are affected by various factors, including noise induction in digitizers and the vertical amplifiers of oscilloscopes, quasi-static electric and magnetic field penetration in signal cable [12], clearances to nearby grounded or live objects, stray inductances and capacitances, intercomponent distances, and grounding. Therefore, it is not possible to ensure the adequate execution of such fast rise time tests and reproducible results for these measurements [13].

1.2 Aim of Research

The aim of this work is to develop a reference calibration circuit for measurement of current steps that has rise times below 5 ns, current levels up to 50 A, and an expanded uncertainty of less than 0.5%. After successfully achieving the current step having an amplitude of 50 A, the target will be raised to 100 A. The rise times for these current steps will be made as low as 2 ns to ensure steeper step, maintaining an expanded uncertainty close to 1%. The thesis will also develop a traceable infrastructure and measurement techniques for very fast current impulses. In addition, the thesis will suggest improvements to the present test procedures and measurement capabilities with an emphasis on the calibration of resistive shunts used for current step measurement.

1.3 Methodology

In order to achieve this aim, a fast-current step generator will be developed for generating current steps in order to extend the calibration range for surge current measuring instruments. Resistive shunts and Rogowski coils will be used as measuring sensors. Step current measurements and step calibration will be performed for impulse shunts using fast current-sensing Rogowski coils as a transfer reference. In addition, the calibration methodology will be developed for the new system.

This calibration methodology will be developed by reviewing for the current step generation along with research survey to determine a reliable method and a combination of circuit components which will help in developing the current step generator. This generator will be used for generating required current steps. Research will be done on various current sensor available in High Voltage Laboratory at VTT Mikes, and factors will be studied which can affect the shape and generation of the current step. Primary practical experiments will be performed to generate current steps, and to collect measurement results. The initial practical measurement results obtained will be analyzed to improve the shape of the current step for proposing the best calibration circuit. The results of the research survey will be used to perform extensive and final practical experiments to possibly generate current

steps with required parameters. At the end, the current sensors used will be calibrated using recorded data for current steps.

1.4 Scope

The thesis will focus on generating and measuring current steps for 90 – 100 A peak current having rise time below 5 ns. Resistive shunts and other available current sensors will be calibrated to develop a traceable infra-structure for very fast shunts and other current sensors. The work reported here has received support from the EMPIR programme co-financed by the Participating States and from the *European Union's Horizon 2020 research and innovation programme*. Public documentation and further details of this project are available at [5].

1.5 Organization of thesis

The rest of the thesis is organized as follows; Chapter 2 reviews the literature covering the methods previously used for current step generation and the theory of circuit components, current sensors for step measurement and factors affecting the shape and the waveform of generated current step. Chapter 3 describes the simulation and practical circuit used for current step generator. Chapter 4 presents the measurement of current step, techniques used to improve measurement circuit and therefore its accuracy. Results and the relevant discussions of the conducted testing are presented here. Chapter 5 presents the methods used for the calibration of the resistive shunts and current sensors. Finally, Chapter 6 summarizes the work and presents the most important conclusions along with guidelines and suggestions for further possible improvements in the future.

Chapter 2

Theory and Background

As the thesis aim is to develop a reference calibration circuit for current steps, it is first necessary to generate a current step and to identify monitoring techniques for measuring current steps. Therefore, this chapter presents a broad overview of different current monitoring techniques, their performance and limitations, as well as reviews the literature concerning current step to determine the most reliable method for current step generation, measurement of current step, and factors affecting current step measurement. Section 2.1and 2.2 provide a generic overview of sensors used for current step measurement. Section 2.3 defines the current step in terms of its purpose and the methods used by different authors for current or voltage step generation. Section 2.4 introduces the spark gap as a switch and its role in current step generation. Section 2.5 and Section 2.6 discuss the measuring system and the factors affecting the current step measuring system. Section 2.7 defines the calibration that will be performed in Chapter 5 for current sensors used in this project. Finally, Section 2.8 summaries the whole discussion in this chapter.

Current sensing techniques can be classified based upon four underlying physical principles [14]:

- The Ohm's law of resistance;
- The Faraday's law of induction;
- Magnetic field sensors; and
- Faraday Effect.

In this work, the current measuring techniques follow the first two physical principles. Therefore, the measurement techniques will be explained in terms of these two principles.

2.1 Current sensing based on the Ohm's law

One commonly used approach for current sensing following the Ohm's law are shunt resistors. These are called with different names such as shunt resistors, current viewing resistors, or current viewing sensors. Shunt resistors are established industry favorites among resistive products (passive products) and the majority of these are surface mounted. They are named shunt resistors as their main purpose is to monitor the current in a circuit according to Ohm's law by translating the amount of current in a particular circuit into a voltage which can easily be measured (Figure 1). The current is measured as

$$I_{load}=V/R_{shunt}, \quad (1)$$

where I_{load} , V ,R_{shunt} are load current, supply voltage and resistance of the shunt respectively. They have typically a low resistance of 50 mΩ or less. Shunts are high frequency resistors designed to sustain high peak current inputs and power generated by impulse generators, capacitive banks, and steady state current loads.

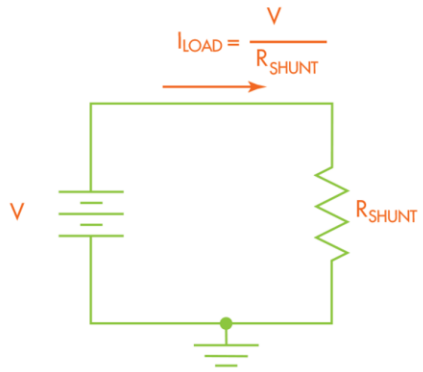

Figure 1 The working principle of current viewing resistor.

A potential drop across these shunt resistors is used as the proportional measure of the current flow. Shunts can be used both as alternating current (AC) and direct current (DC) sensors. It should be noted that the use of shunt resistors is limited and can be restricted in high current applications due to their power loss. Different types of shunt resistors or current viewing resistors are used, including high performance coaxial shunts (Figure 2(a)) and low-cost surface mounted devices (SMD) depending on the applications and current ratings.

2.1.1 High performance coaxial shunts for impulse current measurement

High performance coaxial shunts are widely used in the measurement of transient current pulses having fast rise times and high amplitudes. The high frequency behavior of these current sensing resistors is of critical importance in such applications. The equivalent circuit diagram for these shunts is shown in Figure 2(b).

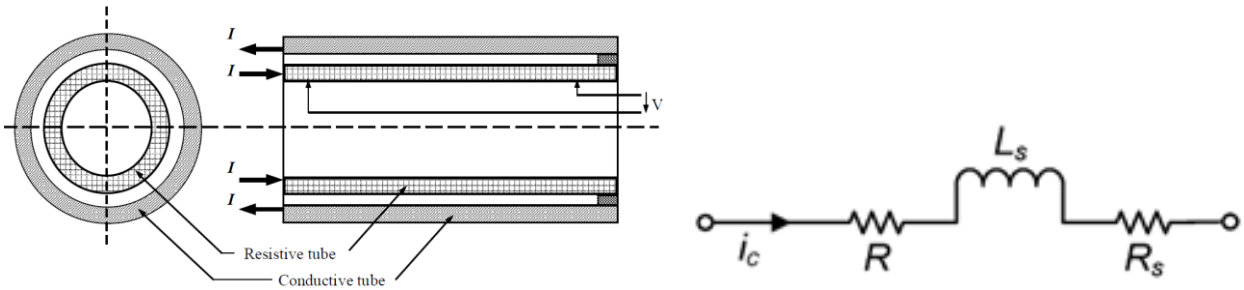

(a) (b)

Figure 2 (a) Coaxial-tube shunt: Front and lateral sections [7], (b) Equivalent circuit diagram for impulse shunt [14].

Here, R is the nominal resistance, L_s is the parasitic inductance and R_s is the series resistance due to skin effect that can be ignored in the case of DC currents. Parasitic inductance L_s results from the mutual-inductance M of the loops built by the main current and the sense wires [15]. Therefore, the connection of the sense wire is of more importance to achieve high performance. This parasitic inductance due to mutual inductance should not be confused with the self-inductance of the current viewing resistor. Reduction in L_s increases the measurement bandwidth. The geometrical shapes play a vital role in reduction of L_s, like coaxial resistive tube which significantly reduces the flux that couples into the sense wire [16]-[18].

If coaxial shunt resistors are used for DC current measurement, the series resistance due to skin effect can be ignored and the parasitic inductance is negligible due to the coaxial construction. However, when heavy-duty shunts are used for measuring the AC pulse currents of high magnitude, the skin effect becomes a limiting factor

that determines measurement bandwidth [19]. Flat strap geometry is also one of the techniques used that increases the measurement bandwidth [20]. All these types allow the measurement of current pulses with the rise time of a few nanoseconds and of several kilo amperes current magnitudes. Concluding the research survey, the Ohm's law of resistance offers the simplest solution to measure currents. However, the main disadvantage of current sensor using this method is the unavoidable electrical connection between the sensor circuit and the current to be measured. In this project, three high performance coaxial shunts by T&M Research Products and one by HILO-TEST are used. Structural details of these shunts are available in Appendix A.

2.2 Current sensing based on the Faraday's law of induction

In safety standards of electrical isolation, the current sensors following the Faraday's law of induction as physical principle are used for current sensing. They provide inherent electrical isolation between the output signal and the current being measured. By providing a ground related output signal, isolated current sensing technique enables the measurement of current on the high and floating voltage potentials. Rogowski coils are one of the current measuring sensors that are based on the principle of Faraday's law of induction.

2.2.1 Rogowski Coil

One of the main examples of an application using the Faraday's law of induction is the Rogowski coil, as shown in Figure 3.

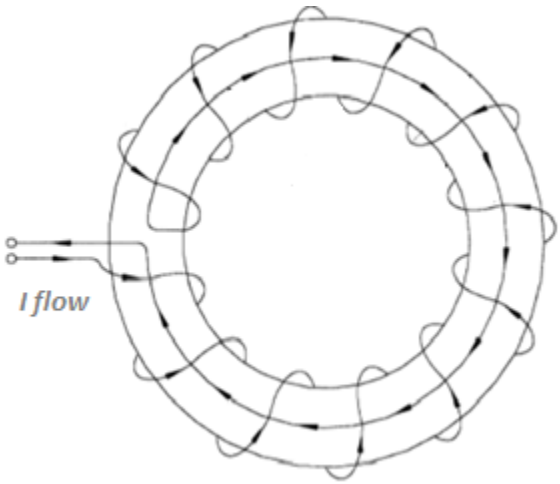

Figure 3 Rogowski coil.

These coils work by sensing the magnetic field produced by the current without requiring any electrical contact with the conductor whose current has to be measured. The working principle of the Rogowski coil is explained starting with ampere's law, which is the path integral of the magnetic flux density B in the coil. Mathematically

$$\oint_0^c \vec{B} . d\vec{l} = u_0 i_C, \tag{2}$$

where i_c is the current that flows through an area enclosed by some curve C and u_0 is the permeability of free space. For simplicity, we assume much smaller cross-sectional diameter than the radius r of Rogowski coil, which is valid for most coil designs. The equation for magnetic flux density B can be written for the current i_c centered inside the coil as

$$\boldsymbol{B = \frac{u_0 i_C}{2\pi r}}. \tag{3}$$

Now Faraday's law of induction can be applied here to determine the voltage induced into the Rogowski coil with N turns due to change in the current i_c [21] as

$$\boldsymbol{v = -N\frac{d\phi}{dt} = -NA\frac{dB}{dt} = -\frac{NAu_0}{2\pi r}\frac{di_C}{dt}}\ , \tag{4}$$

where N is the number of turns and A is the cross-sectional area of the coil body formed by the windings. Voltage v is therefore proportional to the derivative of the primary current i_c which is to be measured. Using infinitely high input impedance and an integrator with integrating constant k can yield the exact results as

$$\boldsymbol{v_{out} = -\frac{NAu_0}{2\pi r}\ k\int_0^t \frac{di_C}{dt}.dt + v(0)_{out} = -k\frac{NAu_0}{2\pi r}\ i_C + v_{out}(0).} \tag{5}$$

Note that the above equation is theoretically valid even if the geometry of the coil is not circular or the coil around the conductor is not centered [21]. However, the datasheets for commercial Rogowski coils explain that the measurement errors are increased, if the coil is not at the center (coaxial) as explained by Figure 4 [14], [22].

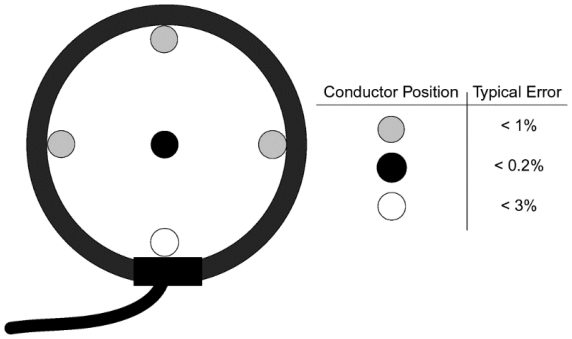

Figure 4 The influence of conductor position on accuracy of Rogowski coil [14].

This is because the winding density is never perfectly constant round the coil. Accordingly, if the conductor carrying current that has to be sensed is positioned close to the clip together mechanism, which is the point where output from the winding end is connected, the accuracy obtained is poorest. The reason is the winding density, which is never perfectly constant around the coil in this region.

The practical Rogowski coils are not suitable for measuring low frequency currents [21], [23-24]. To extend the range to DC current measurement, it is recently proposed to use a Rogowski coil in combination with other sensors that can also provide information about DC [25].

For current measurement based upon the Faraday law of induction, two Rogowski coils from Pearson Electronics called as wide band current monitor devices are used in this project work. Data sheets and structural details for these Rogowski coils are available in Appendix A. These sensors are claimed to have a potential for measuring small currents in sub milliamps like in the beam of charged particle, or large currents in kilo amperes caused by fault currents in power systems. These products are using a patented distributed termination technique, which allows them to measure, and monitor pulse currents with the rise time in nanoseconds. They have greater immunity to noise for small currents than the coils of any other product and can be connected directly to digitizers and oscilloscopes [26].

Structures and models using coils and windings such as Rogowski coils, toroids, solenoids, current and voltage transformers etc, capacitance and inductance are important parameters. Capacitance is mainly caused by electric coupling between the winding and the other parts of the structure like core, while magnetic coupling mainly causes inductance. Usually a Rogowski coil has capacitance associated with each winding and a large value of inductance due to turns of wire. These high valued inductances and capacitances can form resonant circuits within the current measuring instrument and can cause frequency distortion. Therefore, the Pearson Products are using the coils of improved characteristics such that the load resistance is distributed in each winding of the coil. Pearson current monitors have an improved pulse rise time response and good pulse flat top characteristics. Another parameter of consideration is the cable that is used with the current measuring sensor connected to oscilloscope having definite impedance. For best transient and frequency response, it is necessary to have an impedance match for this cable and the loading resistance of the measuring instrument to avoid reflections. This cable is then fed directly to a high frequency oscilloscope having high input impedance [27].

2.3 Current step

A typical waveform of a current step is shown in Figure 5. The value of the current step or the impulse current is the maximum value of current, inclusive of superimposed oscillations. Rectangular current steps have more or less pronounced droop. This current step waveform is characterized by its peak current value I and the two time parameters: duration of the peak T_d and the total duration T_t.

- Time T_d is the time during which the current is consistently greater than the 90% of the peak current value I.
- Parameter T_t, called the total duration, is the time during which the current is greater than the 10% of the peak current value I with a requirement that $T_t \geq 1.5\ T_d$.

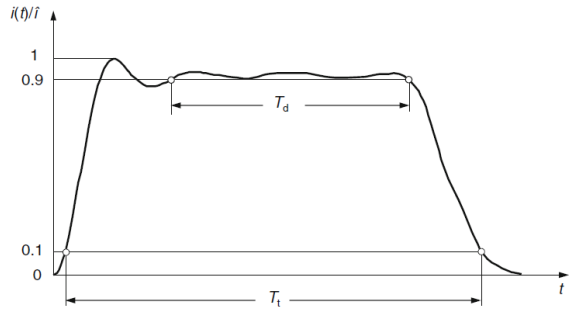

Figure 5 Current step with superimposed oscillations [28].

Rise time and bandwidth are the important parameters to be considered for current step generation. Figure 6 explains the rise time of the step or impulse. ***Rise time*** is the time required for a pulse to rise from 10% to 90% of its steady value. Alternatively, it is the time between two points at 10% and 90% of the peak value of an impulse. In contrast, the term *front time* is used in high voltage measurements. While measuring the rise time, it is also important to consider the rise time of the measuring instrument.

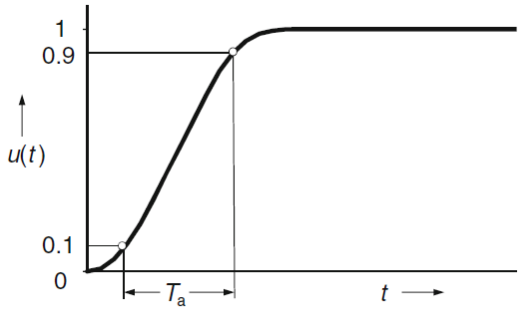

Figure 6 Definition of rise time Ta of a current step [28].

Bandwidth is the 3-dB frequency limit in frequency domain equivalent to the definition of rise time in the time domain. The relation between the rise time and the bandwidth B of a system is given by

$$\boldsymbol{B = \frac{0.35 \ldots 0.45}{Ta}}, \tag{6}$$

where T_a is the rise time. The factor 0.35 is valid if the system's step response attains the final value without overshoots (first order system), while the factor 0.45 is valid for a system with about 10% of overshoot in rise time (higher order system) [28].
This thesis will use the generated step current for characterizing the performance of the shunts and other available current sensors.

2.3.1 Previous research

Various methods have been proposed for generation of voltage pulses and steps with rise time in the range of nanoseconds [29-34]. Most of these methods used for generating voltages pulses can also be applied for the generation of current steps. For example, a coaxial cable was used in [29,33-34] as a pulse forming line, a pulse generator based on ferrite pulse sharpener was used in [30], high-voltage step recovery diodes were used in [31] to generate voltage steps with peak value of 500 V and approximately 0.8 ns rise time. Similarly, Power MOSFETS were used in [32] to produce the voltage steps in excess of 1 kV having the rise time of 15 ns. However, only limited work has been specifically devoted to current steps. This limited work includes generation of current steps by [7] using coaxial cable.

In all the previous work done on the generation of current and voltage steps, it is found that the most inexpensive and reliable method is using coaxial cable generator. The method is based on discharging length of a charged coaxial cable by using fast switch. Various kinds of fast switching devices are used, such as two pressurized spark gaps were used in [29], power MOSFETS in [32], mercury-wetted reed relays were used in [30-31,34], and a simple air spark gap was used in [7]. In addition to coaxial cable being considered as the most reliable method for producing well-defined rectangular current steps, simple spark gap devices with air or other pressurized gas are used as switching device which are found simple, low-cost, and easy to construct.

Figure 7 shows a simple version of coaxial cable generator described in [7] for testing the dynamic behavior of impulse current shunts. An open-ended coaxial cable with the length of 800-m and the characteristic impedance Z of 50 Ω was charged to voltage V supplied by high voltage DC generator through charging resistor R_d. L is the

inductance of circuit, R_x represents the thin walled current shunt with 1 mΩ resistance, and T_c is the reference current measuring transducer. Digital oscilloscope was used to measure the voltage across the shunt. A long trace of current steps and the first current step are shown in Figure 8.

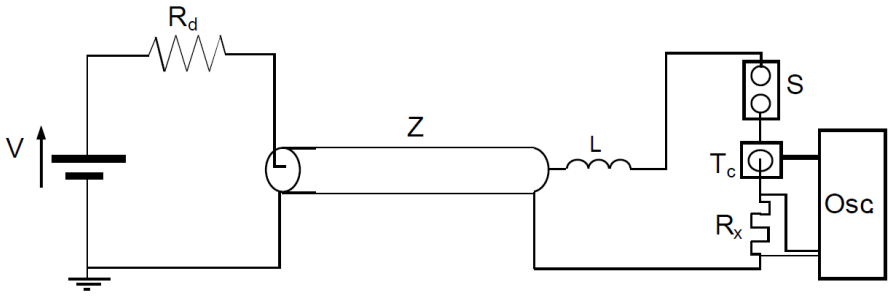

Figure 7 Circuit diagram of the current step generator for testing the dynamic behaviour of impulse current [21].

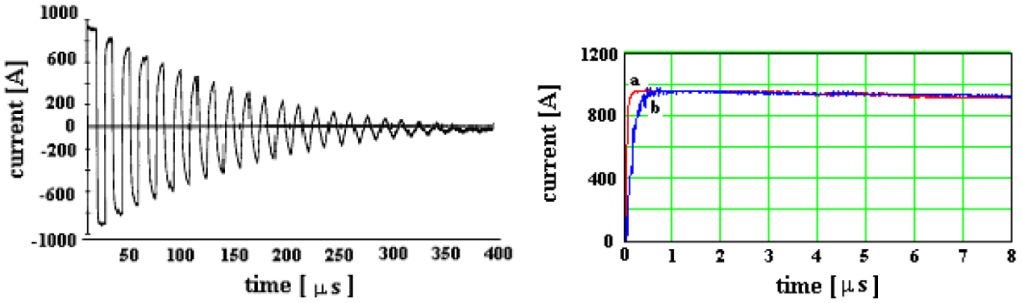

Figure 8 Left: 800 m long coaxial cable discharge current, Right: Measured current in the first 8 μs: a) with impulse current transformer, b) with thin walled shunt [21].

The length of the current step can be adjusted by changing the length of coaxial cable used in current step generator. For such purpose, it is impractical to build the generator by having the charging resistor at the opposite end to the switch, though, it is easier to visualize the operation as shown in Figure 7. Current step generator with changing resistor R_d and supply voltage V at the switch end of the line is shown Figure 9. This circuit is practical and can be built for generating current steps [34].

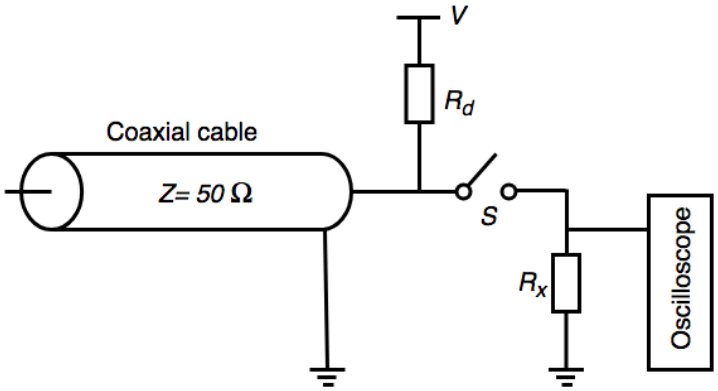

Figure 9 Simplified circuit diagram of the coaxial cable generator shown in Figure 7 with a charging resistor and a switch at the same side of coaxial cable.

The Blumlein generator can also be used for current step generation [6]. To understand the waveform of current steps produced in Figure 8, it is important to understand the Blumlein configuration for transmission lines achieving charged voltage into matched load for a pulse length equal to double the transmit time of one of the two lines.

Consider two lines charged as shown in Figure 10 which have characteristic impedance Z_o and driving a load Z with the impedance twice that of single line $Z=2Z_o$. The cable is connected to a switch S and the DC power supply V through a charging resistor R.

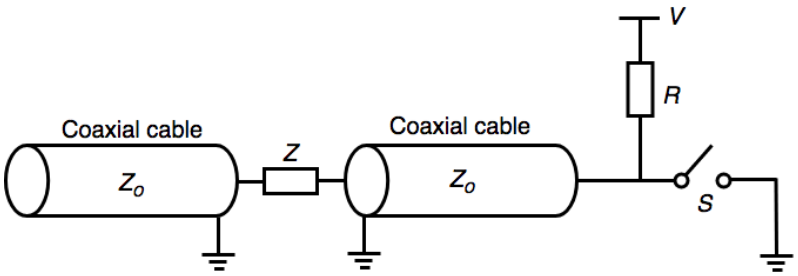

Figure 10 Circuit diagram for explaining Blumlein configuration and impedance difference.

In the Initial state, the voltage across the cables is given by,

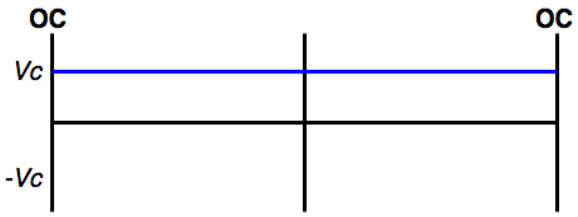

Figure 11 Voltage across the cables and load impedance when the switch in the circuit diagram of Figure 10 is open.

Where OC= open circuit, SC= short circuit. When the switch S closes, the voltage wave follows the path as shown in Figure 12.

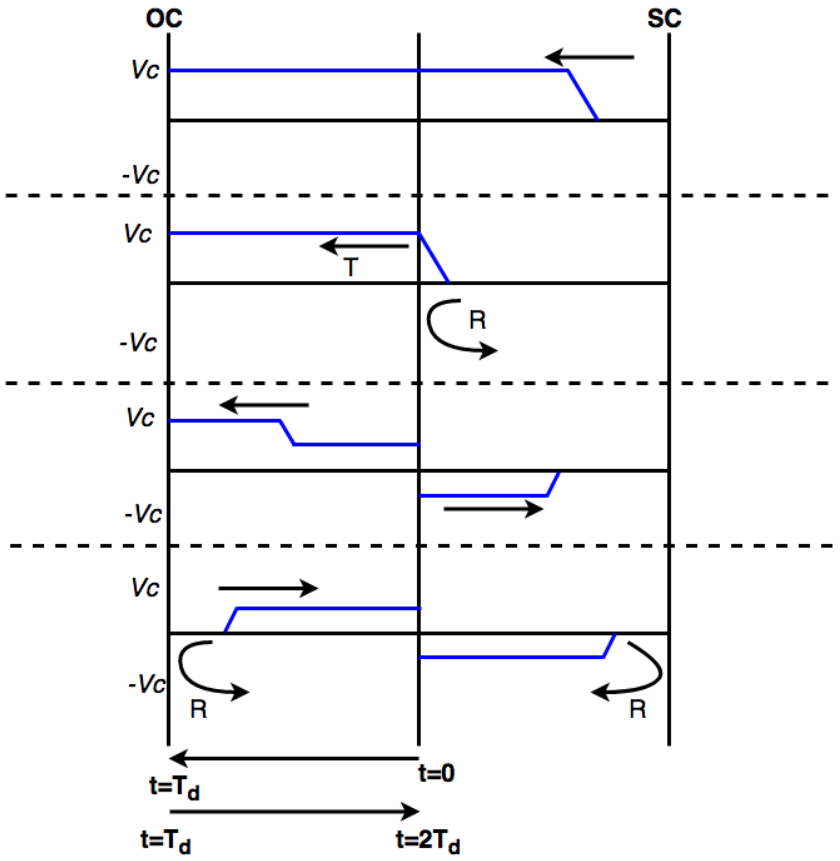

Figure 12 Behaviour of voltage wave when the switch *S* in the circuit diagram of Figure 10 is closed.

Here *T*= Transmitted wave, *R*= Reflected wave and T_d = travelling time of the wave in coaxial cable [35]. The pulse width in this case with one end open-circuited is twice the wave travelling time. No reflections occur if the impedance of load is same as the cable impedance (for $Z=2Z_o$). Various types of reflection due to impedance difference can occur i.e. if $Z\neq2Z_o$, as shown in Figure 13 [6].

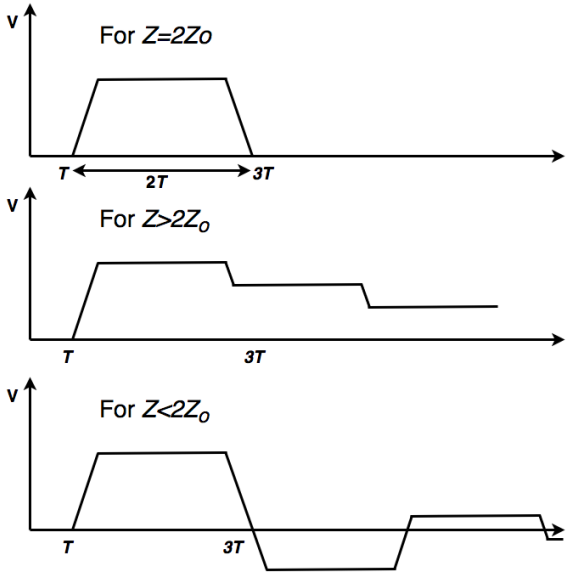

Figure 13 Behaviour of voltage waveform with and without impedance difference.

The waveform of current steps produced in Figure 8 had followed the condition $Z<<2Z_o$.

2.4 Spark gap as a switch

In a pulsed system, the large amount of energy is stored for relatively long time and then released in a much shorter time. As in the pulsed power systems, some type of closing switch is required to deliver the energy from the storage medium to the load, a closing switch is also required in systems to generate high currents with a very small rising time. The most widely used closing switch is a simple spark gap which was also used in [7] for current step generation. The spark gap switch closes to discharge the charged coaxial cable and opens to charge it again producing current step with the rise time in the range of nanoseconds.

The working principle of spark gap is straight forward. It consists of two conducting electrodes separated by some gap distance. This gap of the spark gap electrode is filled with some medium, such as air or SF_6 gas. When the voltage across the spark gap electrodes exceeds the breakdown limit of gas medium, spark is formed that ionizes the gas or the medium of spark gap electrodes, reducing electrical resistance. An electric current therefore flows until the path of this ionized gas is broken by means of some quenching medium or the current is reduced below minimum value called as "holding current"[36]. It is worth mentioning that the material of the electrode used in the spark gap does not affect the breakdown voltage i.e. the breakdown voltage is independent of the electrode material used in the spark gap [37].

For the generation of fast pulses or steps, a charged line is discharged into a load having some characteristic impedance by means of the spark gap switch. This switch has to be fast enough to reopen quickly after each closure to enable the line to be recharged again, generating repetitive pulses. The switch has to open at the end of pulse because the current dies or ceases to flow when all the energy stored in the line capacitance has been dissipated. Therefore, the switch or the spark gap in case of such fast phenomenon should be close enough to ideal switch in performance, because the relay switch forms a part of overall delay time [34].

2.4.1 Achievable rise time for the spark gap inserted in a coaxial transmission line

Three methods have been mentioned in [38] to achieve higher rise times with a spark gap in order of 1-10 ps. One of the method presented is to design a low inductance compensated spark gap. In the ultrafast switching, as in case of the current step generation having high rise time, interelectrode spacing in the spark gap should be made very short to reduce the inductance of spark cannel. In general, the switch performance is dominated by the inductance of spark channel in spark gap. Therefore, the additional cross-sectional area of a spark gap in relation of electrode area should be removed to reduce the inductance. For long channels, this can be achieved by the addition of taper in the outer conductor as shown in Figure 14. Reduction in inductance helps in matching the inductance per unit length of electrode gap region to the inductance per unit length of the hardware[38].

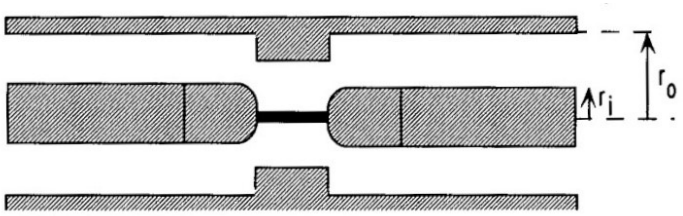

Figure 14 Compensated spark gap [38].

2.4.2 Spark gaps used in this project

Figure 15 shows two of the spark gaps assemblies used as a switch to produce repetitive current steps. In this project, spark gaps with different media were used as a switch for the current step generation. Air, Argon and SF_6 were used as a medium. Discharging coaxial cable having the characteristic impedance of 50 Ω using the spark gap having the break down voltage of 300 V results in generation of current step with peak current amplitude of 6 A (according to Ohm's law, $I=V/Z$). The SF_6 spark gap was used with adjustable electrodes and variable gas pressure to achieve the higher rise time of generated current step. This low inductance design presented in Section 2.4.1 was also built and used in this work. Significant results were achieved for rise time of current step with the low inductance compensated spark gap.

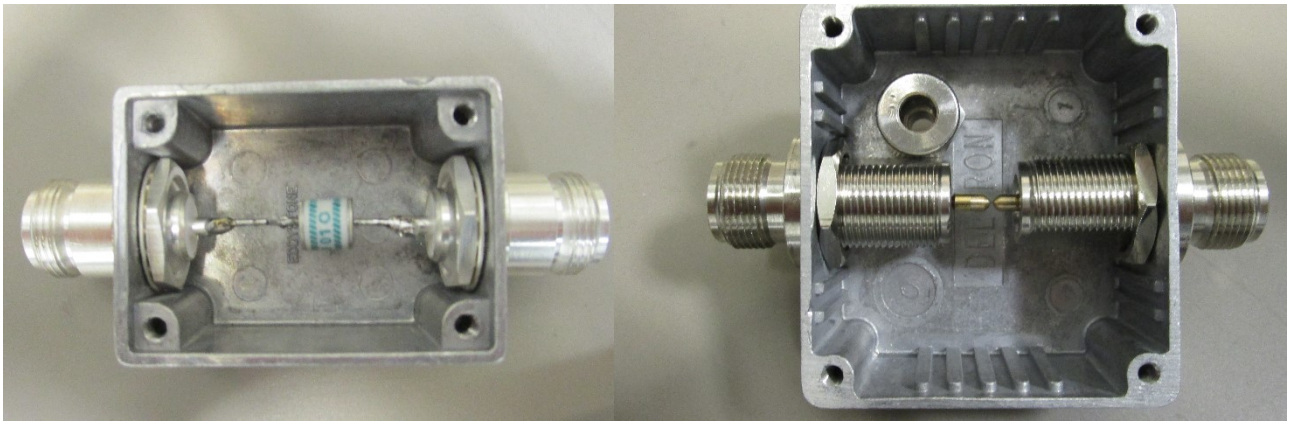

(a) (b)

Figure 15 (a) Assembly made for argon spark gap, (b) Assembly made with adjustable electrodes using air and SF_6 as a medium.

2.5 The Current step measuring system

The current step measuring system includes all the devices that are used for current step measuring which agree with the high voltage measurement standard IEC-60060-2 [9]. Figure 16 shows different components of the measuring system. These components are: a) The converting device, b) The transmission line, and c) The measuring or recording instrument.

2.5.1 The Converting device

The device which converts or capable of converting its input quantity into a quantity which is in the input range of the measuring instrument and maintains the parameters like shape, time, frequency components, etc of input quantity up to a certain accuracy. Converting device gives the replica of the measurand to the instrument. In this project, resistive shunts and Rogowski coils are used as converting device. Other types of converting devices

include voltage divider, transformers and electric field probes. Every converting device scales down the input quantity by its scale factor.

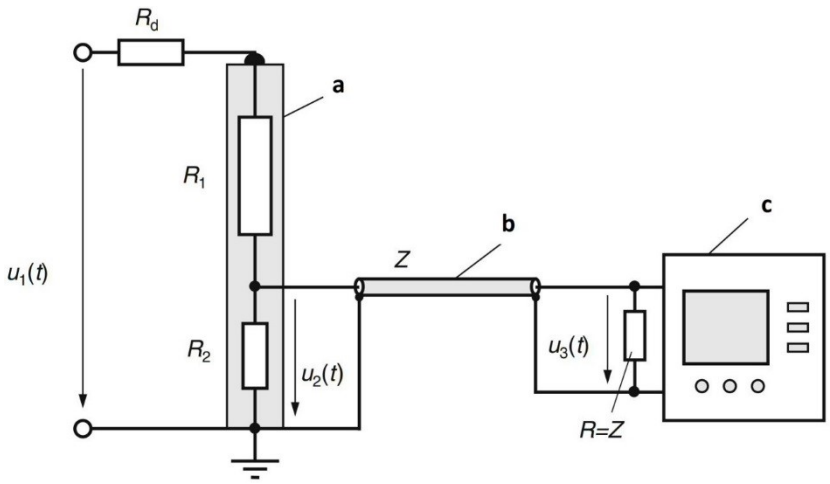

Figure 16 Impulse measurement system showing, (a) Resistive divider as a converting device (it can be any other instrument e.g. shunt, Rogowski coil etc). (b) Coaxial measuring cable with surge impedance *Z* as a transmission line, (c) Oscilloscope or Digital measuring instrument used as a recording instrument [28].

2.5.2 The Transmission line

Transmission line transmits the output of the converting device to the measuring device. It is usually a coaxial or a tri-axial cable with its termination connection or impedance. The cable has its own surge impedance or characteristic impedance *Z*. To analyze the behavior of the waveform with accuracy and better results, optical type transmission systems are also used having a set of a transmitter and a receiver. In some cases, impedance attenuators may also be used to decrease the voltage even further. Presence of attenuators is considered when calculating the scale factor.

2.5.2.1 Assigned scale factor of the system

The assigned scale factor of the whole system is actually a combination of all scale factors in the system, such as divider, sensor, cable, attenuators, instruments etc. This assigned scale factor of the system has to be calibrated and those calibration values should be used for voltages to get the respective values for the current.

2.5.3 The Measuring instrument

Measuring device is a device which measures, displays and calculates any relevant parameters of input voltage. Digital recorders or digital scopes are used nowadays as the measuring instrument instead of analog peak voltmeters. Oscilloscopes and digitizers are a few examples of measuring instruments. The voltage received from the transmission line is fed to the instrument that multiplies the pre-fed scale factor of the system with it. Every measuring instrument usually has its own native software which is the part of the measuring system considering as a whole. This software can calculate different parameters, such as impulse front time, the time of chopping or the cut-off etc. as per standards. As an example, a complete system with high-resistance divider having high voltage and low voltage arms and impedance matching resistance *Z* is shown in Figure 16.

2.6 Factors affecting the results of current step measurement

The initial operation of a current step measuring system consists of shunts, Rogowski coils, voltage dividers, signal cables, and oscilloscopes. The waveform displayed by these oscilloscopes or digitizers have interferences that is not the correct representation of the original waveform being measured. Different factors are found in literature that affect the results of a current step measurement.

2.6.1 Factors related to measurement systems

According to the Nyquist criterion, the sampling rate should be at least twice the bandwidth. If the system is used for measuring a rise time of 5 ns, the bandwidth according to the relation of bandwidth/frequency and the rise times as per equation 6 will be 70 MHz. Therefore, to show the clear picture of the phenomenon that has to be investigated, the measurement system or instrument should have a minimum sampling rate of 140 MS/s.

2.6.2 Factors related to interference

Due to their fast-occurring phenomenon, impulse and step measurements are liable to the high level of electromagnetic interference which can be due to conduction or radiation. One of the main cause of interference is the interference currents in the braids of the measuring cables, introduced by the nearby spark gaps in the circuit of steep rise time current step generator. The firing of a nearby spark gap produces interferences if the high values of current and voltages are used that can superimpose on the beginning part of the measured impulse or step. Hence, this hinders the determination for 90% point on the rising edge of current step which is required to calculate the rise time [12]. In this project, the length of the coaxial cable from current sensor to oscilloscope was reduced to avoid interferences due to the firing of nearby spark gap. Figure 17 shows the improvement in the current signal during various states of the interference reduction which are superimposed on the current signal.

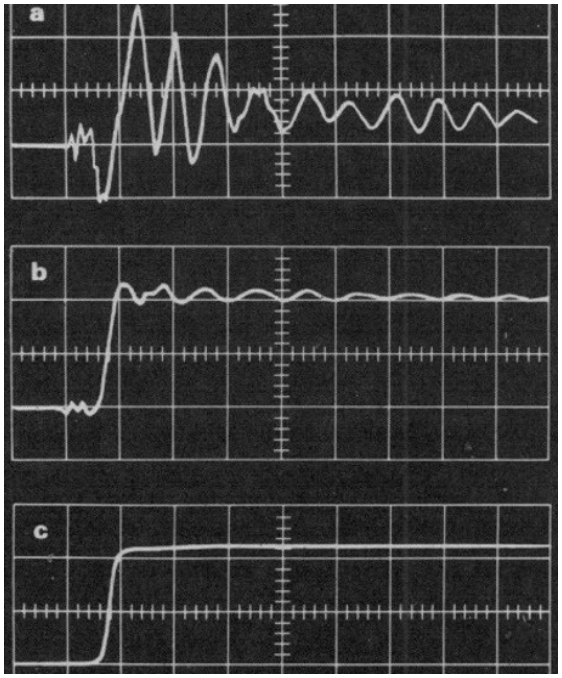

Figure 17 Improvement of the pulse fidelity of current signal during various states of interference reduction [12].

2.6.3 Factors related to instruments and software

The rise time of an instrument is an important parameter when evaluating the instrument for current step measurements. The rise time should considerably be shorter than the rise time of the current step which is to be measured. Similarly, an instrument with small sampling rate results in smaller number of points in the sampled data for current step as compared with an instrument with a higher sampling rate. The instrument with too much small sampling rate will result in loss of critical points on the sample data of current step, resulting errors in the time parameters and peak values [28]. Higher sampling rate for better performance can be obtained by incrementing the number of bits of the instrument's native AD converter. Nowadays, the oscilloscopes are available with much higher limits of sampling rate and speed. LabMaster 10-100Zi is the digital oscilloscope from the TELEDYNE LECROY with the bandwidth of 100 GHz and the sampling rate of 240 GS/sec. It has a rise time of 3.5 ps (20-80%) [39]. The instrument like this can be of importance to record steep current steps with high accuracy.

Digital oscilloscopes nowadays come with installable software for measurement from the manufacturer. These programs can be installed in commercial operating systems like Windows from Microsoft. A custom software can also be written for recording and evaluating the impulse or step parameters of one's own choice. The software used must be able to recognize the superimposed oscillations so that the parameters can be evaluated properly [28]. For the purpose of evaluating the efficiency, verification for the impulse can be done using the predefined data sets of some selected shapes rather than evaluating the individual software. An international comparison was made for this purpose via non-variable data sets [40].

2.6.4 Factors related to errors during signal recording

Figure 18 shows the basic block diagram of a digital recorder. The analogue and digital components of digital recorders used for the measurement of step currents cause characteristic measurement errors. Even the ideal digitizing is associated with errors due to the factors, including time resolution and limited amplitude. These errors are described as sampling errors or quantization errors and their maximum values can theoretically be estimated. The analogue circuits of a real AD converter used in the recorder for digitizing causes additional errors due to its technical imperfections. Therefore, the effect of errors can be subdivided into those that are already present while sampling the DC voltage, and those that additionally arise with high frequency signals. Other error sources of recorders include input attenuators and amplifiers [28].

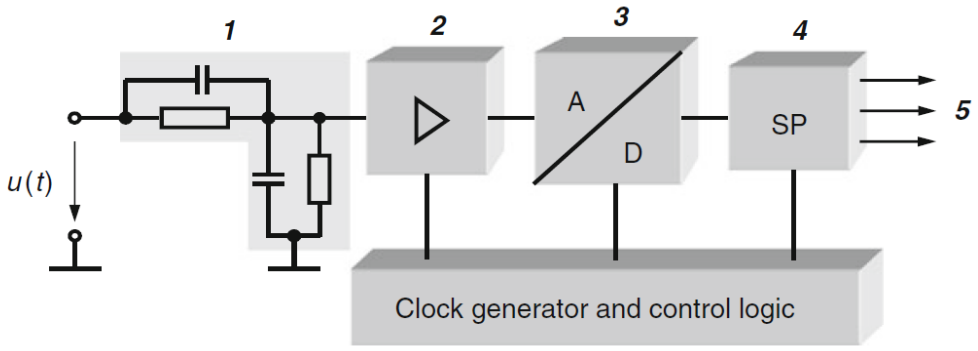

Figure 18 Simple block diagram of a digital recorder. 1 input attenuator. 2 amplifier, 3 analogue to digital converter, 4 data storage, 5 data output to external equipment [28].

2.7 Calibration

Calibration is essentially the measurement of the systematic error that characterizes a device. A device can be calibrated if a systematic error that can be moved to and from a calibration laboratory i.e. if the systematic error is transportable and stable, without significant change. The calibration is done to correct for the systematic error, and the initial systematic error is effectively replaced by calibration uncertainty. Some of the important definitions used in the process of calibration are defined below.

Error: The unavoidable difference between the measured value and the true value of the measurand which is never precisely known is referred to as an error. Two main types of errors are
(a) Systematic error: An error that characterizes the particular device or 'system' which is used. The magnitude of this error remains the same as long as the device is same.
(b) Random error: Error in measurements caused by the factors which vary from one measurement to the other. e.g. temperature.
Uncertainty: The estimate of how wrong the measurement may be is uncertainty. It should be noted that the calibration uncertainty amounts to the estimate of the systematic error, even if the calibration uncertainty is entirely due to a random error [41].

For measurements to be traceable to standards, the characterization of current measuring sensors is done by calibrating them. The calibration of current sensors in this project will be done by selecting best shunt as reference and calibrating rest of the sensors with respect to reference shunt as per Section 5.2 of standard IEC-62475, which explains high-current test and measurement techniques [11]. The calibration of current sensors with a reference current sensor is explained in Chapter 5. It consists of the following two step:

- Estimating the uncertainty of current sensor with respect to reference current sensor having suitable accuracy,
- Considering the dynamic behavior of different current measuring sensors.

After the calibration of sensors keeping in view the limits presented in standard IEC-62475[11], the system acts as an approved measuring system which can be used in high voltage labs.

2.8 Summary

This chapter introduces and compares the two different current monitoring sensors, resistive shunts using the Ohm's law and Rogowski coils using the Faraday's law of induction. Both methods will be used for measuring current steps. Current steps are explained along with brief discussion on previous research done in this field. Various methods are analyzed which are used in the past for current step generation. This chapter presented the theory of current step measurement systems, factors which affect a current measurement system, and a brief theory of calibration, which will be done in Chapter 5 for all the sensors used in this project. From this background study of current and voltage step generation, it is concluded that a coaxial cable generator with the spark gap as a switch is the most inexpensive and reliable method used for the current step generation. Therefore, a coaxial cable generator is made for current step generation with the spark gap as a switching device in this Thesis. The generation of current step is presented in Chapter 3, followed in Chapter 4 by an explanation of current step measurement.

Chapter 3

Generation of Current Step

This chapter presents the simulation and practical circuit for the coaxial cable generator used to generate current steps. In addition, the working principle of this cable generator is explained. Section 3.1 discusses the general circuit for current step generation. Section 3.2 and 3.3 explain circuit simulation and practical circuit for the current step generator. Finally, Section 3.4 summaries the whole chapter.

3.1 Generation of rectangular current step

Figure 19 presents an arrangement for coaxial cable step generator that can generate negative or positive step currents. It consists of a coaxial cable having surge impedance Z charged from one end with a direct voltage U_o through a series charging resistance R_1, and the other end of this coaxial cable is left open. L is the inductance of the overall circuit including the inductance of connections and spark gap. Z_a is the impedance of load connected, such as shunt in this project. The peak current of the current step generated is the ratio of the applied voltage U_o at which the spark gap switch S operates and the circuit's total impedance at the time of switching. The overall impedance of circuit when the switch S closes is the characteristic impedance of the coaxial cable Z and the connected load Z_a.

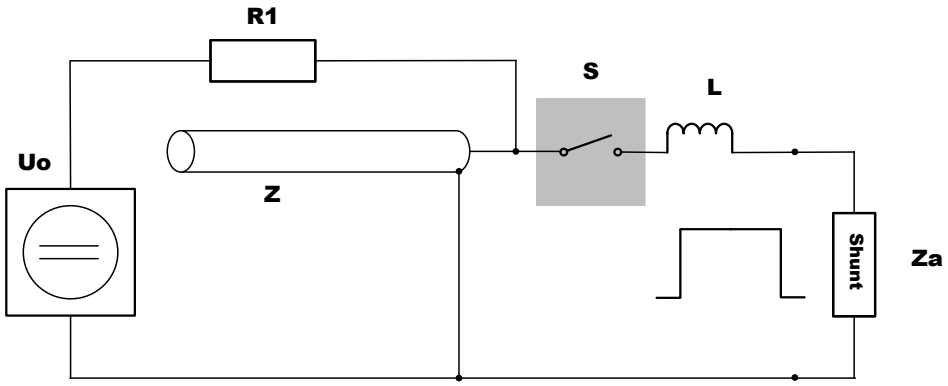

Figure 19 Circuit diagram of coaxial cable current step generator charged via charging resistor *R1* when the switch *S* is closed [43].

According to [42], the magnitude of the generated current step is given by

$$I = \frac{Uo}{(Z+Za)} \ , \qquad (7)$$

where I is the magnitude of the current step generated, and U_o is the applied DC voltage. Z is the characteristic impedance of the coaxial cable and Z_a is the impedance of the connected load. Since the characteristic impedance

of the coaxial cable generator is a dominating factor as compared to the small impedance of the connected load in this project, the final equation can be approximated as

$$\boldsymbol{I = \frac{Uo}{(Z)}} \ , \qquad (8)$$

which gives the magnitude of the current step generated ignoring the negligible impedance Z_a of connected load.

One possible method of generating a current step is a cable generator as represented in Figure 19. The charging resistance R_1 is selected large enough to slowly charge the cable for the duration of the cable transmission delay. Initially, the coaxial cable is charged by varying voltage U_o of DC generator through a series charging resistance R_1 to the breakdown voltage (e.g. 2.5 kV for 50 A current step) of the spark gap *S*. During the charging, a steep wave of current enters the coaxial cable and reflects at the open end. This reflected wave travels back from the open end to the entry point of the cable with same amplitude and polarity as explained in Figure 12 of section 2.3.1. At the breakdown voltage, the spark gap switch *S* ignites (closes) and the charged coaxial cable is discharged to the load Z_a, which is a resistive shunt in this case. Therefore, discharging this coaxial cable generates the current steps with step length of twice the cable transmission delay. Current steps are generated at the terminating impedance whose amplitude is determined by the ratio of the impedance of the connected load, Z_a, and *Z*. The current steps are generated which has the waveform according to the condition $Z_a << Z$, described in Figure 13, Section 2.3.1.

The electromagnetic wave propagates at the speed of light through free space. When the current wave is surrounded by the insulating medium other than air or vacuum, the propagation delay increases proportionally. The propagation delay with known dielectric constant *Dk* is given by the following equation

$$\boldsymbol{tdp = \frac{\sqrt{Dk}}{c}} \ , \qquad (9)$$

where *tdp* is the propagation delay, *Dk* is the dielectric constant and *c* is the speed of light in free space. The material used for cable insulation of coaxial cable used in this project was foam polyethylene obtained from the data sheet. The dielectric constant of foam polyethylene according to [42] is 1.37. The transmission line propagation delay of approximately 450 ns was calculated for the coaxial cable using equation 9. Therefore, for twice the transmission delay, a 900 ns step length can be generated. A current step length of approximately 960 ns was generated practically which agreed with theoretically calculated step length.

The steepness of the step depends on the spark gap switch *S* and the inductance of the leads in the discharge circuit. In a low-inductive construction of a step generator, rise times of the step voltage less than 1 ns can be attained. If a recorder or a coaxial shunt is connected to the generator by means of a coaxial cable, introduction of a series resistance equal to the cable surge impedance is recommended to avoid reflection phenomena.

For $Z_a = Z$, the current dies out or ceases at the terminating impedance after twice the cable travel time. In the meantime, the switch operates again forming successive current steps. For, $Z_a \neq Z$, the reflection phenomenon happens again at the load, now with opposite polarity. According to [42], the duration of a current step generated depends on the physical length *l* of the coaxial cable and the cable travel time given by

$$t = 2l/v, \tag{10}$$

where $v = \frac{1}{\sqrt{LoCo}}$. L_o and C_o are characteristic inductance and capacitance of the coaxial cable. Note that the length of the current step is always limited by the drooping of the current step due to damping losses in the cable. Relation between the rise time of the generated current step, τ, and the inductance, L, is given by the equation

$$\tau = \frac{L}{(Z+Za)}\ , \tag{11}$$

where L is the total inductance of overall circuit such as inductance of spark gap, connections etc [42]. Therefore, the rise time is limited by the L/Z time constant of the circuit. Inductance or inductive loops in the circuit should be reduced to get lower rise times. Rise time is also affected by the type of switch used, while it depends on the type of medium used in case of the spark gap used as a switch [37].

3.2 Circuit simulation of current step generator

The simulation tools Micro-Cap [44] and Castle transmission line circuit simulator [45] were used for simulating the circuit diagram of the current step generator. The purpose for simulations was to compare the obtained waveforms with those which will practically be generated at High Voltage Laboratory. The Castle transmission line circuit simulator had the advantage of simulating lossy transmission lines in time domain using transmission line equations. It was therefore used for simulating the circuit which helped in getting required aims. Figure 20 shows the circuit diagram made with castle simulation tool. Shunt was used as a load with resistance of 99 mΩ and parasitic inductance of 0.2 nH. A spark gap was simulated by using the ideal switches *S1* and *S2*, their position and switching times were arranged in such a way that the coaxial transmission line *T1* was charged for the time twice the transmission delay τ (the time for which the switch remains closed). Thus, the cable was continuously charged and discharged generating current steps with the same decay time as calculated practically. The simulated current steps and the magnification of the first current step are shown in Figure 21. The droop in the current step depends on the resistance of the coaxial cable *R,* overall inductance of the circuit *L6*, and the swiching losses of the spark gap.

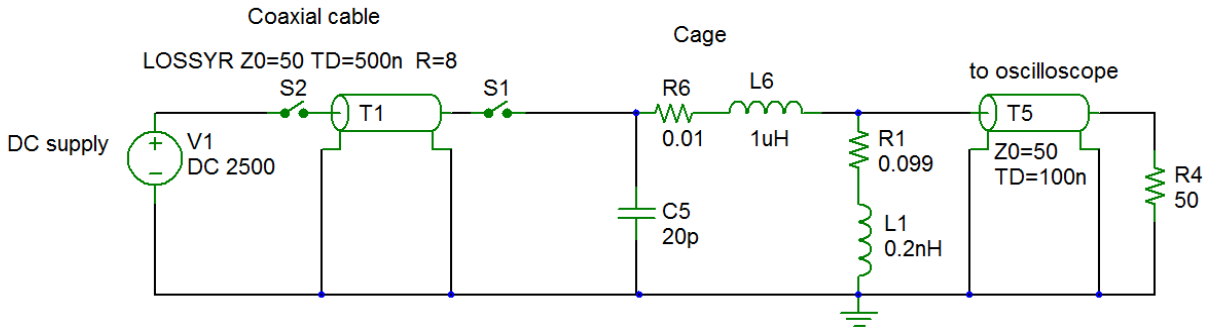

Figure 20 Circuit diagram of current step generator simulated on the Castle circuit simulator with a 0.099 Ω shunt for measuring current step.

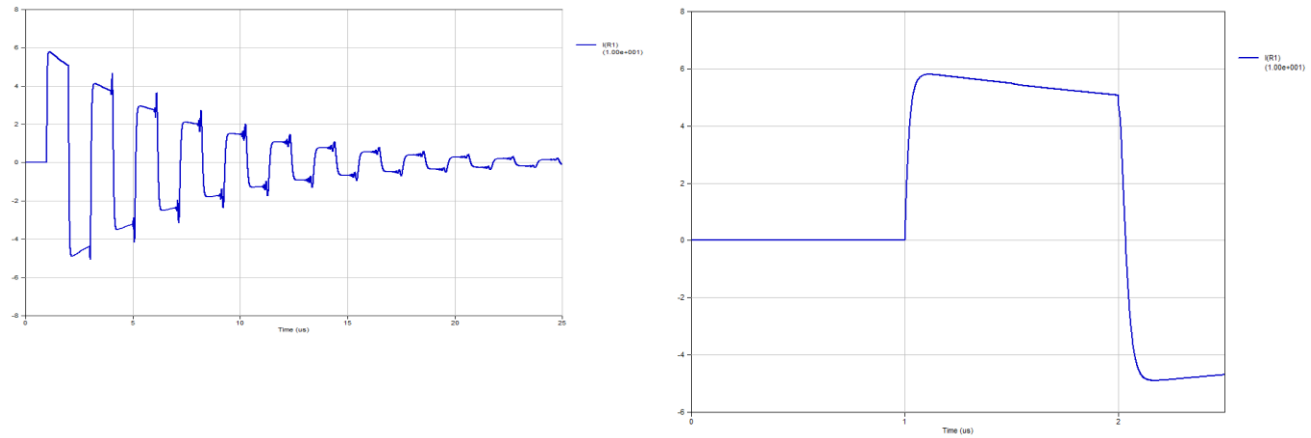

(a) (b)

Figure 21 Simulation results of Figure 20 simulated with the Castle circuit simulator for current steps using circuit. a) Simulation results for long trace of current steps generated, b) Simulation result of the first current step (1000 ns).

3.3 Practical setup for generating a current step

Figure 22 shows the setup for generating current steps built in the High Voltage Laboratory at VTT Mikes [51]. A DC generator capable of providing voltage up to 200 kV was used to charge a ½" Heliax cable 110-m in length having characteristic impedance of 50 Ω. The charging resistor of 32 MΩ and spark gaps of different media were used as the switch *S*.

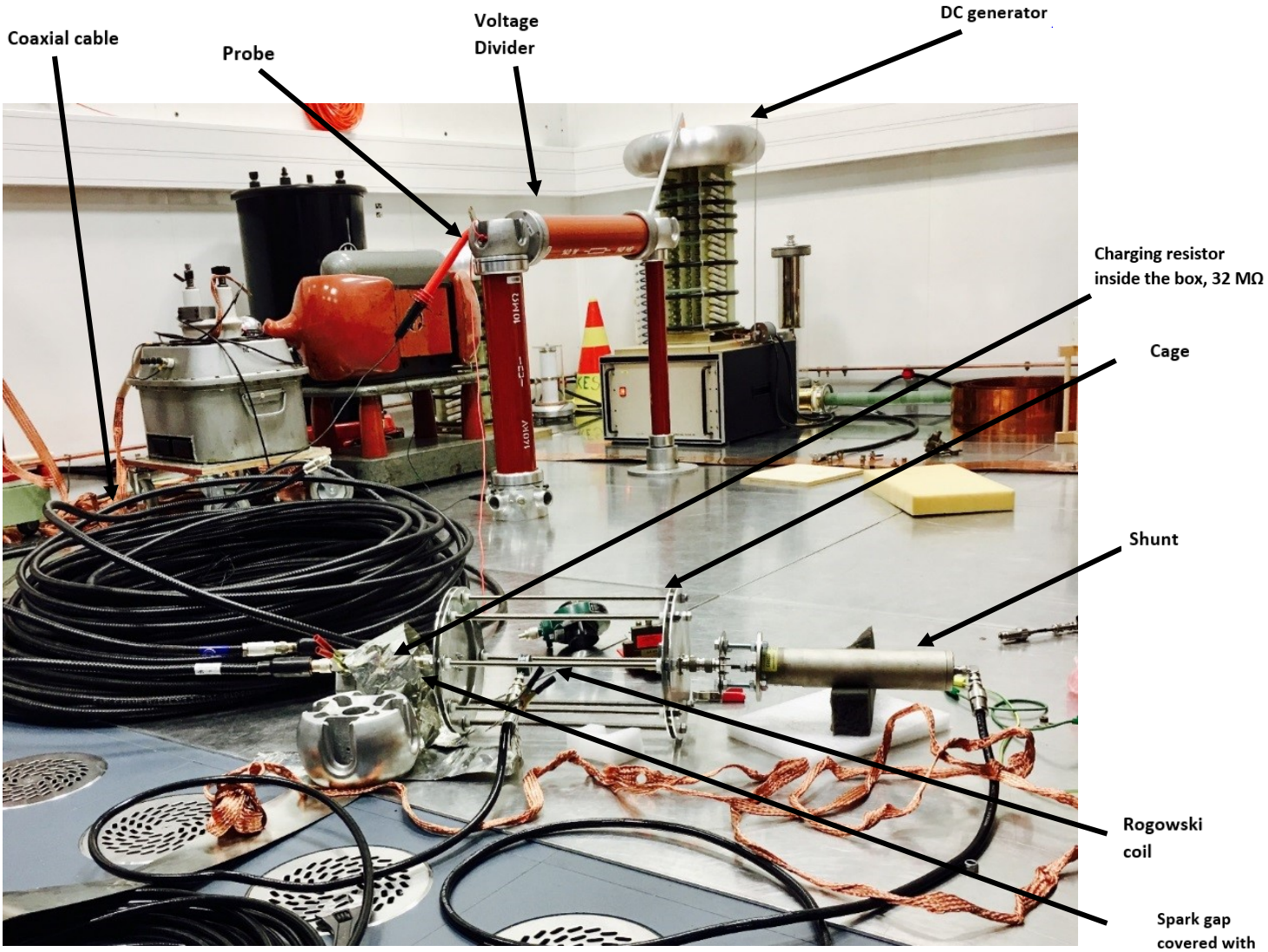

Figure 22 Circuit assembly for the current step generation in High Voltage Laboratory at VTT MIKES. The 110-m cable can be seen on the left charged with the DC generator through a voltage divider and series charging resistance. The spark gap used is located between cable and the cylindrical cage like structure made for placing sensors coaxially with respect to the return path of the current. The cage has two round disc-like plates with central conductor for current flow and 8 rods for return current. The Rogowski coil which can be seen inside the cage and shunt resistor to the right of cage are connected to oscilloscope via coaxial cables.

The coaxial cable was charged with the DC generator from one end and left open at the other end. With the help of a spark gap switch, the cable was charged by varying DC supply through a series resistor of resistance 32 MΩ. The cable was discharged to a shunt (or coil) at the specified breakdown voltage of the spark gap (e.g. 2.5 kV for current step of 50 A and 5 kV for current step of 100 A) to get the required current step as per equation 8. The current steps generated were identical and comparable to the simulation results shown in Figure 21. Figure 23 shows one of the practically generated current steps and its magnified first current step. To increase the step-length of the current step generated, the length of the coaxial cable used for generation was increased from 100-m to 110-m. Figure 24 shows the comparison of two current steps with different length of coaxial cable in generation circuit.

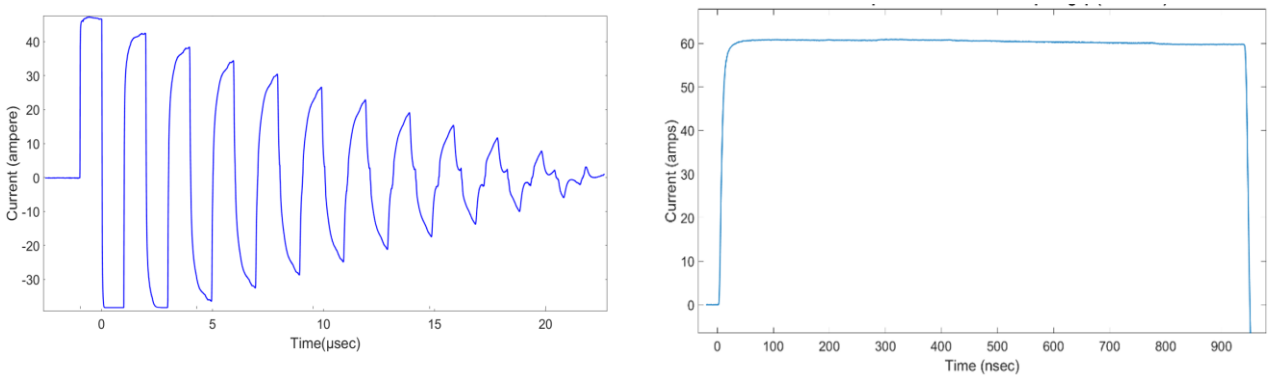

(a) (b)

Figure 23 Practically generated current steps at VTT Mikes High voltage laboratory using shunt resistor. (a) The long trace of generated current steps. (b) First current step of generated steps with shunt resistor.

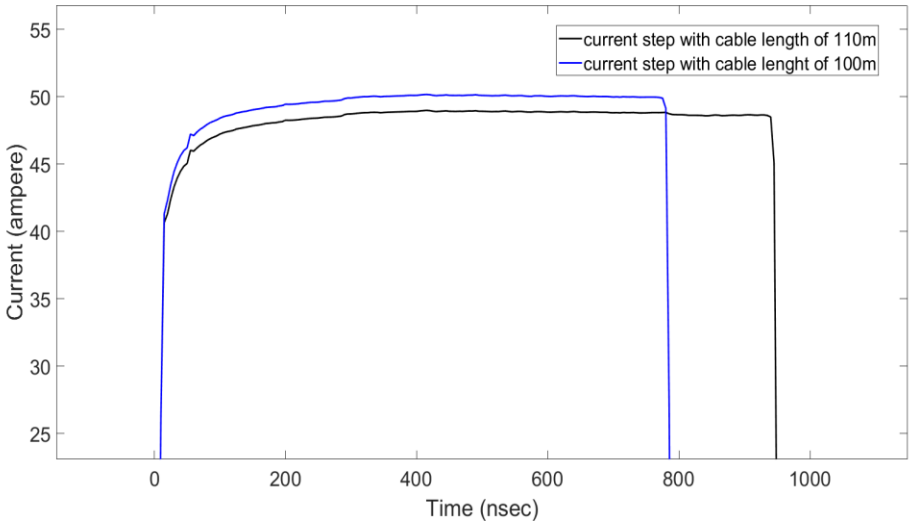

Figure 24 Current steps generated with different cable lengths showing increase in the step length.

Tektronix impulse generator was also used in the initial stages of practical lab tests. Figure 25 shows the impulse generator used and its specifications are listed in Table 1. The coaxial cable was charged using this impulse generator instead of supply from DC generator, and the current step was generated by discharging the cable through a 300 V spark gap switch.

Table 1 Specifications of the Tektronix impulse generator.

Device	Manufacturer	Model	Output impedance	Rise-Time
Impulse generator	Tektronix	110	50 Ω	0.25 ns

Figure 25 Tektronix impulse generator.

According to [43], a rise times of 6 to 8 ns can be achieved using normal spark gaps with atmospheric air as a medium. Results achieved practically by using designed current steps generater almost agreed with this statement by getting a rise time in the range of 10 ns. Similarly, pressurized or multiple spark gaps allow even shorter rise times [43]. Therefore, to improve the accuracy of generated current steps, various spark gaps, including pressurized SF_6 gas filled spark gap was used later instead of an air-filled spark gap. Table 2 shows different types of spark gaps used in this project. Gaps number 1 and 2 were commercial argon filled two-electrode surge arresters. Gaps number 3 and 4 are the same self-made gap box shown in Figure 15 of Section 2.4.2, filled either with atmospheric air or pressurized SF_6.

Table 2 Various spark gaps used in current step generation.

S. No.	Gas	Gap length	Breakdown Voltage	Type
1	Argon	Fixed	300 V	Commercial surge arrester
2	Argon	Fixed	2.5 kV	Commercial surge arrester
3	Air	0.1--1.1 mm	1.7--4.7 kV	Adjustable self-made gap
4	SF_6	0.1 mm	varied with gas pressure	Adjustable self-made gap

Figure 26 shows a coaxial cage like structure made to provide return path for current and coaxial connection to current step measuring sensors. In order to reduce the rise time of the generated current step, the circuit was kept coaxial to minimize its inductance. The inductive loops and thereby inductance in the circuit were reduced by a coaxial structure made at the workshop of VTT MIKES to place current sensors coaxially with respect to their return currents. Inductance directly effects the rise time of the generated current step according to equation 11. Thus, modifications were made throughout different test sessions performed to achieve the lower rise times.

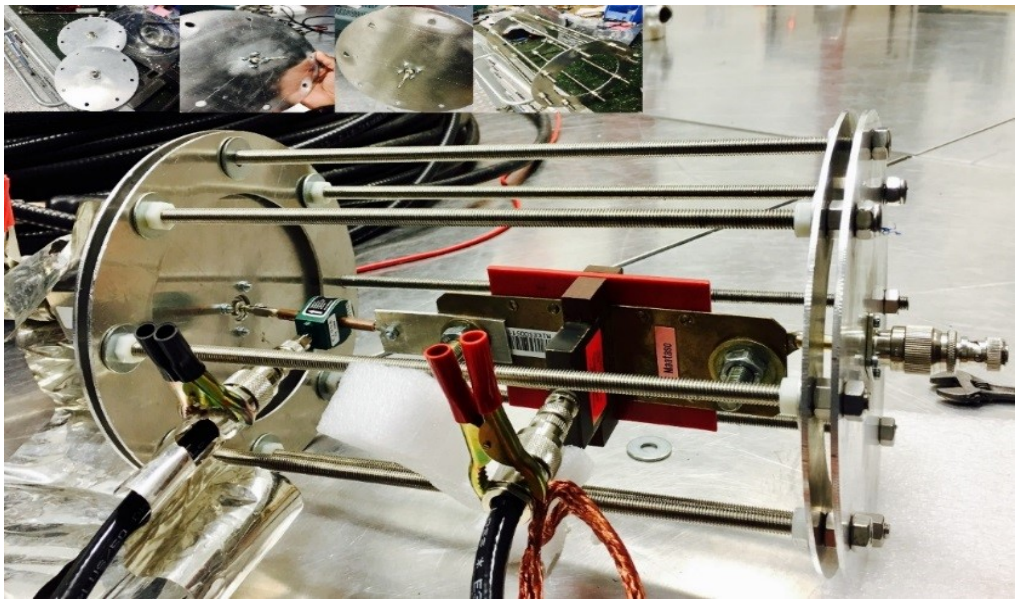

Figure 26 Cage-structure made to provide return path for current and coaxial connection for current sensors.

To further analyze the generated current steps, the coaxial cable used as current step generator was also charged from its opposite end, i.e., from the end normally left open, to examine its effect on the waveform of current step. The results showed that the change in the cable orientation does not affect the rise time of generated current step. The cable from different manufacturer (*Ecoflex*) was also used for current step generation having the same impedance of 50 Ω as previously used 110-m long coaxial cable. No improvement in the rise time or the waveform of current step was observed. Appendix B shows all the current steps generated with coaxial cable charged from opposite end, and with *Ecoflex* cable of approximately 15-m in length.

Inductive grounding at different positions and its effect was studied on the generated current step. Inductive grounding connections were made at the end of the sensor where it was connected to the transient recorder with a cable through a BNC and N-connector to get the best current steps generated. A slow pitched droop cannot be prevented due to the dampening of the cable. Generated current steps were measured with different sensors and recorded with various oscilloscopes available.

3.4 Summary

This chapter presented coaxial cable generator and its working principle made in HV Lab at VTT Mikes for the generation of rectangular current steps. The circuit simulation results for current steps and practical generation circuit results were compared, showing identical output. The circuit components, various spark gaps used as a switch and modifications to the generation circuit were described. The measurement of current steps generated using this step generator is explained in Chapter 4.

Chapter 4

Measurement of Current Step

This chapter describes the measurement of generated current steps presented in Chapter 3. Section 4.1 describes the sensors used for current step measurement and their specifications, practical step measuring circuit and its working, procedure followed for recording measured data and block diagrams of measurement circuit. Section 4.2 discusses the factors affecting current step measurement, waveform and the rise time of current step measured. Section 4.3 shows the measurement of rise time and the rise times recorded with various current sensors used in different test sessions. Section 4.4 provides the result for interference tests performed. Section 4.5 presents reference calibration circuit for step measurement and the calibration of current sensors. Finally, Section 4.6 summaries the whole chapter.

4.1 Measurement setup

The generation and measurement of current step are overlapping phenomena that are performed together. The current steps generated were always measured and recorded with current sensors. Figure 27 shows pictures of the tested sensors whereas Table 3 shows their specifications.

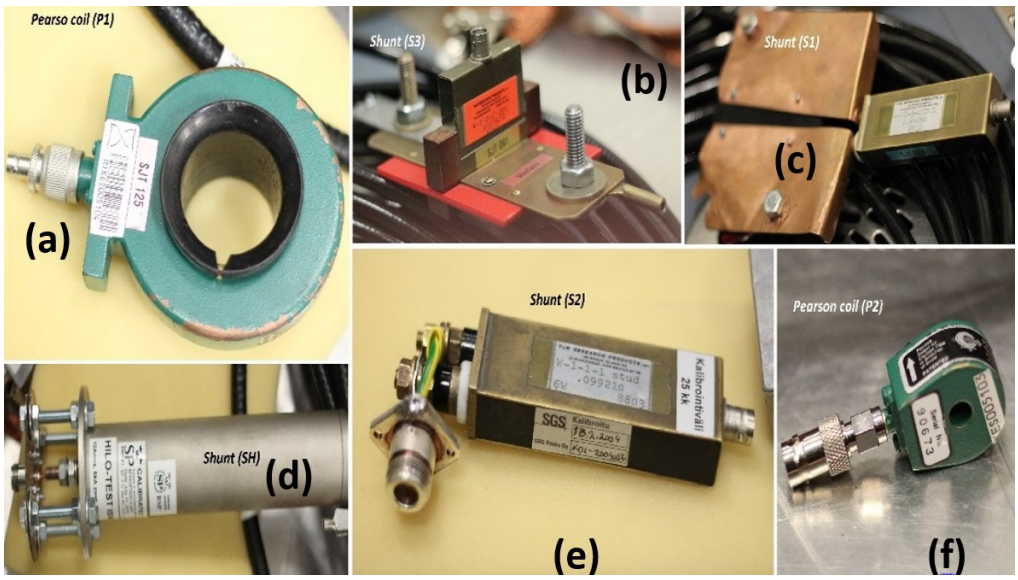

Figure 27 Sensors used for measuring the current step; (a) The *P1* Rogowski coil from Pearson Electronics, (b)The *S3* shunt from T&M Products, (c)The *S1* shunt from T&M Products, (d) The *SH* shunt from HILO TEST, (e) The *S2* shunt from T&M Products, (f) The *P2* Rogowski coil from Pearson Electronics.

The current sensors used were 2 Rogowski coils and 4 resistive shunts. One of the main aim of the current step measurement was the step calibration of shunts. The DC calibration for most of the shunts had already been carried out at VTT Mikes previously, followed by new DC calibration for shunts presented in Section 5.1 in Chapter 5. However, no step calibration for any of the sensor was previously available. Due to common mode grounding

problems, two shunts cannot be directly compared against each other. However, it was possible to compare the response of a shunt with a current sensing Rogowski coil as a transfer reference represented in Figure 28. Therefore, in most of the measurement sessions, one shunt and one coil were used together in the same measurement setup to record the measured data for the step calibration of shunts and to analyse their behaviour towards the generated current step of the same rise time and peak current value. Other than recording data for calibration and the characterization of resistive shunts, generated steps were examined to look for the factors affecting the waveform of the current step and its rise time. Only first current step was studied in this thesis.

Table 3 Measuring sensors used and their specifications.

Symbol used	Sensor	Manufacturer	Model	Nominal sensitivity or Resistance	Sensitivity/ Resistance (calibrated at VTT Mikes)	Bandwidth (MHz)	Rise-time (ns)	Max. Current (A)
P1	Rogowski coil	Pearson Electronics	110A	0.1 V/A	-	20	20	10,000
P2	Rogowski coil	Pearson Electronics	2877	1 V/A	-	200	2	100
S1	Shunt	T&M Research Products	W-1T-5-1STUD	0.5 Ω	(0.490509 ± 0.000018) Ω	400	1	-
S2	Shunt	T&M Research Products	W-1-1-1STUD	0.1 Ω	(0.099337 ± 0.000002) Ω	400	1	-
S3	Shunt	T&M Research Products	W-1-01C-2FC	0.01 Ω	(0.010338 ± 0.00000021) Ω	800	0.45	-
SH	Shunt	HILO-TEST	ISM 5P/50	0.05 Ω	-	200	1.8	5000

Figure 28 shows the general assembly of how current measuring sensors were used in a circuit. As an example, one coil and one shunt are used together in measurement setup. The shunt is connected to an oscilloscope via an attenuator to scale down the readings in the acceptable range of shunt. A spark gap is used as a switch *S*.

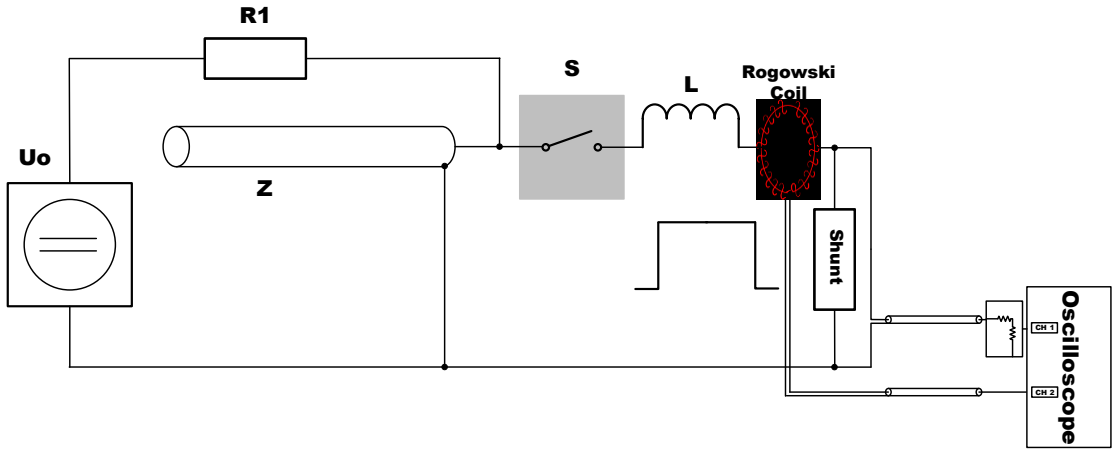

Figure 28 Circuit diagram for the measuring current step using shunt, coil, attenuator and oscilloscope. *S* and *L* representing spark gap and the total inductance of circuit, respectively.

The Rogowski coils and shunts were connected to one of the oscilloscopes from *Tektronix*, digitizers from *National Instruments*, and *LeCroy*. Table 4 shows the details and specifications of the oscilloscopes used. During the testing, the oscilloscopes were remotely controlled via optical fiber. The purpose of using different oscilloscopes was to measure the current steps with various sampling rates and bandwidths. The optimal sampling rate for the setup was 1 GS/s. Except the LeCroy oscilloscope with bandwidth of 600 MHz, sampling rates higher than 1 GS/s resulted in oversampling. The LeCroy oscilloscope was used in case of fast switching SF_6 spark gap that resulted in a rise time of less than 5 ns for most of the current sensors. This oscilloscope helped in analysing details in the rising edge of the current step measured.

Table 4 Oscilloscopes used as a recording instrument with the current sensors.

Scope	Model	Bandwidth (MHz)	Sampling rate (GS/s)	Uncertainty (%)	Sampling rate used (GS/s)
Tektronix	TDS 784C	1000	4	0.8	1
National Instruments	PXI-5124	150	0.2	0.38	0.2
LeCroy	64MXs-B	600	10	1	10

Figure 29 shows the practical setup assembly for the current step measurement. Current sensors were connected to the oscilloscopes through the coaxial cables of 50 Ω characteristic impedance to study the waveform and the rise time of the current step. Using possibly short lengthen coaxial cables of 50 Ω characteristic impedance between the sensor and oscilloscope provided impedance match to avoid reflections caused by impedance mismatch. The data was recorded with a software developed at VTT Mikes for the purpose of data reading from the oscilloscope.

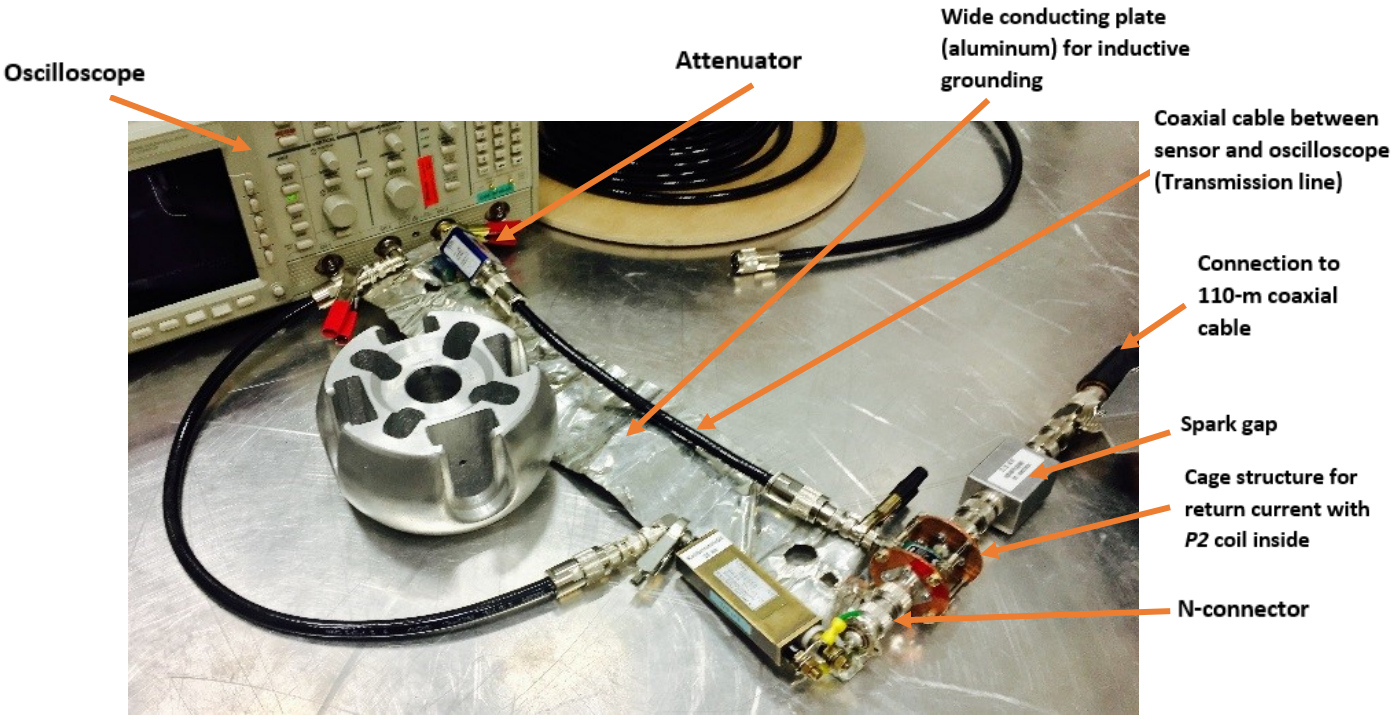

Figure 29 The setup assembled on a grounded aluminium sheet to provide the inductive grounding to the connections of components, connected through BNC and N-connectors. From the right, there is a spark gap switch followed by cage like structure with the *P2* Rogowski coil inside and the *S1* resistive shunt to the left. The cage like structure provided the return path and almost 50 Ω impedance match to the circuit. The possible short coaxial connection from sensors *S1* shunt and *P2* coil to the oscilloscope can be seen. Also, an attenuator is used with the *P2* coil at the input of oscilloscope.

While measuring generated current steps, the shunt *S1* and the Pearson coil *P2* were used with attenuators to attenuate the signal and get the output signal on oscilloscope within the required range. Figure 30 shows a simplified schematic of the principle design for an attenuator. A change in the scale factor of the attenuator was expected during test sessions due to the input impedance of an oscilloscope, temperature dependence, and self-heating due to application of current steps [46]. This was confirmed when the two sensors used together in the same measurement circuit measured different amplitude of the current step with one of the sensor using an attenuator. It was realized that using a 50 Ω input impedance of an oscilloscope was responsible for the change in the scale factor of the attenuator. The input impedance was in parallel with the attenuator and a new scaling factor was therefore calculated accordingly. Table 5 shows the attenuators used and their change in the scale factor with a 50 Ω input impedance.

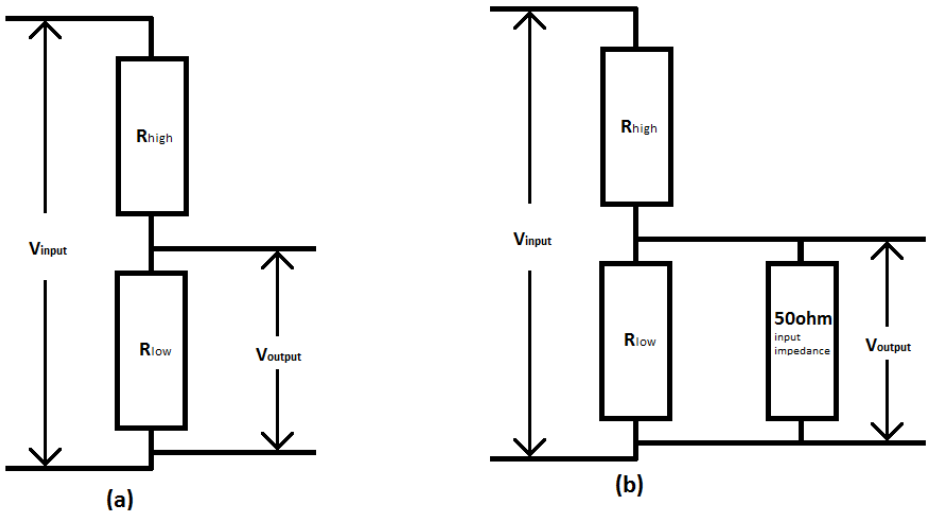

Figure 30 Simplified schematics showing the principle design of a resistive attenuator (a) without input impedance (b) with input impedance.

Table 5 Attenuators used in this project.

S. No	Attenuator	Used with	Change in the scale factor with 50 Ω input impedance
1.	5:1	Shunt S1	5.8:1
2.	6.6:1	Coil P2	7.5166:1

Initially, low amplitude current steps in the range of 6 A were generated using the Tektronix impulse generator shown in Chapter 3(Figure 25). These current steps had oscillations throughout the step measured with the *SH* shunt, but the measurement session with this impulse generator provided path for understanding generation and measurement of the current step. Appendix B shows the rising edge of a current step measured with the *SH* shunt using the impulse generator. Later, high amplitude current steps were generated with peak current range up to 50 A using DC generator available in the High Voltage Laboratory at VTT Mikes. Different test sessions were performed for measuring current steps using current sensors in various combinations following the similar setup assembly as shown in Figure 28.

Table 6 is an example of the test sessions with the Tektronix oscilloscope. The block diagrams of each circuit used for generation and measurement in this session are shown in Figure 31. These current steps were generated with 50 A peak current as per equation 8, using the sampling rate of 1 GS/s, acquisitions number of 100, and Argon spark gap of 2.5 kV. In each test session, parameters like grounding connection, coaxial connection, and impedance difference in circuit components were examined using the obtained waveforms. Current steps generated for this test session and other test sessions with various current sensors and oscilloscopes used are presented in Appendix C.

Table 6 Tests performed for high amplitude current step measurement using the Tektronix oscilloscope as a recording instrument.

S. No	Pearson coil 5104 *(P1)*	Pearson coil 5103 *(P2)*	HILO-TEST Shunt *(SH)*	Shunt 5113 *(S2)*	Shunt 5114 *(S3)*	Grounding	Coil position	Purpose of measurement
Test 01	✓		✓		✓	✓	not in center	Waveform& rise time
Test01 (reading 2)	✓		✓		✓	✓	in center(coaxial)	waveform study
Test 02	✓				✓	✓	in center(coaxial)	Waveform& rise time
Test 03	✓		✓		✓	✓	in center(coaxial)	waveform study
Test03 (reading 2)	✓		✓			✓	in center(coaxial)	waveform study
Test 04	✓			✓		✓	in center(coaxial)	waveform study
Test 05	✓					✓	in center(coaxial)	Waveform& rise time
Test 06	✓	✓				✓	in center(coaxial)	waveform study
Test 07	✓	✓					in center(coaxial)	waveform study
Test 08		✓		✓			in center(coaxial)	waveform study
Test 09		✓		✓		only S2	in center(coaxial)	waveform study
Test 10		✓					in center(coaxial)	waveform study
Test 11		✓					in center(coaxial)	Rise time
Test 12				✓		✓	in center(coaxial)	Rise time
Test 13				✓		✓	in center(coaxial)	long trace study
Test 14			✓			✓	in center(coaxial)	waveform study

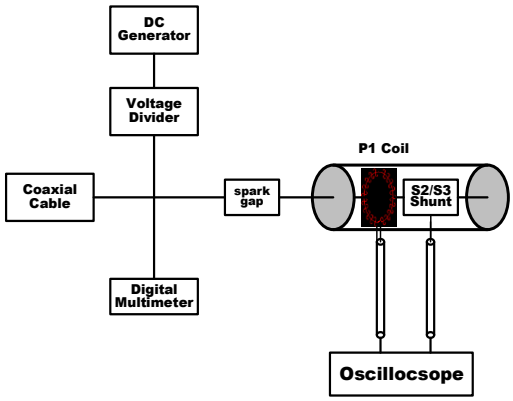

Measurement circuit for test 1A/2/4
(S2&S3 shunts used separately)

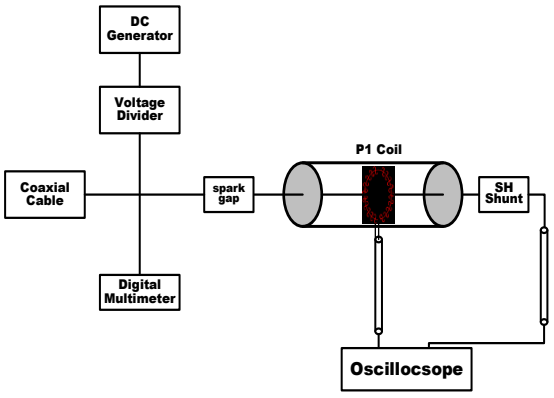

Measurement circuit for test 1/3/3A

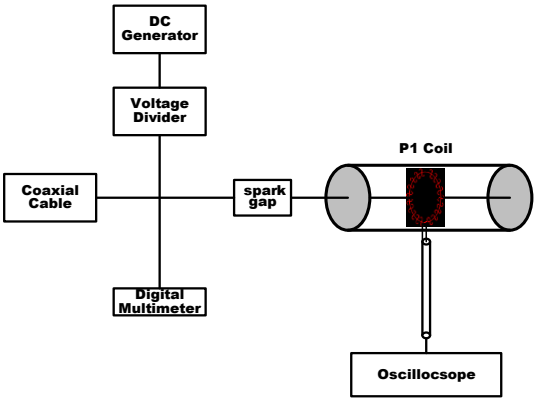

Measurement circuit for test 5

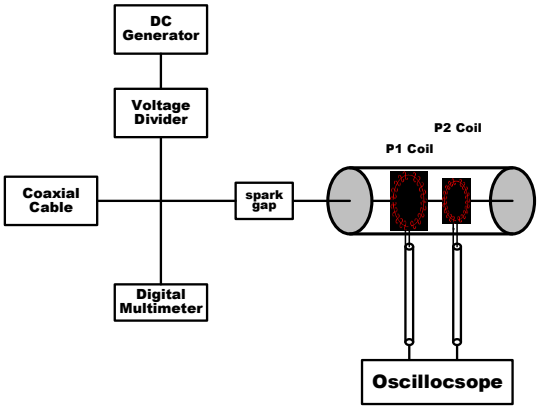

Measurement circuit for test 6/7

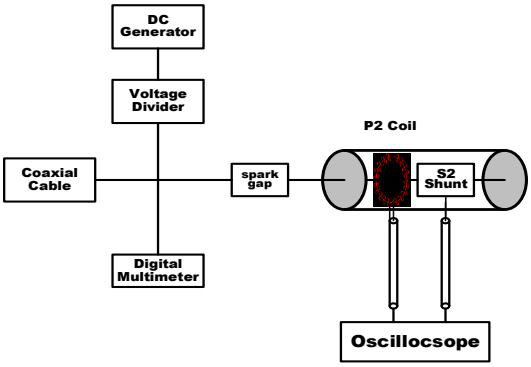

Measurement circuit for test 8/9

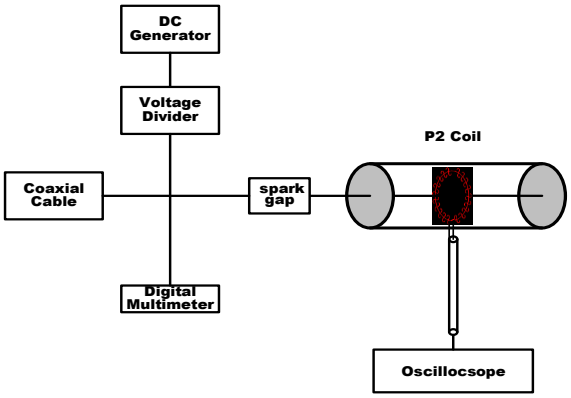

Measurement circuit for test 10/11

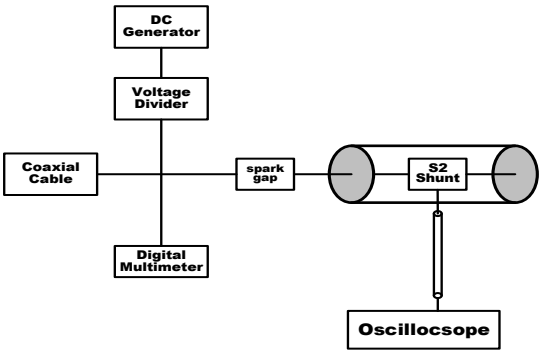

Measurement circuit for test 12/13

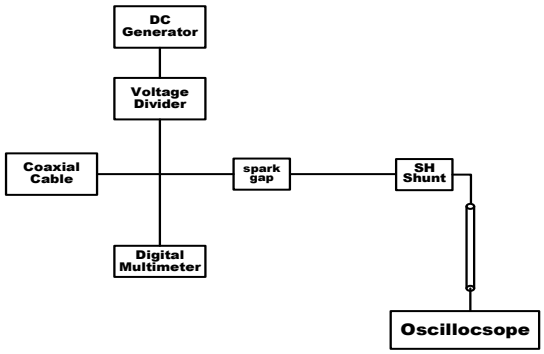

Measurement circuit for test 14

Figure 31 Block diagrams of all the tests performed for current step measurement using different combination of sensors.

As an example of current step measurement, the current steps for *P1* and *P2* coils are compared in Figure 32 while the current steps and their rising edge for *S1* and *S2* shunts are shown in Figure 33.

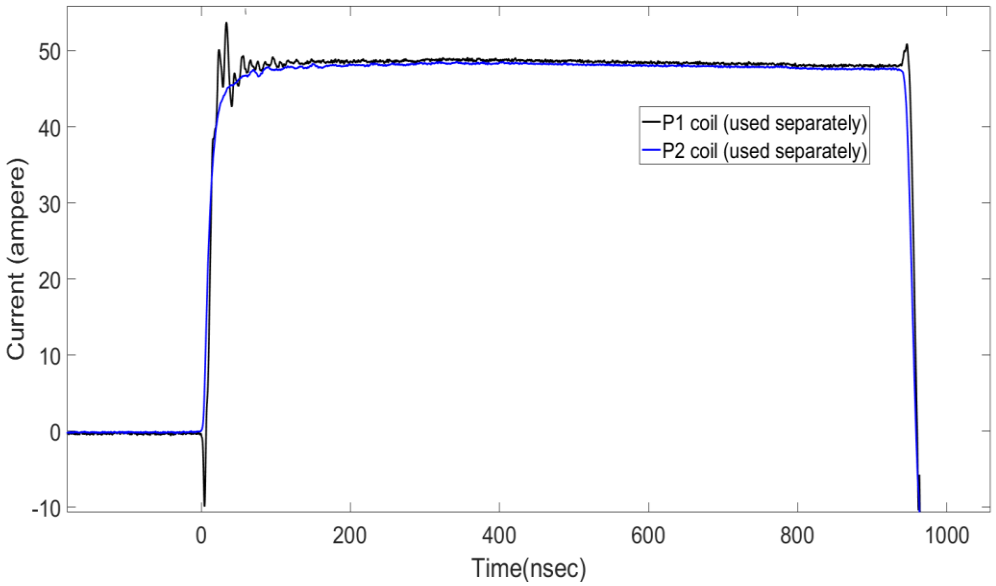

Figure 32 Current step measured with the *P1* and the *P2* coil separately in different test sessions. There are some oscillations in the rising edge of current step measured with the *P1* coil while no oscillations were recorded for the *P2* coil.

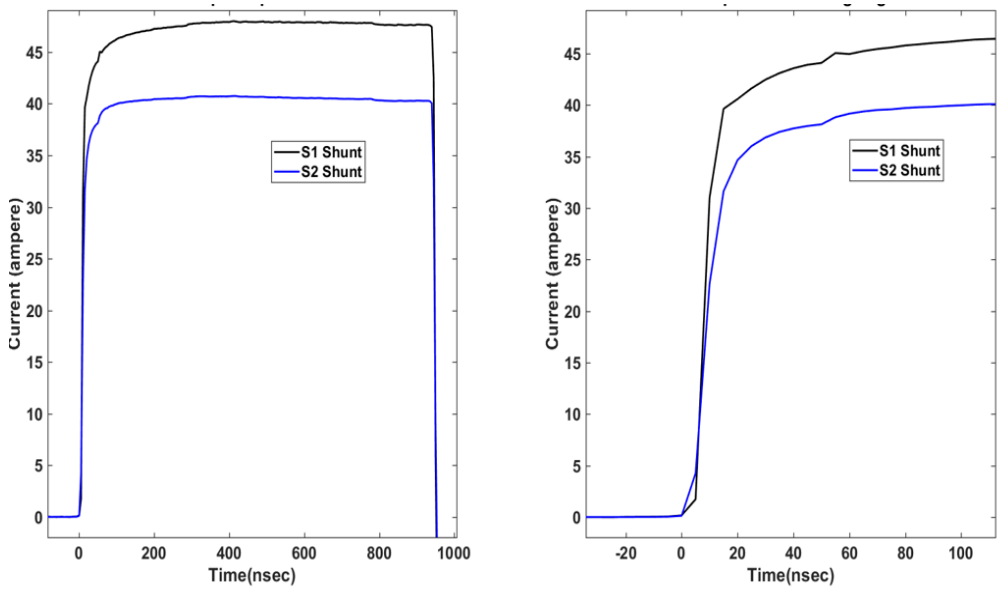

Figure 33 Current step and the magnified rising edges measured with shunts *S1* and *S2* used separately in current step measurement circuit in one of the test sessions.

4.2 Factors affecting current step measurement and the rise time

Various factors including grounding connection, the coaxial assembly of the sensors, reflections due to impedance difference, the arc length of spark gap electrodes, the gas pressure of spark gap medium, and the nominal values of current sensors were observed which affected the shape of the current step waveform and its rise time.

A. Grounding connection

The BNC and N-connector were used for connecting different components together, including oscilloscope, shunts, Rogowski coils, spark gaps, charging cable etc. The inductive grounding of these BNC and N-connectors in the measurement circuit had direct effect on the waveform of the generated current step. Figure 29 shown in Section 4.1 is the measurement setup on aluminium plate, where the connections of the cables used for connecting sensors to oscilloscope are grounded on both ends using these wide aluminium conductors for the inductive grounding. It should be noted that only connectors should be grounded and not the body of the current step measuring sensor, as grounding them resulted in a small leakage current, thus affecting the waveform of the current step. Figure 34 shows the rising edge both with and without the grounding connection for the current step measured with the two Rogowski coils *P1* and *P2* used together in the same measurement circuit for measuring of current step. It can be seen that the oscillations are reduced with grounding connection.

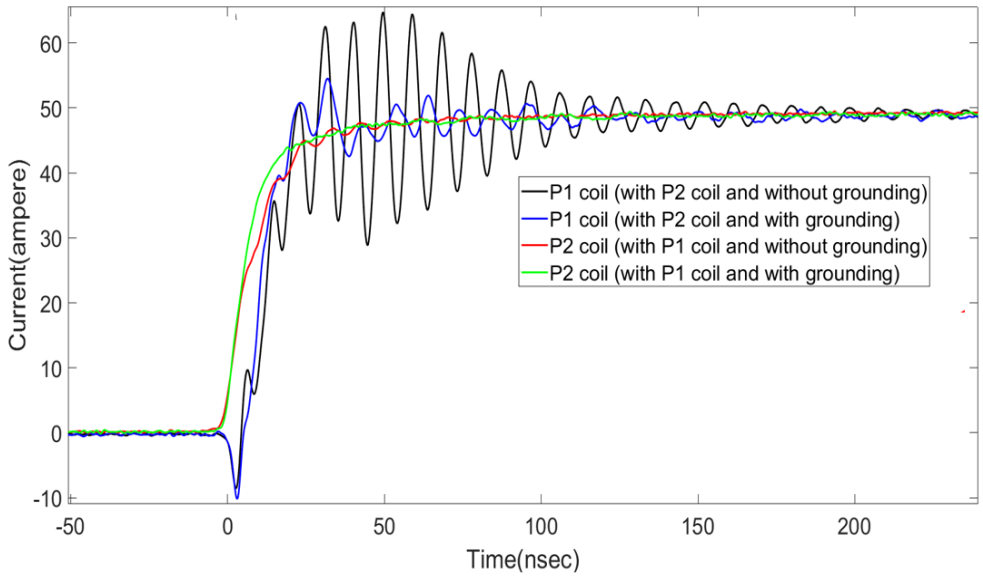

Figure 34 The rising edge of current steps measured with the *P1* and the *P2* coil. Oscillations are reduced with grounding connection.

B. Coaxial assembly of the sensors and components

In the initial tests performed without taking much care of coaxial connection, oscillations were observed in the rising edge of the measured current steps that appeared to be the main cause of increased rise times. By making the coaxial assembly for sensors and other components in the measurement step, these oscillations were reduced. In later test sessions, coaxial cage structures were made in the workshop Labo at VTT Mikes. Figure 35 shows the cage-like structures with sensor *S3* placed coaxially in larger cage and the *P2* coil in small cage. Inductive loops always exist in non-coaxial connections which directly effects the rise time of the current step as per equation 11. The cage structures made for placing current sensors provided coaxial connection to the various current measuring sensors and the other circuit components, such as the spark gap assembly.

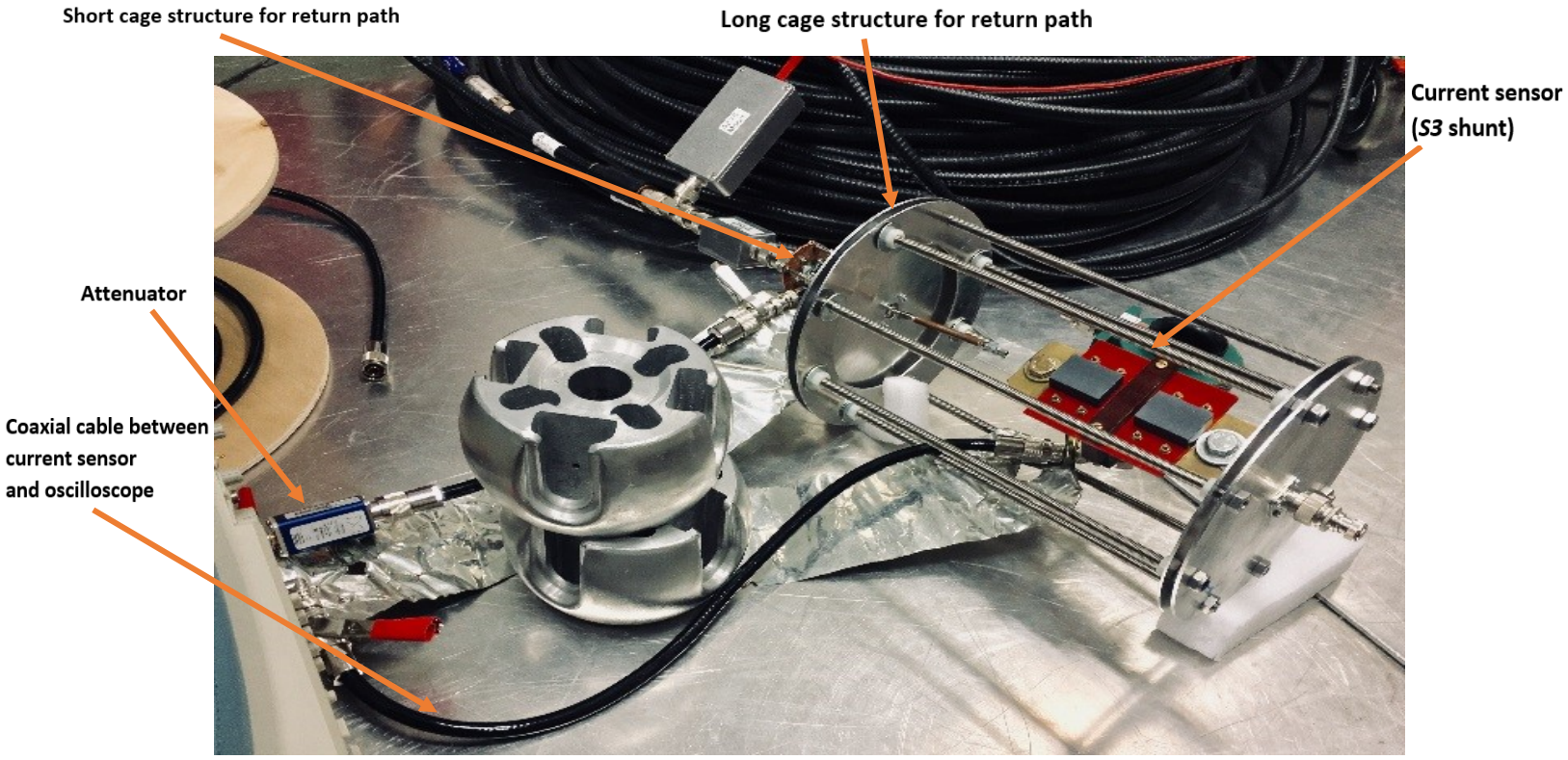

Figure 35 The cage-like structure providing coaxial connection to the *S3* shunt placed inside. The *P2* coil is placed in small cage-like structure to the left of the larger cage structure. Short coaxial cables from sensor to oscilloscope are used to avoid inductive loop and achieve coaxial connection.

In addition to provide the coaxial assembly for sensors, these structures also provide the return path for the traveling current wave without forming an inductive loop. Figure 36(a) shows the step measurement of the *P1* coil measured with and without a coaxial connection. Oscillations in the rising edge were reduced when the *P1* coil was placed coaxially in the cage structure of Figure 35, replacing the *S3* shunt. Similarly, Figure 36(b) shows an improved rising edge, when the inductive loop was avoided by using N-connector to provide coaxial connection for the *S1* shunt. Steeper rising edge with reduced rise time was therefore obtained for the current step.

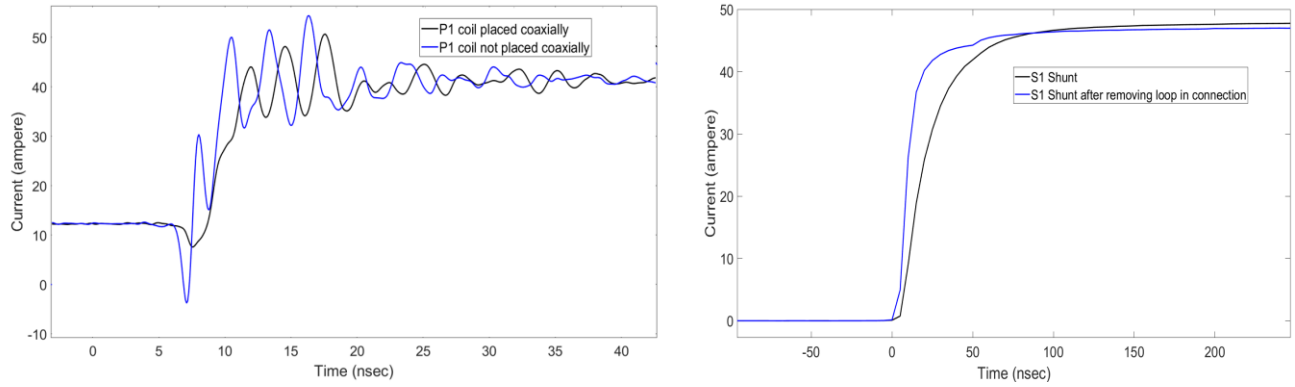

Figure 36 (a) Reduced oscillations in rising edge of the *P1* coil when placed coaxially. (b) Current step showing steeper rise after removing inductive loop in the *S1* shunt connection using the N-connector.

C. Reflections and impedance mismatch

The oscillations observed in the rising edge of the current step were mostly removed by proper grounding and coaxial connections; however, there were still some reflections within the rising edge of measured step. To examine the cause of these reflections, sensors using attenuators were used with attenuators of different scale factors, but same results were obtained. Later, circuit simulations were performed in the Castle transmission line simulator to understand the cause of reflections within the rising edge of current step. The simulation results showed that impedance mismatch of various circuit components caused these reflections. Figure 37 shows simulation results for the coaxial cage structures with different impedances made for the coaxial assembly of sensors.

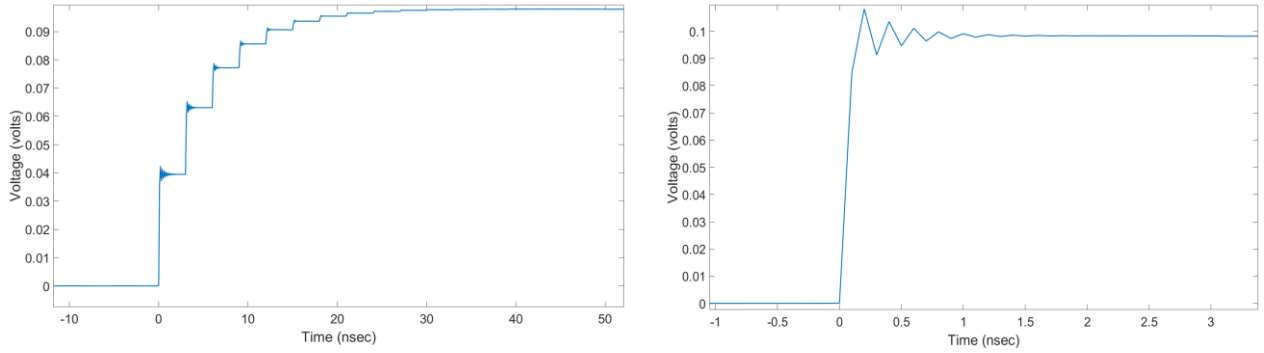

(a) **(b)**

Figure 37 Simulation results for coaxial cage structures of different impedances made for placing sensors coaxially, explaining impedance difference between cage structure and other components of the measurement circuit; (a) Impedance of 200 Ω, (b) Impedance of 60 Ω, showing improvement in rising edge of the current step and reduction in reflections due to impedance match as the rest of the circuit components had the impedance of 50 Ω.

As the type of connection and grounding affected the steepness of measured current step and therefore the rise time, these reflections caused by impedance difference were also one of the main cause of increased rise times. Reflections in the rising edge of current step were reduced when the impedance of the coaxial cage structure used for current sensors was made approximately 50 Ω, due to impedance match as rest of the components of the current measuring circuit had an impedance of 50 Ω. It was observed that the oscillations in the rising edge of the current step were caused by the inductance and the inductive loops of measurement circuit, while the reflections in the rising edge of current step measured were due to impedance mismatch. Figure 38 shows the coaxial structure with reduced length as compared to Figure 35 for placing the *P1* Rogowski coil. The length of the cage-structure with the *P1* coil was decreased from 28 cm to 12 cm for reducing the impedance to match 50 Ω. The *P2* coil with possibly reduced length of coaxial cage structure and the impedance approximately 50 Ω can also be seen in Figure 38. Figure 39(a) shows further modification made to the coaxial structure of the *P2* coil for impedance match. With this modification, rise time measured with the *P2* coil was further reduced from 2.02 ns to 1.64 ns. Figure 39(b) shows results measured with the *P1* coil having different lengths of coaxial structure. Due to improvement in the impedance match, reflections in the rising edge as per simulation results were reduced while using the coaxial structure of shorter length.

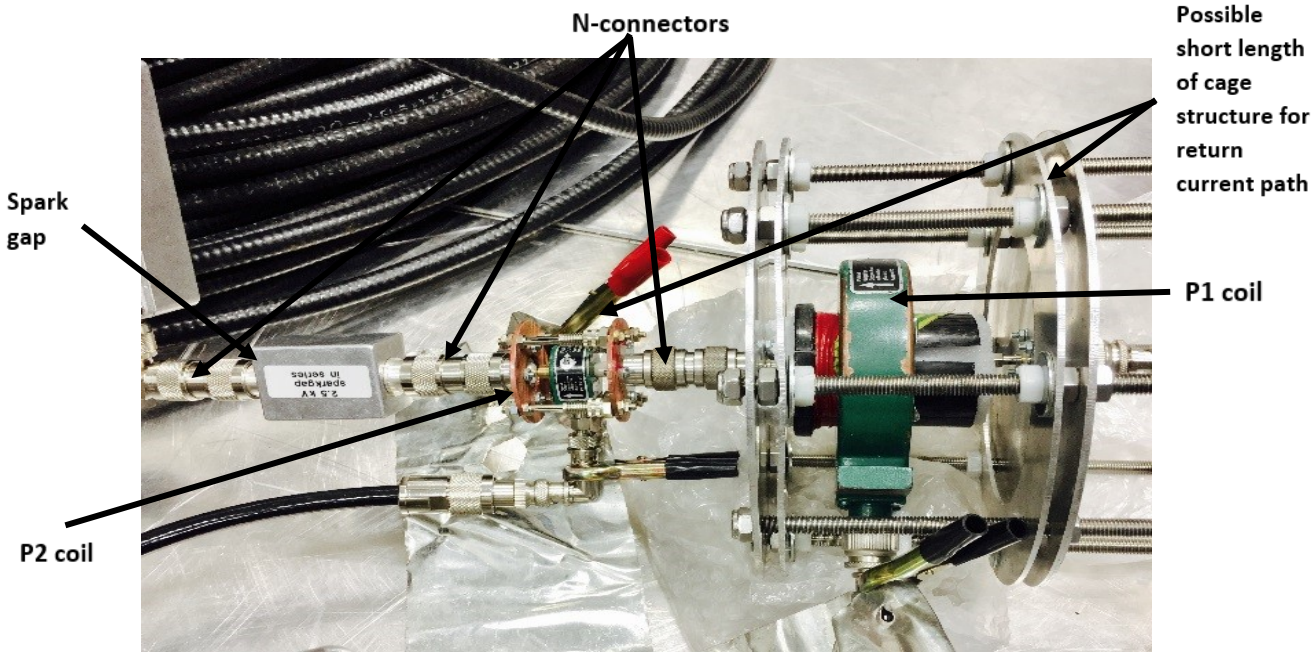

Figure 38 The short length of coaxial structures possibly made for return current path and placing the *P1* and the *P2* coil sensors. N-connectors are grounded.

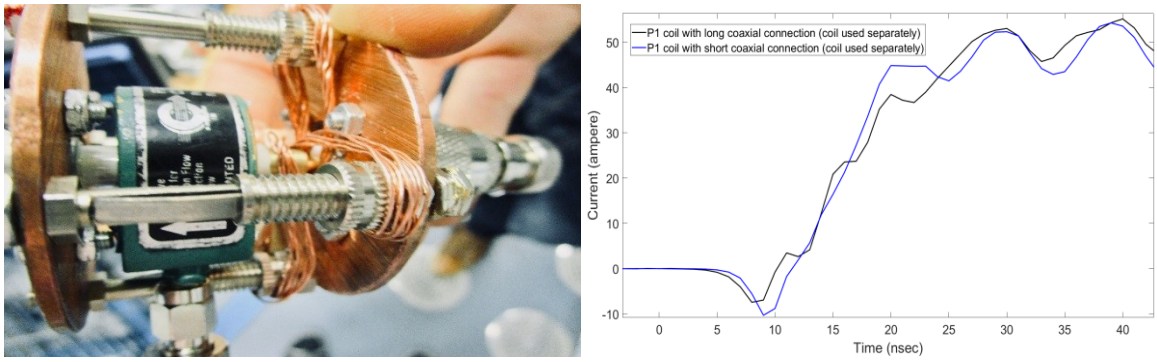

(a) (b)

Figure 39 (a) New arrangement for the *P2* coil made by further reducing the return path with copper wire to get reduced impedance difference, an improvement in rise time from 2.02 ns to 1.64 ns was achieved with this modification. (b) The rising edge of current step measured with coil *P1* by varying the length of the coaxial structure used as return path for the current. The black solid trace represents measurement with a 28-cm long cage length while the blue solid trace represents improvement in the rising edge of current step with short cage length of 12 cm.

Another main cause of the reflection within the rising edge of current step measured with the Rogowski coil in the coil-shunt combination was that the shunt can only be placed at the end of the current step measuring circuit due to common mode grounding problems as shown in Figure 35 and Figure 50. The wave of current step reflects at the shunt end making reflection in the rising edge of current step measured with the Rogowski coil. This reflection in the rising edge of the current step measured with the coil is due to a small distance between the shunt end and the coil. Consequently, the rise time of the current step measured with coil also increases. Figure 40 shows the rising edge of the current step measured with the *SH* shunt and coil *P2* used together. Voltage waveforms were recorded with the oscilloscope and the SF_6 spark gap was used as a switch. The coil *P2* had a rise time of just 1.64 ns when used separately for current step measurement. Because of the reflection in the rising edge caused by impedance mismatch, the rise time of this coil was increased to 5.8 ns when used together with the *SH* shunt.

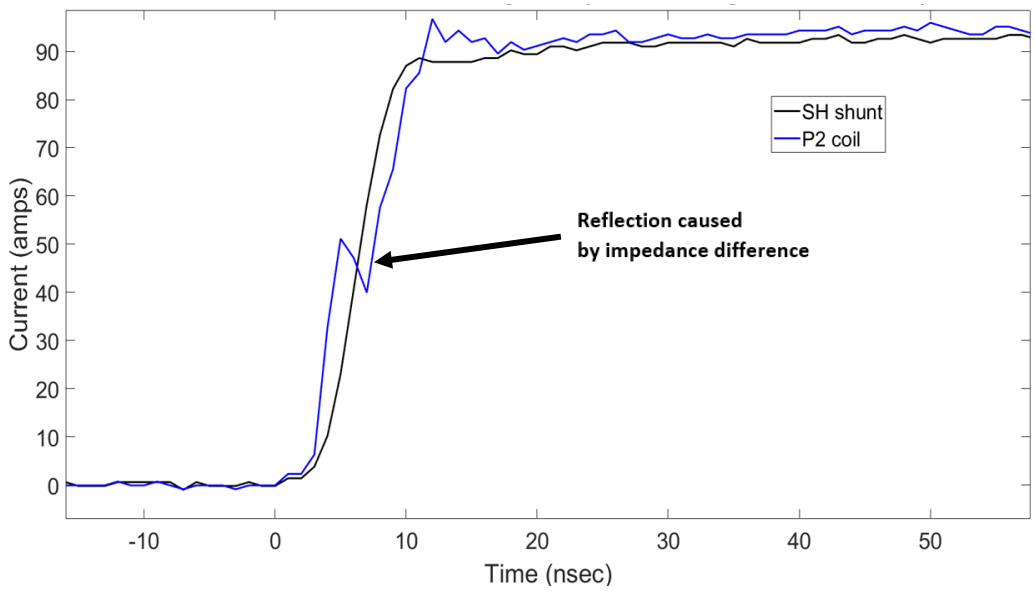

Figure 40 Reflection in rising edge of current step measured with the *P2* coil when used together with the *SH* shunt in the same measurement circuit. The SF_6 spark gap was used in step generator. The rise time of the *P2* coil was increased from 1.64 ns to 5.8 ns due to reflection in rising edge of current step when used with *SH* shunt caused by the impedance mismatch.

D. Arc length of the spark gap electrodes

Figure 41 shows the rising-edges of the current steps measured and their respective rise times.

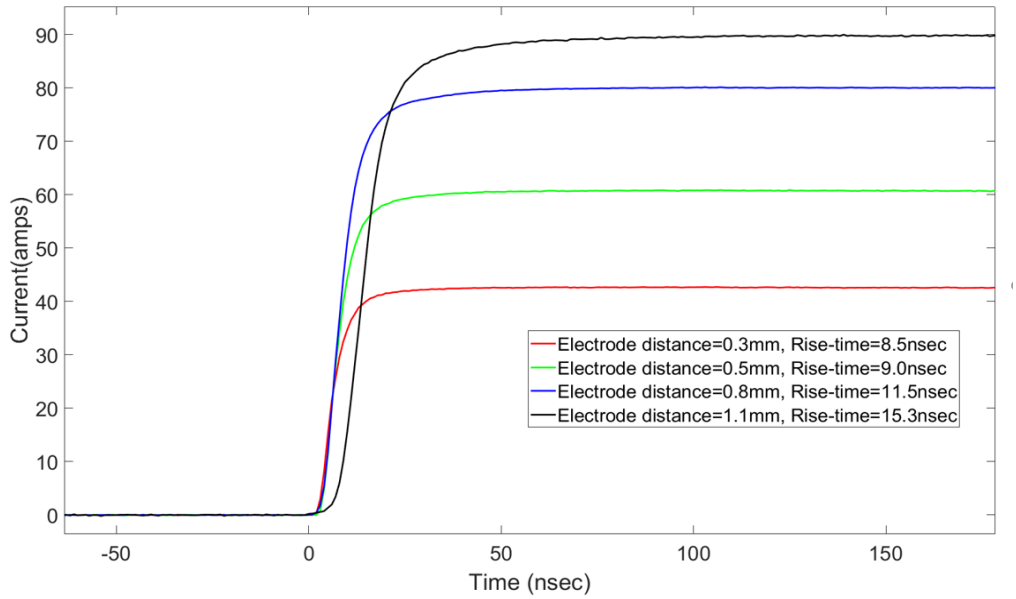

Figure 41 Effect of arc length of the spark gap electrodes on the rise time. Rise times of 8.5, 9.0, 11.5 & 15.3 ns were obtained with 0.3,0.5,0.8 & 1.1 mm spark gap electrode distances, respectively. The generation circuit used air spark gap while the *SH* shunt was used for step measurement.

The electrode gap of spark gap with air as a medium was precisely adjusted from 0.3 to 1.1 mm and the rise time was calculated for each current step. Only the *SH* shunt was used for this purpose. The peak value of the current

step was increased with increase in the spark gap electrode length. With the hypothesis made during this thesis work that the arc length of the spark gap affects the rise time of the current step, this test session was performed with spark gap having air as a medium. It was verified practically that the arc length affects the rise time such that the rise time increases in response to increasing arc length. The rise time increased from approximately 8 ns at 40 A to approximately 15 ns at 90 A, while the slew rate remained constant.

E. Gas pressure of the spark gap medium

In order to reach the faster rise times, the gap length of spark gap electrodes was reduced to 0.1 mm, and the insulation gas was changed to SF_6. The spark over voltage was controlled by changing the pressure inside the gap assembly keeping the spark gap electrode length constant to get the full use of the higher dielectric constant of the SF_6 gas. Tests were performed, and the results were analyzed to see the effect of gas pressure on the rise time of measured current step. It was observed that the increase in pressure reduced the rise time to some extent as shown in Figure 42. The breakdown level of the spark gap increases with increasing pressure and it results in higher value of current step generated. A rise time in the range of 3 to 4 ns was recorded with SF_6 spark gap having an electrode length of 0.1 mm and the SF_6 gas pressure of 2-atm w.r.t vacuum. Note that only 1 acquisition was used in this test rather than several acquisitions, which is explained by some oscillations in the step.

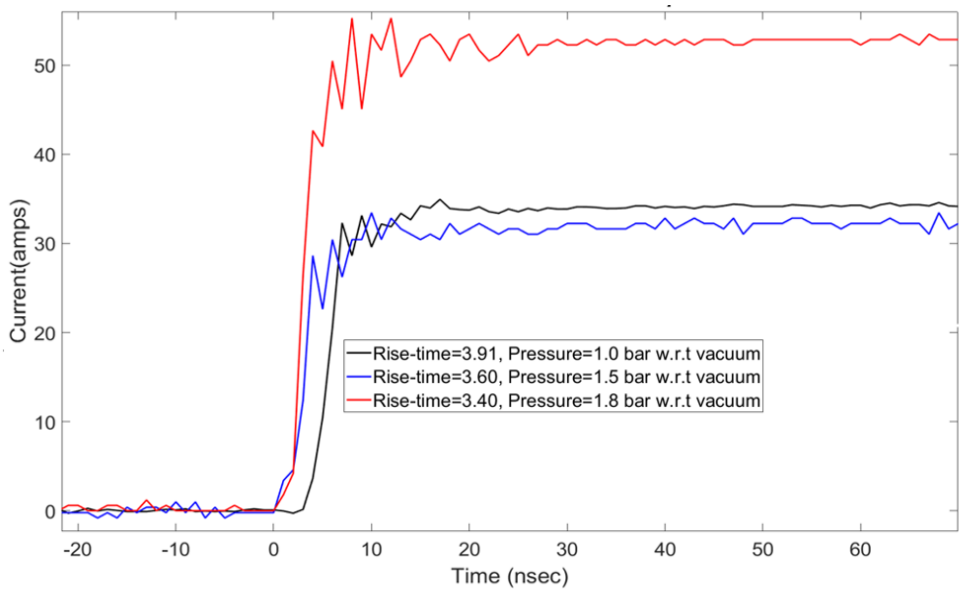

Figure 42 Effect of the SF_6 gas pressure in spark gap on the measured rise time. Rise times of 3.9 ns, 3.6 ns, 3.4 ns were obtained using the *SH* shunt with 1bar, 1.5 bar and 1.8 bar respectively gas pressures with respect to vacuum.

F. Effect of the sensor's nominal values on measured current step

Coil *P1* was used in few test sessions to measure the current steps of different rise times generated by various spark gaps. These steps recorded with the *P1* coil always had oscillations at the peak of the current step which were further increased when current steps with lower rise times were measured. Rising edge of current step measured with the *P1* coil can be seen in Figure 32, Figure 34 and Figure 36. As per data sheet of the *P1* coil shown in Appendix A, this coil was suitable for the measuring peak currents up to 10 kA, but it had a nominal rise time of 20 ns. Current steps generated in this project had the rise times lower than 20 ns and therefore, the *P1* coil was not the optimal sensor to be used for such lower rise time measurement due to its higher nominal rise

time and oscillations at the peak of the rising edge. It was also observed that sensors with a higher nominal rise time increased the measured rise time for the sensor used in the same measurement circuit. For example, Figure 43 shows increase in the measured rise time of the *SH* shunt from 4.8 ns to 11 ns when the *P1* coil with nominal rise time of 20 ns was used in the same circuit. Comparison of current steps and the rising edge for the *P1* coil sensor with the *S1* shunt using Digitizer of *National instruments* is shown Appendix C.

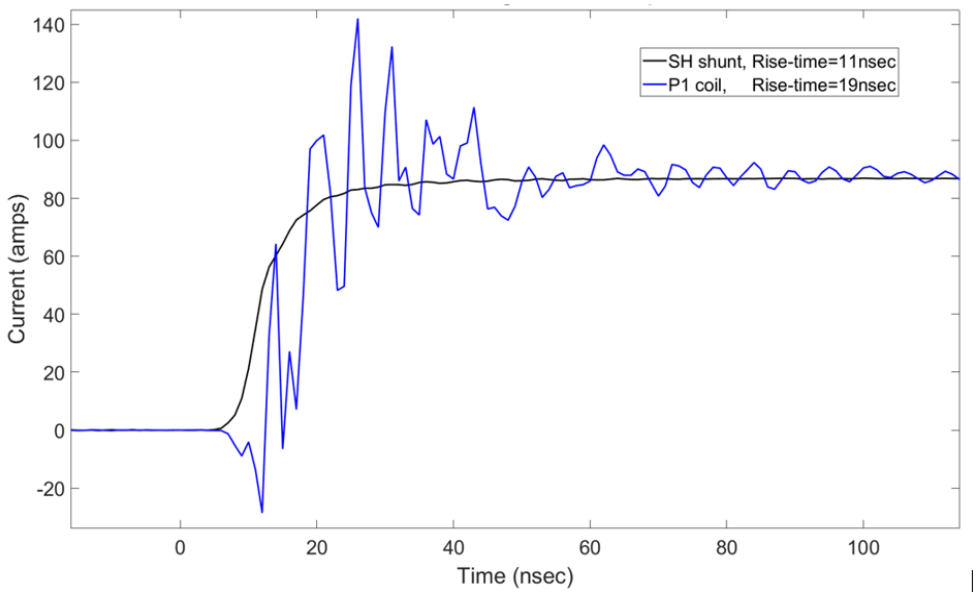

Figure 43 Rising edge of the current step measured with the *P1* coil and the *SH* shunt used together in same measurement circuit. The *P1* coil measured the rise time of approximately 19 ns which has a nominal rise time of 20 ns. Rise time measured with the *SH* shunt was increased to 11 ns which measured rise time of only 4.8 ns when this shunt was used in combination with the *P2* coil sensor instead of *P1* coil.

4.3 Measurement of rise time

Current steps were generated with spark gaps of different media and their rise times were measured. An overview of the measured rise times with different spark gaps and sensors is shown in Figure 44. The sensors and oscilloscopes mentioned in Table 3 and Table 4 were used for the measurements, but the results shown are in most cases not limited by the characteristics of the measurement system. The peak current of the current step was varied by adjusting the spark gap electrodes of different spark gap media. It was found that the rise time is affected by the peak current value and the medium used in the spark gap, with SF_6 giving the best results.

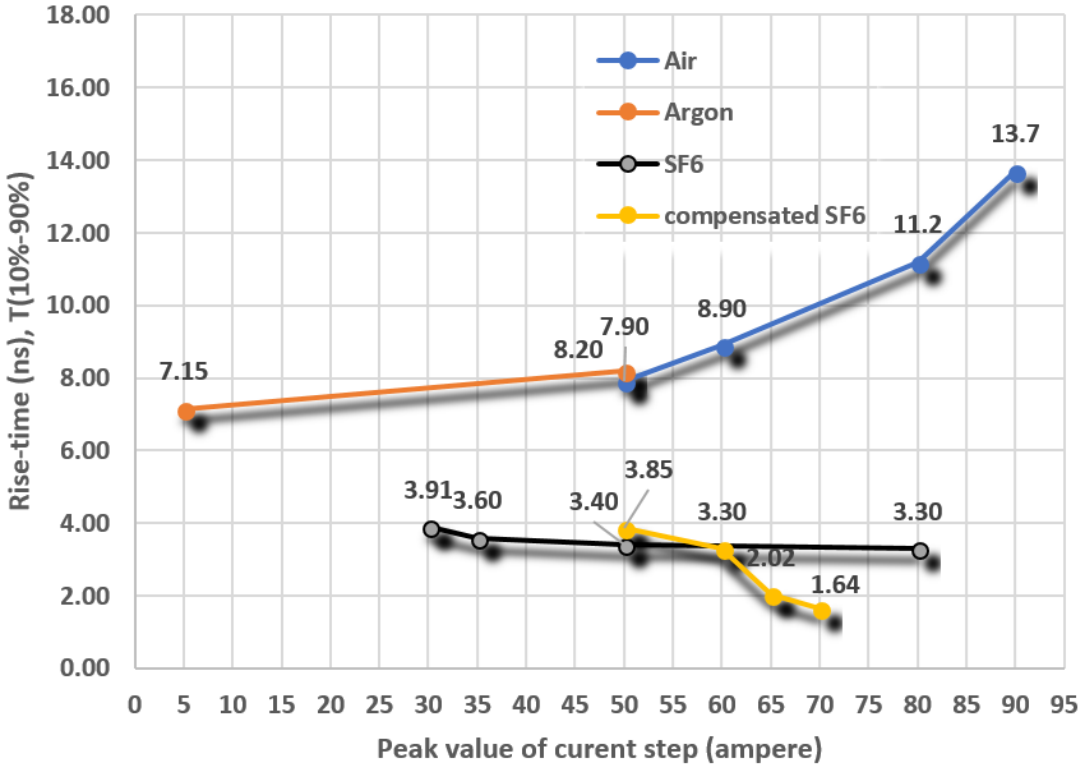

Figure 44 Relation of the rise time and step current values with various spark gaps used.

Effort was taken to keep the circuit as compact as possible and match the circuit to the 50 Ω impedance of coaxial cable as much as possible. To achieve this, modification was made to the spark gap based on 50 Ω N-connectors shown in Figure 15(b). An additional cover was made to provide coaxial return path for the current. Figure 45 shows pictures of the compensated SF_6 spark gap modified from the SF_6 spark gap shown in Figure 15(b), section 2.4.2. The modification to a compensated low inductance design followed the discussion as explained in section 2.4.1.This compensated design not only further improved the rise time for sensors, but also reduced the interferences that were caused by the spark gap. This test session with compensated spark gap was performed with the LeCroy oscilloscope which had a bandwidth of 600 MHz and a sampling rate of 10 GS/s. Much lower rise times were achieved with this design.

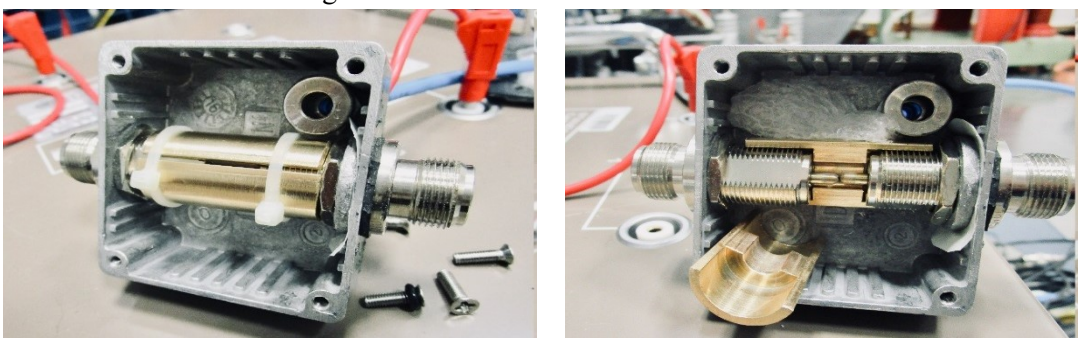

Figure 45 The compensated SF_6 spark gap made at VTT Mikes HV Laboratory. Modifications made by placing taper structure using brass plates to the SF_6 spark gap of Figure 15(b) making it the low inductance compensated spark gap design.

The rise time was calculated from the data recorded with computer software for oscilloscopes available in the High Voltage Laboratory at VTT Mikes. The difference between the time at which the magnitude of the current

step was 10% and 90% of the peak current step was carefully calculated for the rise time measurement. Peak current was considered at the most stable peak current level of the step. In this project, total step length of approximately 960 ns was generated and measured. The current step was most stable for the time epoch from 750 ns to 900 ns, which was used for peak current measurements. As an example, Figure 46(a) shows the smooth and clear current step measured with the *P2* coil only using the compensated SF_6 spark gap, while Figure 46(b) explains the procedure followed for measuring the rise time of the *P2* coil sensor. Table 7 shows the rise times measured by current sensors for the current steps of different peak values using various spark gaps. The spark gaps used as a switch were changed to achieve better results for the rise times in various test sessions. The sensors which were suitable for particular spark gap resulting in lower rise times were considered in each test session.

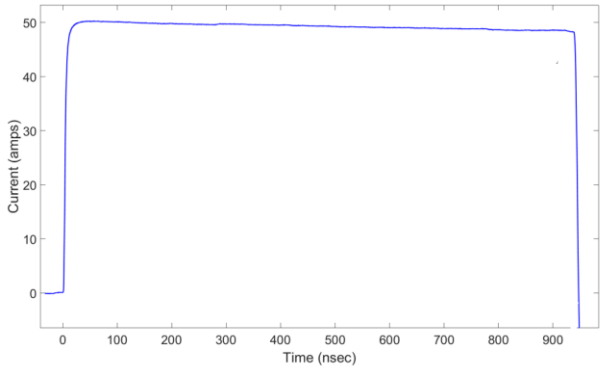

(a)

Step measurement type	= 50 acquisitions
Pressure	= 2 bars w.r.t vacuum
Spark gap length	= 0.1 mm
Current peak value at 750-900 ns step region	= 62.6 A
90% of peak current	= 56.3A
Time at 90% of peak current	= 1.8 ns
10% of peak current	= 6.2 A
Time at 10% of peak current	= 0.15 ns
Rise-Time	**= 1.64 ns**

(b)

Figure 46 (a) Current step measured with the *P2* coil only, using compensated SF_6 spark gap with SF_6 gas pressure = 2 bar w.r.t vacuum, (b) The calculation of rise time measured with the *P2* coil using the *LeCroy* oscilloscope with sampling rate of 10 GS/s.

Table 7 Rise times measured with different sensors and spark gaps in various test sessions.

Spark gap and spark gap medium		**Air**									
Amplitude of current step		**5A**	**30A**	**35A**	**50A**	**60A**	**65A**	**70A**	**80A**	**90-100A**	**Nominal rise time of sensor**
Sensor used and measured rise time (ns)	***P2***	-	-	-	7.90	8.90	-	-	11.2	13.7	2.0
	SH	-	-	-	8.50	9.0	-	-	11.5	15.3	1.8
Spark gap and spark gap medium		**Argon**									
Amplitude of current step		**5A**	**30A**	**35A**	**50A**	**60A**	**65A**	**70A**	**80A**	**90-100A**	**Nominal rise time of sensor**
Sensor used and measured rise time (ns)	***P1***	17.0	-	-	14.5	-	-	-	-	-	20
	S2	7.15	-	-	8.20	-	-	-	-	-	1
	S3	32.1	-	-	34.7	-	-	-	-	-	0.45
	SH	18.5	-	-	23.5	-	-	-	-	-	1.8
Spark gap and spark gap medium		**SF_6**									
Amplitude of current step		**5A**	**30A**	**35A**	**50A**	**60A**	**65A**	**70A**	**80A**	**90-100A**	**Nominal rise time of sensor**
Sensor used and measured rise time (ns)	***P1***	-	-	-	23.0	-	-	-		19.0	20
	P2	-	3.91	3.60	3.40	-	-	-	3.30	-	2
	S1	-	5.80	5.60	4.70	-	-	-	3.14	-	1
	SH	-	-	11.0	5.90	5.80	-	-	4.8	-	1.8
Spark gap and spark gap medium		**SF_6 (Compensated)**									
Amplitude of current step		**5A**	**30A**	**35A**	**50A**	**60A**	**65A**	**70A**	**80A**	**90-100A**	**Nominal rise time of sensor**
Sensor used and measured rise time (ns)	***P2***	-	-	-	3.85	3.30	2.02	1.64	-	-	2
	SH	-	-	-	-	-	6.34	5.95	4.95	-	1.8

4.4 Interference test

Figure 47 shows the rising edge of a current step measured with the *SH* and the *S1* shunts used separately. A rise time of 5.9 ns was recorded with the *SH* shunt and 3.1 ns with *S1* shunt. The current steps with rise times lower than 5 ns were more prone to interferences, as in case of the *S1* shunt (Figure 47(b)), due to a fast switching phenomenon of the SF_6 spark gap. Therefore, two types of the interference tests were performed, one with open connection to the *P2* coil used for current step measurement, and other with short-circuit to the return path of the *P2* coil. Figure 48 shows the waveforms for interference tests performed when the SF_6 gas was used as spark gap medium for generating current step. It was observed that there was some interference. An interference of 40 mA was recorded in the case of open circuit test, and 20 mA was recorded in the case of the short circuit test.

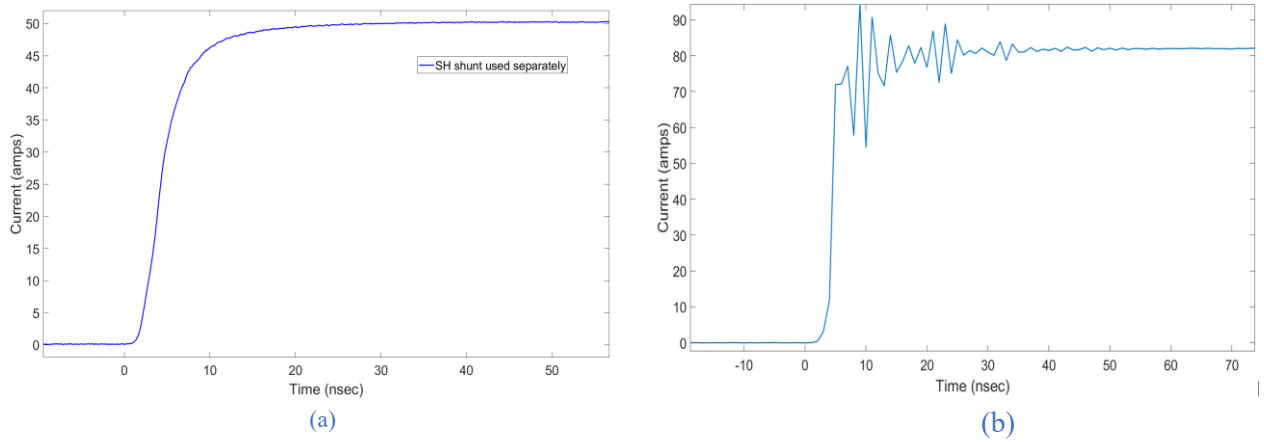

Figure 47 (a) The rising edge of current step measured with the *SH* shunt, Rise time = 5.9 ns, SF_6 gas pressure = 2 bar w.r.t vacuum ,spark gap length=0.1mm, (b) The rising edge of current step measured with the *S1* shunt, Rise time = 3.1 ns, SF_6 gas pressure = 1.8 bar w.r.t vacuum ,spark gap length=0.1mm.

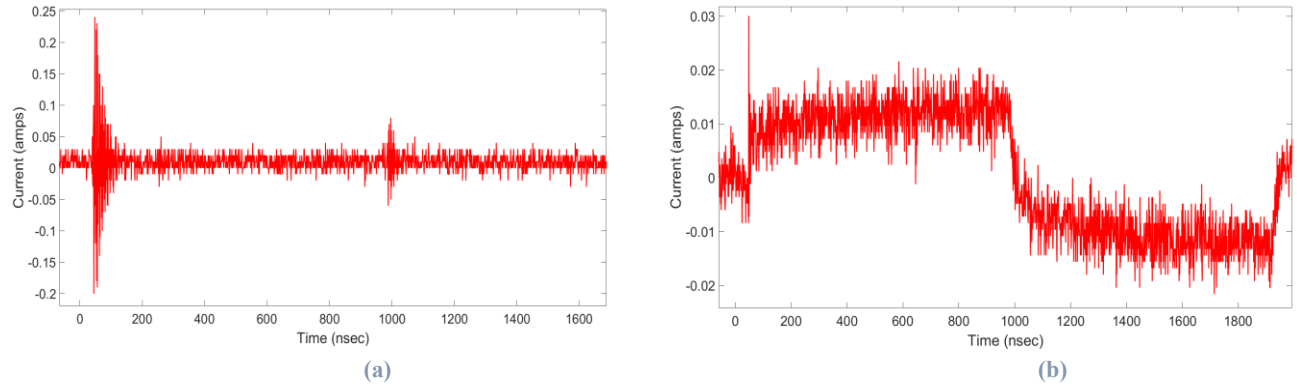

Figure 48 Interference test with a magnitude of 40 mA using the SF_6 spark gap, (a) Interference test with open connection to coil, (b) Interference test with the short circuit to return path of the coil.

An interference test was conducted again when the compensated SF_6 spark gap shown in Figure 45 was used in step generation circuit. Figure 49 shows the interference tests performed with the compensated spark gap. In this case, much lower interference of just 5 mA was observed compared to the interference test shown in Figure 48 due to taper-modification used on the electrodes of spark gap (Figure 45).

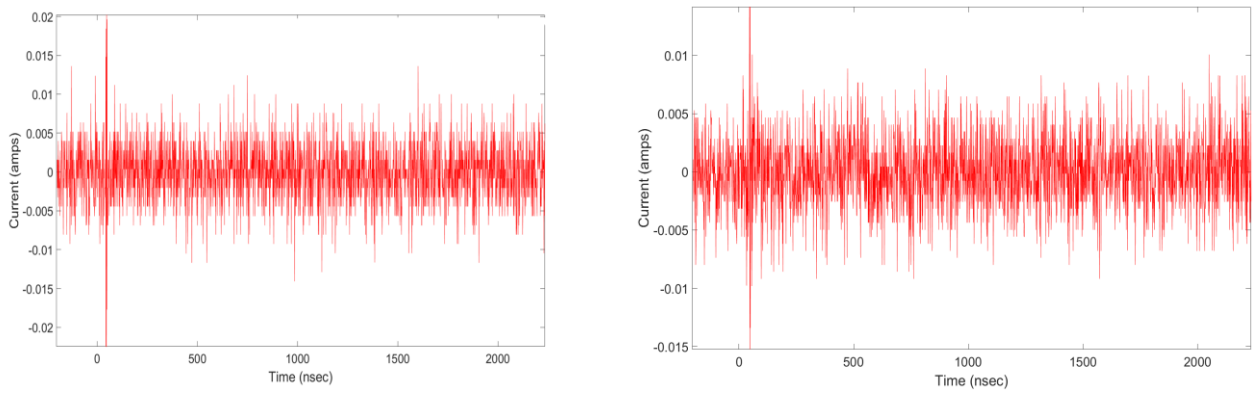

Figure 49 Interference test with magnitude of 5 mA using compensated SF_6 spark gap (a) Interference test with open connection to *P2* coil, (b) Interference test with ends of *P2* coil grounded.

4.5 Reference calibration circuit for current steps

Figure 50 shows the best current step measuring circuit achieved which had the with lowest oscillations and interference. The small length of coaxial cables from sensors to the oscilloscope were used, components were placed coaxially, smallest possible length of the cage structure was used to achieve impedance match having the impedance approximately 50 Ω, and the SF_6 spark gap was used which made this combination as the best reference current step measuring circuit used for the calibration of resistive shunts. This circuit measured a rise times of less than 5 ns using the compensated SF_6 spark gap.

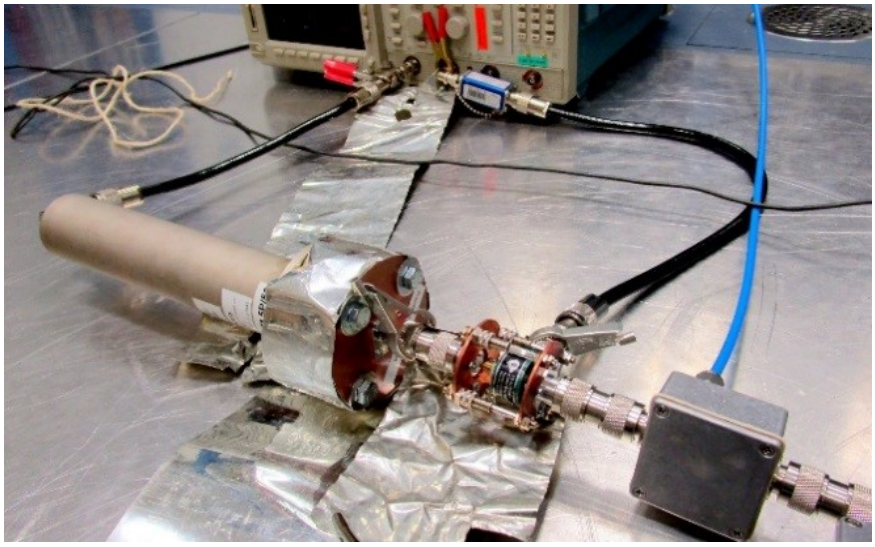

Figure 50 Reference calibration circuit showing the *SH* shunt and the *P2* coil used together in the same measurement circuit as an example. N-connectors between the two sensors are used to achieve possible small distance between them, avoiding reflection in the rising edge of current step measured with the *P2* coil caused by impedance difference.

4.6 Summary

Practical measurement setup of current steps was presented in this chapter. Current step measurement procedure, factors affecting current step measurement, measurement of rise time, and interference tests performed are

presented here. Finally, a reference calibration circuit achieved during current step measurement was presented which is used for step calibration of sensor in Chapter 5.

Chapter 5

Calibration of sensors

In Chapter 4, a reference calibration circuit to use with various current sensors was proposed in order to measure the current step. The measurement results using the reference calibration circuit were recorded for the calibration of the current sensors. This chapter extends the results for current step measurement by describing the methods used to calibrate the current sensors and presenting step calibration results. Section 5.1 describes DC calibration of the shunts. Sections 5.2 and 5.3 explain the step calibration and the transient behaviour of different current step measuring sensors. Section 5.4 describes the transient behaviour of few current sensors using low inductance compensated SF_6 spark gap in the generation circuit. Section 5.5 summarizes the calibration done for the sensors.

5.1 DC Calibration of shunts

The shunts were calibrated in DC mode with the Agilent 3458A digital multimeter using the four-wire measurement. The results are presented in Table 8. The uncertainties with a 50 Ω input impedance have been estimated based on the previous uncertainty analysis made with 1 MΩ input impedance in the High Voltage Laboratory at VTT Mikes.

Table 8 DC calibration of the shunts used in this project with expanded uncertainties (k = 2).

Shunt	Attenuator used	Nominal value with attenuator	DC calibration (including 50 Ω impedance at oscilloscope input)
S1	5.8 : 1	0.0862 Ω	(0.083701 ± 0.000003) Ω
S2	-	0.1 Ω	(0.097702 ± 0.000002) Ω
S3	-	0.01 Ω	(0.010180 ± 0.000001) Ω
SH	-	0.05 Ω	(0.049331 ± 0.000002) Ω

5.2 Step calibration of shunts

Step calibration of the sensors was carried out by using data obtained from the current step measurement. The current measuring sensors were calibrated by simultaneously measuring current step with a coil-shunt combination and then comparing the two against each other. For the coil-shunt combination, one shunt at a time was used with the coil in each test session. Shunt responses were compared using this coil-shunt combination. One of the shunts, *S1*, was used as a reference, and the rest of the shunts were compared with the known responsivity of the *S1* shunt. Coil sensor *P2* was calibrated using the DC calibrated value of shunt *S1* as a reference. Other shunts were then compared with the *P2* coil. Results were analyzed for their relative error and uncertainty. Waveforms were recorded for calibration using an oscilloscope, or a digitizer. Those waveforms were used for further analysis of transient behavior. The sensor was connected to an oscilloscope, and the oscilloscope was connected to a computer through a fiber optic cable for recording the data in digital form. The *P1* coil was also tested; however, it could not be used for calibration because of its higher nominal rise time and consequent oscillations at the peak of its current step's rising edge.

While evaluating the recorded data, the offset was removed for the zero and unity levels. The zero level was calculated by taking an average of all data before 0 ns and then subtracting this average value from the measured data. For the peak value (unity level) of the current step, the average value of the data for the time epoch from 750ns to 900ns was used, as the current step was most stable in that region. The shunts *S2* and *S3* required more than 960 ns of current step length for stable current step measurement, as explained by their transient behavior in Section 5.3. This is because that the maximum current step length generated was approximately 960 ns using the available coaxial cable in this work. Based on relative error, uncertainty, settling of curves and waveform obtained, the *S1* shunt showed much better performance than the other shunts. Therefore, the *S1* shunt was selected as the reference shunt for current step generation. This shunt measured stable current after approximately 150 ns of step length with a peak current up to 100 A and a rise time of less than 5 ns. In the calibration process, the sensitivity of coil *P2* was first calculated using reference shunt *S1* as

$$Sensitivity\ of\ Coil\ (S) = \frac{V(coil) \times Sensitivity\ of\ reference\ shunt}{V\ (reference\ shunt)}. \tag{12}$$

This sensitivity of the coil was then used to calibrate the sensitivities of the other shunts used, one at a time, in the same measurement circuit with the *P2* coil as

$$Sensitivity\ of\ shunt = \frac{V(shunt) \times Sensitivity\ of\ Coil\ (S)}{V\ (coil)}\ . \tag{13}$$

Here, V is the voltage recorded by the oscilloscope. Table 9 describes the calibration results for one of the test sessions measured with various sensors using the National Instruments 150 MHz digitizer. An impedance of 50 Ω was used at the input of the oscilloscope for the readings in every test session.

Table 9 Results of step calibration. *P2* was first calibrated against *S1*, the rest of the shunts were then calibrated against *P2*. The uncertainty values are given as standard uncertainties with a coverage factor *k* = 2.

SENSORS	P2	S1	S2	S3	SH
Attenuator used	7.5166:1	5.8: 1	-	-	-
Nominal sensitivity (V/A)	0,0665	0,08621	0,1000	0,0100	0,0500
DC sensitivity (V/A)	--	(0.083701 ± 0.000003) Ω	(0.097702 ±0.000002) Ω	(0.010180 ± 0.000001) Ω	(0.049331 ± 0.000002) Ω
Step sensitivity (V/A)	0,065701 Ω	---	0,098722 ± 0.000008) Ω	0,010822 ± 0.000001) Ω	0,049501 ± 0.000004) Ω
Measured current based on nominal sensitivity (A)	45,3972	44,6259	45,9156	52,1837	48,2932
Measured current based on DC sensitivity (A)	45,3972	45,9624	46,9965	51,2610	48,9492
Current calculated with step sensitivity (A)	45,9624	45,9624	46,5894	48,2921	48,7268
Relative error from nominal sensitivity	-1,2 %	-0,03 %	-1,4 %	8,1 %	-0,9 %
Relative error from DC sensitivity	-0,7 %	0,0 %	1,0 %	6,3 %	0,3 %
Relative uncertainty of error (*k* = 2)	0.4 %	--	0.5 %	0.5 %	0.5 %

The relative error in the step sensitivity from the DC calibrated sensitivity is shown in Table 9. Except for shunt *S3*, the relative error was in the range of 1%. Additionally, the *S3* shunt measured a higher current step compared with the peak value of the current step measured for the same measurement circuit. For the *S3* shunt, the difference in the measured peak current was reduced after DC calibration of sensors, but it was still insufficient to be considered as a reference shunt with minimum uncertainty. Apart from the *S1* shunt, the *SH* and *S2* shunts were also used as a reference, with an uncertainty obtained for all the shunts being in the range of 0.7 %. As an example, Table 10 explains the procedure for calculating the expended uncertainty for the data of Table 9.

Table 10 Example uncertainty budget for step calibration of shunts using the oscilloscope from National Instruments. Components are given as relative uncertainties in percentage.

Sources of uncertainty (*k*=1)	P2	S2	S3	SH
Uncertainty of NI oscilloscope (%)	0.19	0.19	0.19	0.19
Uncertainty of reference shunt S1 (%)	0.001	0.001	0.001	0.001
Standard deviation of mean for peak level or unity level of current step measured with sensor	0.10	0.099	0.13	0.10
Standard deviation of mean for zero level of current step measured with sensor	0.007	0.003	0.009	0.009
Combined standard uncertainty	0.30	0.29	0.33	0.30
Expanded uncertainty (*k*=2)	0.43	0.47	0.52	0.56

In Table 10, the uncertainty of the oscilloscope was obtained from the calibration certificate by VTT Mikes in July 2016. DC calibration values were used as the uncertainty value for the reference shunt *S1*. Standard deviation of mean was calculated for the unity and zero levels of the current step measured with each sensor. This standard deviation of mean was calculated from the data obtained using computer software made for the oscilloscope. Expanded uncertainty was finally calculated according to [41] and Section 5.2 of IEC-62475 [11].

The sensors were calibrated using the same procedure as followed for the oscilloscope from *National Instruments* in Table 10. Step calibrations were repeated with the other two oscilloscopes: Tektronix, and LeCroy. The results and their uncertainties obtained using the three oscilloscopes are compared in Table 11.

The *S1* shunt **(0.083701 ± 0.000003) Ω** used as reference differed by 1.04% from the previous DC calibration certificate calibrated at VTT Mikes High Voltage Laboratory in 2015. This difference is in the acceptable range, as previous calibration was done with an impedance of 1 MΩ, while DC calibration for this project was done with 50 Ω.

Uncertainties were calculated with the *S1* shunt following the methods in [11], [41] and [47]. It should be noted that one major source of uncertainty in the step current measurements is the uncertainty of the oscilloscope. As shown in Table 11, an uncertainties of less than 0.5 % are obtained when ignoring the uncertainties of the oscilloscopes. It is worth mentioning that when the two sensors being compared uses the same oscilloscope and

range, it is possible to ignore the uncertainty of the oscilloscope in that specific measurement. Figure 51 to Figure 54 shows the relative errors and uncertainties (including the uncertainties of the oscilloscopes) for the calibration results of Table 11.

Table 11 Step calibration results with different oscilloscopes.

Oscilloscope used	Uncertainty of oscilloscope (*k*=2)	Sensor	Step responsivity	Difference from DC calibration	Relative Uncertainty (*k*=2)
NI 150MHz Digitizer	0,38 %	*P2*	0,066 Ω	0,1 %	0,4 %
		S2	0,097 Ω	0,1 %	0,5 %
		S3	0,011 Ω	9,2 %	0,5 %
		SH	0,049 Ω	1,2 %	0,5 %
Tektronix (Test session 1)	0,80 %	*P2*	0,066 Ω	-0,7 %	0,8 %
		S2	0,098 Ω	1,0 %	0,9 %
		S3	0,010 Ω	6,3 %	0,9 %
		SH	0,049 Ω	0,3 %	0,9 %
Tektronix (Test session 2)	0,80 %	*P2*	0,066 Ω	0,1 %	0,9 %
		SH	0,0497 Ω	0,7 %	1,0 %
LeCroy	1 %	*P2*	0,0668 Ω	0,6 %	1,0 %
		SH	0,0498 Ω	1,0 %	1,1 %

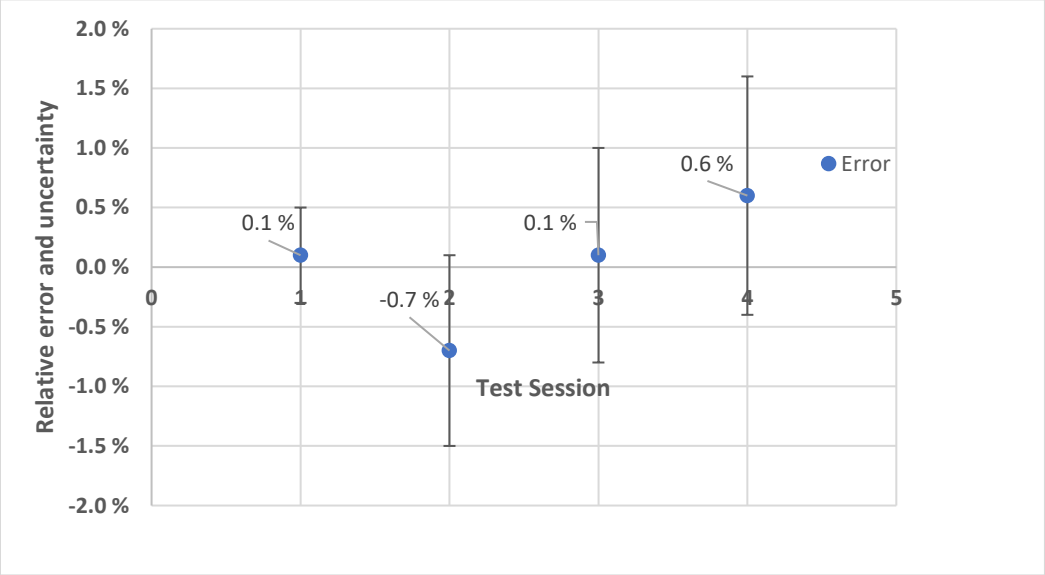

Figure 51 Relative error and uncertainty in different test sessions for coil *P2* used with 7.5166 : 1 attenuator, 50 Ω impedance match and having sensitivity of 1 V/A. Relative uncertainty also includes the uncertainty of the oscilloscope.

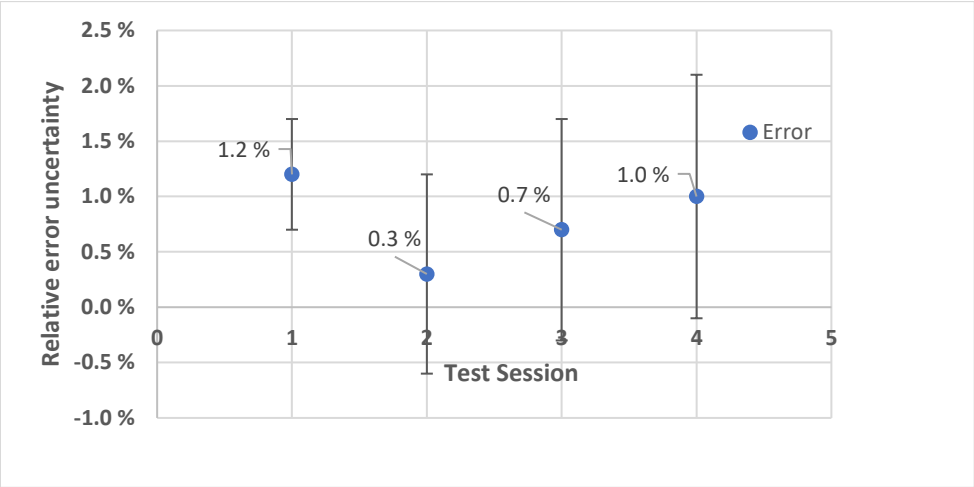

Figure 52 Relative error and uncertainty in different test sessions for the *SH* shunt having sensitivity of 0.04933 V/A. Relative uncertainty also includes the uncertainty of the oscilloscope.

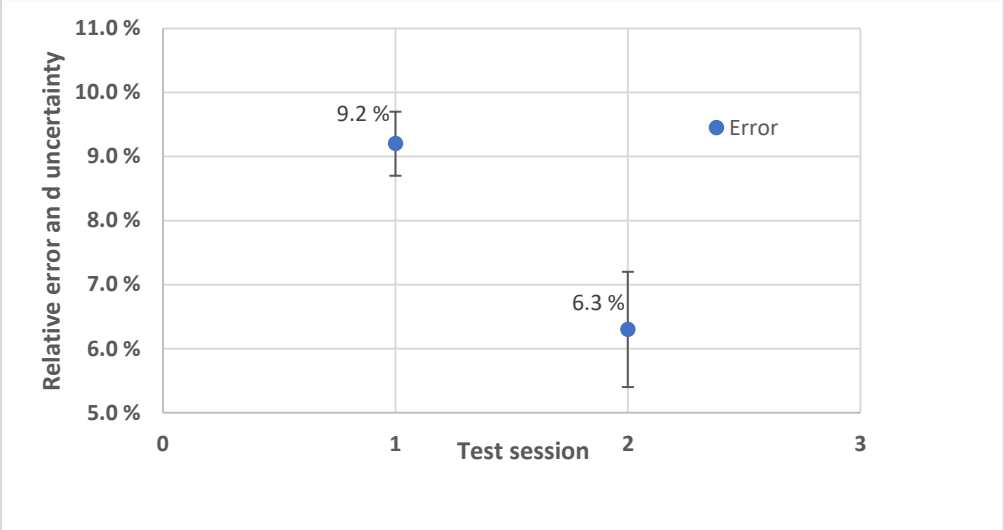

Figure 53 Relative error and uncertainty in different test sessions for the *S3* shunt having sensitivity of 0.01018 V/A. Relative uncertainty also includes the uncertainty of the oscilloscope.

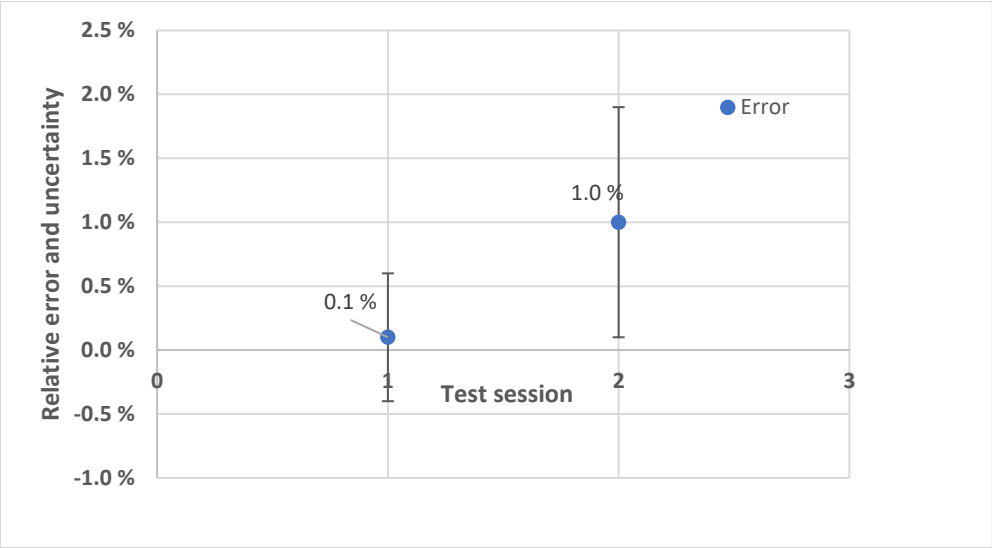

Figure 54 Relative error and uncertainty in different test sessions for the *S2* shunt having sensitivity of 0.09770 V/A. Relative uncertainty also includes the uncertainty of the oscilloscope.

5.3 Transient behavior of different sensors

The coaxial cable generator was capable of providing reasonably constant current. However, contrary to the voltage generated by a mercury-wetted based step voltage generator [34], the step did not settle due to imperfections and losses in the cable. Current steps were measured with all the shunts and coils using their calibrated sensitivities. Since the current level in the time epoch from 750 ns to 900 ns was considered the most stable region of the current step, the average value of current ratios in that region of the current step was considered as the reference line. The ratios of the currents measured with a coil-shunt combination of sensors were plotted after removing offsets to study their transient behavior. The reference line was used to study the settling of curves obtained with two sensors. The current step measured using each shunt in combination with the *P2* coil, as well as their waveform expressed in terms of current ratios are discussed below.

5.3.1 SH shunt and P2 coil

Figure 55(a) shows the current steps measured with the *SH* shunt and the *P2* coil used simultaneously in the measurement circuit. Scaling factors of 0.049501 and 15.0332 were used for the *SH* shunt and coil *P2,* respectively while plotting current step waveforms. The ratio of the two step responses is shown in Figure 55(b). From the figure, it is clear that curves for both sensors settle after 50 ns of current step and agree with each other within the measurement noise level. The reference line in Figure 55(b) indicates the ratio of currents in the stable current region for the time epoch from 750 ns to 900 ns of the current step recorded with the *SH* shunt and the *P2* coil sensors. The reference value of the reference line, 1.017, is not exactly 1 due to different scale factors used for current sensors. It should be noted that this reference line will be exactly 1 when comparing the reference shunt and calibrated shunt using its step calibration values.

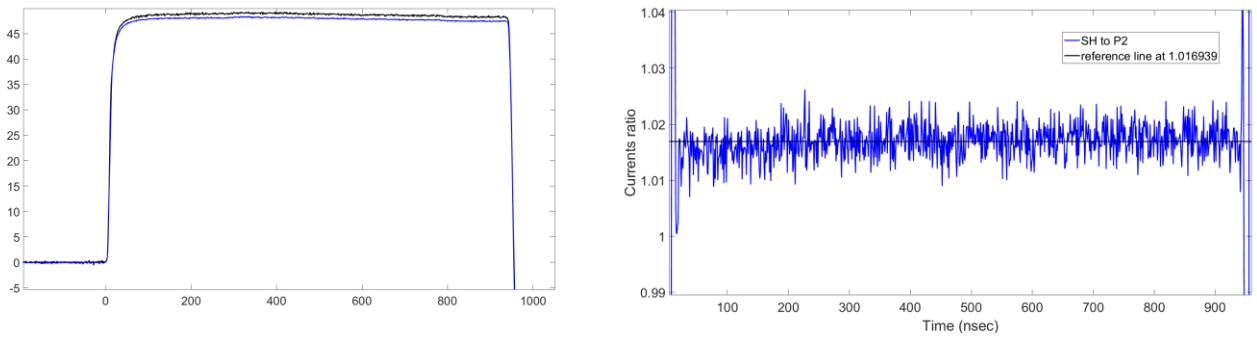

(a) (b)

Figure 55 a) Current step measured with the *SH* shunt (black trace) and the *P2* coil (blue trace) used together in the same measurement circuit. b) Ratio of current measured with the *SH* shunt and the *P2* coil (blue trace) along with the reference line (black line).

5.3.2 S1 shunt and P2 coil

A smooth current step was also obtained for the *S1* shunt and the *P2* coil as shown in Figure 56(a). It indicates that the current steps for the *P2* coil and the *S1* shunt used together were almost same in the shape. A scaling factor of 0.083701 was used for the *S1* shunt while 15.0332 was used for the *P2* coil. The current ratios agreed with measurement noise level after approximately 150 ns, shown in Figure 56(b). Again, the reference line as the ratio of currents measured deviates from 1 due to different scale factors used for plotting the current steps.

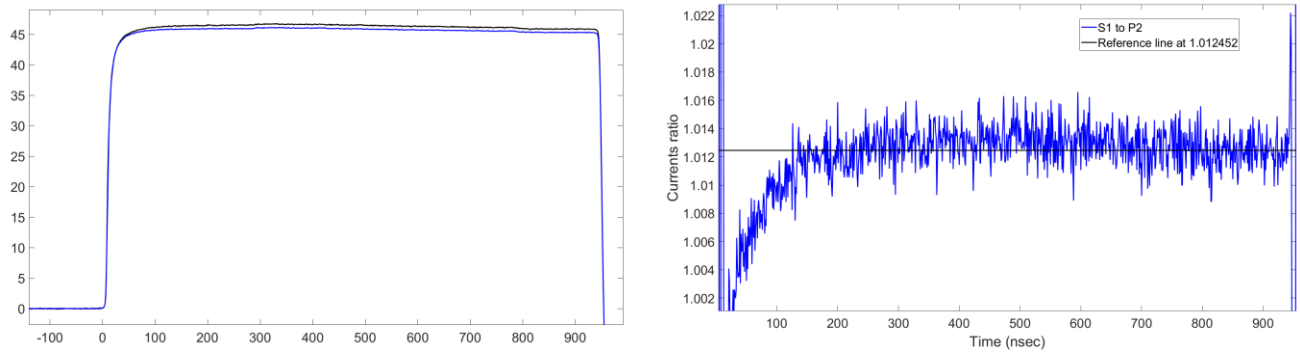

(a) (b)

Figure 56 a) Current step measured with the *S1* shunt (black trace) and the *P2* coil (blue trace) used together. b) Ratio of current measured with the *S1* shunt and the *P2* coil (blue trace) along with the reference line (black line).

5.3.3 *S2* shunt and *P2* coil

Figure 57(a) shows the steps measured with the *S2* shunt and the *P2* coil. A scaling factor of 0.098722 was used for the S2 shunt while 15.0332 was used for the *P2* coil. Figure 57(b) indicates that the ratio of the currents measured is smaller than unity till 750 ns, and it crosses the unity level after that, rather than getting stable at the unity level with some uncertainty. This shows that the coaxial cable used for current step measurement is not long enough to attain a stable current level when the *S2* shunt is used.

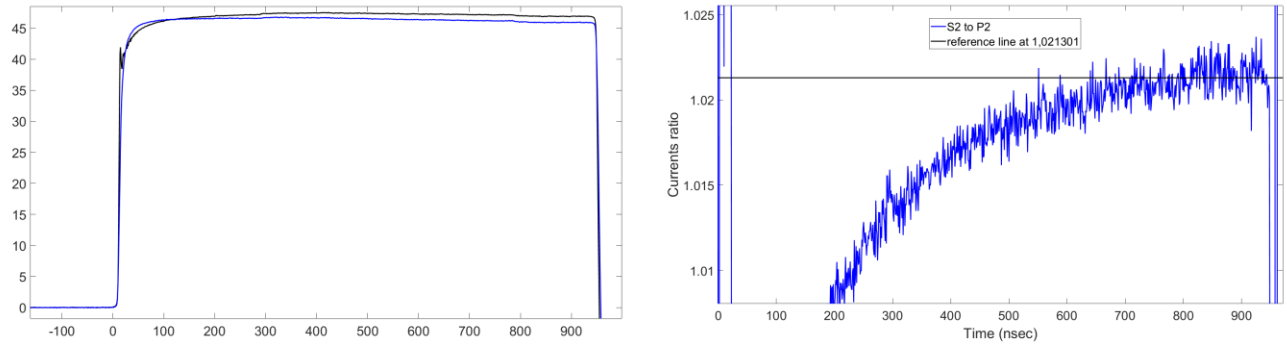

(a) (b)

Figure 57 a) Current step measured with the *S2* shunt (black trace) and the *P2* coil (blue trace) used together. b) Ratio of current measured with the *S2* shunt and the *P2* coil (blue trace) and along with reference line (black line).

5.3.4 *S3* shunt and *P2* coil

As in case of the *S2* shunt, the *S3* shunt showed almost similar behavior as can be seen in Figure 58. Curves not settling at unity level suggested that the coaxial cable used for generation purpose is not long enough to take the current ratio to the stable region. A scaling factor of 0.010822 was used for the *S3* shunt while 15.0332 was used for the *P2* coil. Curves for both sensors crossed the unity level reference line at approximately 500 ns but never stabilized. From the response, it can be concluded that the *S3* shunt takes more than 960 ns to stabilize and measure constant current, which is the maximum current step length obtainable with the coaxial cable used.

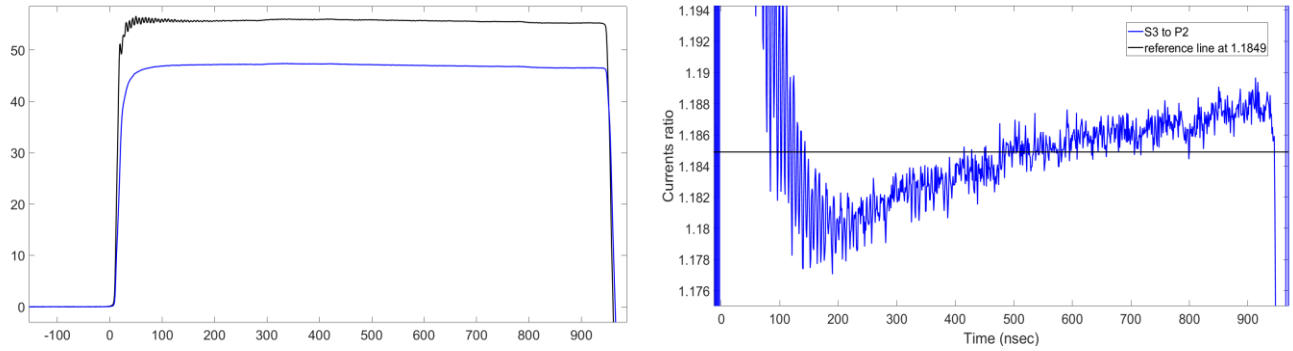

(a) (b)

Figure 58 a) Current step measured with the *S3* shunt (black trace) and the *P2* coil (blue trace) used together. b) Ratio of current measured with the S3 shunt and the *P2* coil (blue trace) along with the reference line (black line).

5.4 Transient behaviour of shunt with *P2* coil using compensated SF_6 spark gap

Current steps obtained with the *S1* and *SH* shunt in combination with the *P2* coil were studied again by analyzing the waveforms obtained using the compensated SF_6 spark gap shown in Figure 45, Section 4.3. This study of transient behavior helped in understanding the stability of shunts with respect to the length of the current step for steep rise times, as the SF_6 spark gap resulted in lower rise times for generated current steps.

5.4.1 S1 shunt and P2 coil

Current steps and the waveform of ratio for currents measured by the *S1* shunt and the *P2* coil used together in current step measuring circuit are shown in Figure 59(a) and (b) respectively. A scaling factor of 0.083701 was used for the *S1* shunt while 15.0332 was used for the *P2* coil. Figure 59(b) indicates that the curves settle after 750 ns in the case of the SF_6 spark gap, due to fast switching of the SF_6 spark gap resulting in fast step generation having lower rise time. The settling time was 150 ns with spark gaps other than SF_6, shown in Section 5.3. As mentioned earlier, reference line is the average value obtained for the peak current ratios measured for the epoch from 750 to 900 ns region of current step and it is not exactly 1 due to different scale factors used for current sensors.

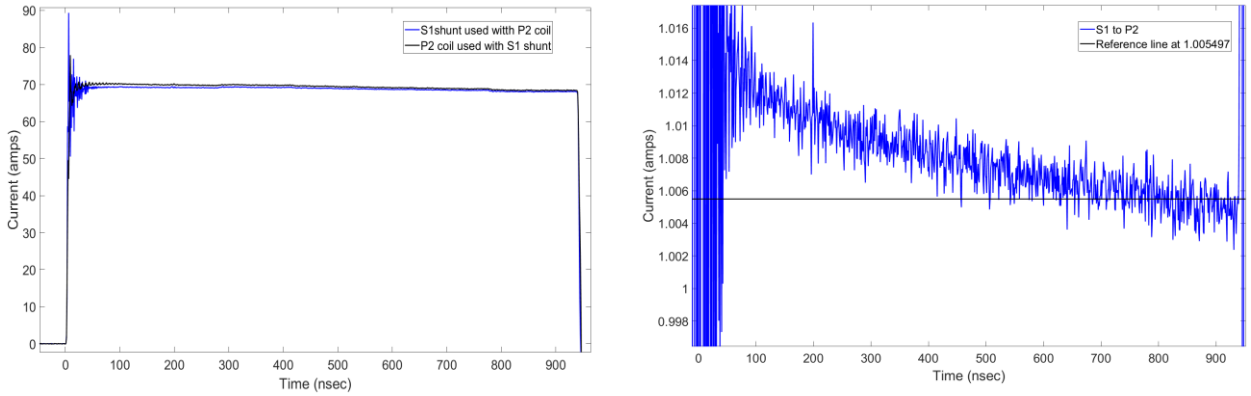

(a) (b)

Figure 59 a) Current step measured with the *S1* shunt (black trace) and the *P2* coil (blue trace) used together in the same measurement circuit. The current step is generated with the compensated SF_6 spark gap. b) Ratio of current measured with the *S1* shunt and the *P2* coil (blue trace) along with the reference line (black line) generated with the compensated SF_6 spark gap.

5.4.2 SH shunt and P2 coil

Figure 60(a) and (b) shows the current steps and the waveform for ratios of currents measured with the *SH* shunt and the *P2* coil when the compensated SF_6 spark gap was used for current step generation. Curves settle after 750 ns time length of current step in the same way as in case of *S1* shunt shown in Section 5.4.1. A scaling factor of 0.049501 was used for *SH* shunt while 15.0332 was used for *P2* coil. These measurements showed that due to lower rise time and fast switching with the SF_6 spark gap, the current sensors take longer step length to measure stable current.

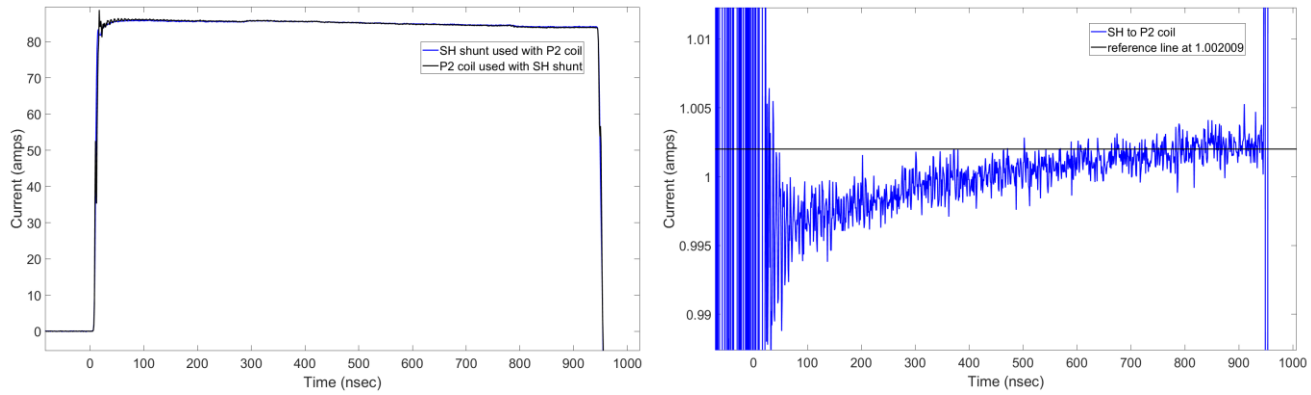

(a) (b)

Figure 60 a) Current step measured with the *SH* shunt (black line) and the *P2* coil (blue line) used together in the same measurement circuit. The current step is generated with the compensated SF_6 spark gap. b) Ratio of current measured with the *SH* shunt and the *P2* coil (blue line) along with the reference line (black line) generated compensated with SF_6 spark gap.

5.5 Summary

The current steps generated using a coaxial cable in Chapter 3 were measured using shunts and Rogowski coils, as explained in Chapter 4. Here, the results and data obtained in current step measurements was used for the step calibration of the sensors. Based on relative error, uncertainty, settling of curves and waveform obtained, the *S1* shunt was selected as a reference for current step generation with a peak current of up to 100 A and a rise time of less than 5 ns. An expanded uncertainty of approximately 1% was obtained for three out of the four shunts when including the uncertainty from the oscilloscopes, while it was less than 0.5% when ignoring the uncertainty of the oscilloscopes. When using a fast switch (e.g., the SF_6 spark gap) for generation of current steps resulting in lower rise times, the sensors required a longer current step length (i.e., coaxial cable length) to measure the stable current region.

Chapter 6

Conclusion and Future Work

6.1 Conclusion

The thesis has successfully designed and tested a coaxial cable generator that produces well-defined, rectangular, fast, and steep steps of peak value up to 100 A having an ultra-fast rise time of less than 5 ns. The produced current step was constant within 0.5% when using a coaxial cable 110-m in length for generating a step length of approximately 1 μs. The generator has been successfully used for current step generation and measurement in the High Voltage Laboratory at VTT MIKES. The techniques have been defined for measuring current step. Additionally, the test procedure and measurement capabilities have been improved for current step generation. The reference calibration circuit for current step measurement has been developed to characterize and standardize the impulse current shunts. An optimal circuit combination has been proposed for current step generation to achieve a rise time of less than 5 ns, along with the proposed reference shunt *S1*, which aims to provide the best stable measurement results with negligible noise, oscillations and droop in current step measurement. Additionally, step calibration has been performed for the current sensors used in this work.

Based on techniques found in the literature review, current steps were generated by designed coaxial cable generator, and different sensors were used to measure the generated steep-front current steps. The step generator consists of a coaxial cable 110-m in length with a characteristic impedance of 50 Ω, which was charged using a DC generator. This coaxial cable was then discharged using a spark gap switch, and the current steps were generated after reflecting back from the open end of the cable with a step length twice that of the cable transmission delay. The current steps were generated with a stable current of up to 100 A. The characteristic impedance changes due to various factors, including twisting of the cable and the resistance of the cable has an influence too, which affects the constant current from the cable.

The measurement system consisted of step measuring sensors (resistive shunts and Rogowski coils), attenuators (5:1 and 6.6:1) based on the requirement of the different sensors, and the recording instrument (oscilloscopes of different bandwidth and sampling rate). The rise time of the step varied from 1.6 ns to 15 ns, depending on the spark gap used for switching.

This study focused on investigating the generation and measurement techniques for current step and different factors affecting the rise time of the current step. Various factors were analyzed that affected the current step measurement, including the type of coaxial cable, type of connection, extra shielding, clearances, interference sources, media of the spark gap and the spark gap electrode distance. The measurement system is influenced by factors, such as the coaxiality of the connection, impedance mismatch, interference, clearances, stray capacitances, and stray inductances. The arc length of the spark gap affects the rise time, such that the rise time increases in

response to increasing arc length. It was also observed that the oscillations in the rising edge of the current step were due to overall inductance of the circuit, while the reflections within the rising edge of the measured current step were due to impedance mismatch. In addition, the sensors with a higher nominal rise time increased the measured rise time for the sensor used in the same measurement circuit. Except for shunt *S3*, the relative error of the step sensitivity from the DC calibrated sensitivity was in the range of 1%. Even though the rise times claimed for all the tested sensors were below 2 ns, these sensors showed different final values for settling times. Three of the four tested shunts agreed within 1% after approximately 750 ns from the onset of the step current. However, the verification of the actual rise time appeared to be difficult due to the steep front of the current step. In addition to the characteristics of the switching element, the geometry of the circuit had a significant effect on the measurement.

Due to common mode grounding problems, it was not possible to directly compare two shunts against each other. Therefore, for calibrating the shunts, Rogowski coil sensors were used with the shunts in measurement circuits. Step calibration was performed for impulse shunts using these fast-current sensing Rogowski coils as a transfer reference and comparing them with the response of impulse shunts.

6.2 Future Recommendations

Although this thesis has achieved all its required experimental targets, several areas can still be improved for current step generation and measurement. In the future, the length of the coaxial cable used could be extended to attain a standard impulse, as the cable available in this work was only 110-m in length, thus limiting the applicability of the method. For example, about two kilometers of cable would be needed in order to cover the full-time epoch of a standard 8/20 µs impulse. Additionally, some of the shunts in this project showed that a higher step length and hence higher cable length is actually required to measure constant current.

A higher peak current value could be reached to investigate the dependency of the rise time on the increasing peak value of the current. In this work, when using fixed electrode length of the spark gap, an increase in the gas pressure of spark gap and thereby the peak value of the current decreased the rise time. On the other hand, it should also be noted that for higher values of the peak current, shunt might not be the best sensor for current measurement because of its dependency on power loss due to an increase in the current. A peak current of 100 A is enough for 1-mΩ shunts. For µΩ shunts, higher currents might be required for best performance.

For rise times of a few nanoseconds, the impedance difference of the measurement circuit should be reduced as much as possible. This could be better done with further circuit simulations to clearly identify the factors causing the impedance differences. These factors of impedance mismatch should then be used for precisely obtaining the uncertainty.

References

[1] Acosta and Orlando N. *Power Plant Stability Capacitors and Grounding: Numerical Solutions*. McGraw Hill Professional, 2012.

[2] N. Arbab. *High Voltage Engineering: Theory and Practice*. Peshawar: Afaq Printers, 2013.

[3] Milić, Saša D., Aleksandar D. Žigić, and Milan M. Ponjavić. "Online temperature monitoring, fault detection, and a novel heat run test of a water-cooled rotor of a hydrogenator." *IEEE Transactions on Energy Conversion,* 2013, pp. 698-706.

[4] M. S. Naidu. *High Voltage Engineering*. Tata McGraw-Hill Education, 2013.

[5] Metrology for the electrical power industry. *Short Name: ElPow, Project Number: 14IND08,* Available: https://www.euramet.org/research-innovation/search-research-projects/details/ ?eurametCtcp_project_show[project]=1321&eurametCtcp_project[back]=546&cHash=2942836947e7f6cb2a47b977cf5e9d91. Accessed: 2018-04-01

[6] Alan Dower Blumlein. “Improvements in or relating to apparatus for generating electrical impulses,” US Patent 589127, filed October 10, 1941, granted June 12, 1947.

[7] C. Cherbaucich, G. Crotti, N. Kuljaca and M. Novo. “Evaluation of the dynamic behaviour of heavy current shunts,” *Metrology in the 3rd Millennium: Proc. XVII IMEKO World Congress*, Dubrovnik, Croatia. June 22-27, 2003, pp. 586–589.

[8] IEC 60076-4 Standard. "Power transformer – Part 4: Guide to the lightning impulse and switching impulse testing- Power transformers and reactors." *International Electrotechnical Commission,* 2002.

[9] IEC 60060-2 Standard. "High Voltage Test Techniques, Measuring System." *International Electrotechnical Commission,* 1994.

[10] IEC 61312-1 Standard. "Protection Against Ligtning Electromagnetic Impulse- General Principle." *International Electrotechnical Commission*, 1995.

[11] IEC 62475 Standard. "High-Current Test Techniques. Definitions and Requirements for Test Currents and Measuring Systems." *International Electrotechnical Commission*, 2010.

[12] A. J. Schwab and J. Herold. "Electromagnetic interference in impulse measuring systems " *in 1EEE International conference, Electromagnetic Compatibility Symposium Record*, 1973, pp. 333-339.

[13] C. Stuckenholz and M. Gamlin. "Overview of impulse current test standards and the impact on test equipment," *in 2012 International Conference on Lightning Protection (ICLP)*, 2012, pp. 1-6.

[14] S. Ziegler, R.C. Woodward, H.H.C. Iu and L.J. Borle. "Current sensing techniques: A review." *IEEE Sensors Journal*, vol. 9, 2009, pp.354-376.

[15] F. W. Grover. Inductance Calculations: Working Formulas and Tables. *Courier Corporation*, 2004.

[16] C. Johnson and P. Palmer. "Current measurement using compensated coaxial shunts," *IEE Proceedings-Science, Measurement and Technology,* vol. 141, 1994, pp. 471-480.

[17] R. Malewski. "New device for current measurement in exploding wire circuits." *Review of Sci. Instrum.,* vol. 39, 1968, pp. 90-94.

[18] J. Ferreira, W. Cronje and W. Relihan. "Integration of high frequency current shunts in power electronic circuits." *IEEE Transactions on Power Electronics,* vol. 10, 1995, pp. 32-37.

[19] Malewski, Ryszard, Chinh T. Nguyen, Kurt Feser and Nils Hylten Cavallius. "Elimination of the skin effect error in heavy-current shunts." *IEEE Transactions on Power Apparatus and Systems*, vol. 3, 1981, pp. 1333-1340.

[20] F. Castelli. "The flat strap sandwich shunt." *IEEE Transactions on Instrumentation and Measurement,* vol. 48, 1999, pp. 894-898.

[21] W. Ray and C. Hewson. "High performance Rogowski current transducers," *in IEEE Conference Record, Industry Applications Conference*, 2000, pp. 3083-3090.

[22] RCT rms Rogowski coal datasheet, Available: http://www.pemuk.com/products/rct-industrial-current-sensor.aspx. Accessed: 2018-04-02

[23] D. A. Ward and J. L. T. Exon. "Using Rogowski coils for transient current measurements," in *Engg. Sci. & Edu. Journal,* vol. 2, 1993, pp. 105-113.

[24] A. Radun. "An alternative low-cost current-sensing scheme for high-current power electronics circuits," in *IEEE Trans. Ind. Electron.,* vol. 42, 1995, pp. 78-84.

[25] L. Dalessandro et al. "Online and offline isolated current monitoring of parallel switched high-voltage multi-chip IGBT modules," *in Power Electronics Specialists Conference PESC*, 2008, pp. 2600-2606.

[26] Pearson Electronics, Available: http://www.pearsonelectronics.com/. Accessed: 2018-04-20

[27] Waters and A.Christopher. "Attenuator for use with current transformer." *U.S. Patent 5,506,550,* issued April 9, 1996.

[28] K. Schon. *High Impulse Voltage and Current Measurement Techniques.* Springer, 2013.

[29] A.W Palmer. "A simple mechanically operated sub-nanosecond rise-time generator for pulses up to 100 kV." *J. phys. E: Sci. Instrum*., vol. 4,1970, pp. 115-118.

[30] N. Seddon and E. Thornton. "A high voltage, short rise-time pulse generator based on ferrite pulse sharpener." *Rev. Sci. Instrum.,* vol. 59, 1988, pp. 2497-2498.

[31] D. Brown and D. Martin. "Subnanosecond high-voltage generator." *Rev. Sci. Instrum,* vol. 58, 1987, pp.

1523-1529.

[32] R.G. Baker and S.T. Ward. "Designing nanosecond high voltage pulse generators using power MOSFETs." *Electron. Lett.,* vol. 30, 1994, pp. 1634-1635.

[33] R.L. Garwin. "A pulse generator for milli-microsecond range." *Rev. Sci. Instrum.,* vol. 21, 1950, pp. 903-904.

[34] C. Hancock, A. Owens and K. O Grady. "Simple voltage generator for producing well-defined nanosecond pulses of amplitudes in excess of 1 kV." *IEE Proceedings-Science, Measurement and Technology,* vol. 144, 1997, pp. 229-233.

[35] Klüss, Joni. *Lectures from the course of High Voltage Engineering S-18.3150*. Aalto University, Finland. 2018

[36] C. T. Allcutt. "Lightning Arrester Spark Gaps. "*Transactions of the American Institute of Electrical Engineers*". vol. 37, 1918, pp. 833-869.

[37] L. Alston. "High-temperature effects on flashover in air," in *Proceedings of the IEE-Part A: Power Engineering*, vol. 105, 1958, pp. 549-553.

[38] J. M. Lehr, C. E. Baum, W. D. Prather and R. J. Torres. "Fundamental physical considerations for ultrafast spark gap switching," in *Ultra-Wideband Short-Pulse Electromagnetics 4*, 1998, pp. 11-20.

[39] Specifications of LabMaster 10-100Zi real-time oscilloscope. Available: http://teledynelecroy.com/100ghz/. Accessed 2018-04-28.

[40] K. Schon, W. Lucas, V. Arndt, C. Cherbaucich, G. Rizzi, F. Deschamps, J.J. Ribot, F. Garnacho, J. Perez, N. Gomes and C. Dias. "International comparison of software for evaluating HV impulses and step responses," in *Proc. 8. ISH Yokohama, Beitrag*, 1993, pp. 289-292.

[41] R. E. Bentley. "Uncertainty in measurement: The ISO guide 2002," *National Measurement Institute,* vol. 11, 2002.

[42] Pulsed Power Formulary. Available: http://www.pulsedpower.net/Info/PulsedPowerFormulary.pdf. Accessed 2018-04-28.

[43] A. J. Schwab. *High-voltage measurement techniques*. *Cambridge, Mass, M.I.T. Press*, 1972.

[44] Spectrum Software. Available: http://www.spectrum-soft.com/. Accessed 2018-04-28.

[45] Circuit Analysis and Simulation with Transmission-Line Emphasis. Available: http://www.rayslogic.com/Software/CASTLE/CASTLE.htm. Accessed 2018-04-28.

[46] Y.Y. Chekurov and J.K. Hallstrom. "Fast resistive attenuators for high accuracy measurements of LI voltages," in IEEE *Conference on Precision Electromagnetic Measurements Digest*, June 2004, pp. 328-329.

[47] B. N. Taylor and C. E. Kuyatt. "Guidelines for Evaluating and Expressing the Uncertainty of NIST Measurement Results." *National Institute of Standards and Technology*, 1994.

[48] T&M Research Products. Available: http://www.tandmresearch.com/. Accessed 2018-04-28.

[49] HILO-TEST Products. Available: http://www.hilo-test.de/. Accessed 2018-04-28.

[50] M.Z. Rehman, J. Havunen and J. Hällström. “Current step generation and measurement with nanosecond rise time using coaxial cable generator,” submitted in *International Conference on High Voltage Engineering*, Athens, Greece. September 2018.

Appendix A

Details of shunts used, Data sheets and Dimensions

1) T&M shunt W-1T-5-1STUD (S1)

6 Watt Units - 4 1/2 Inch Overall Height

Model	Resistance ohms	Bandpass MHz.	Risetime nsec.	Emax joules
W-1T-5-1STUD	.5	400	1	500

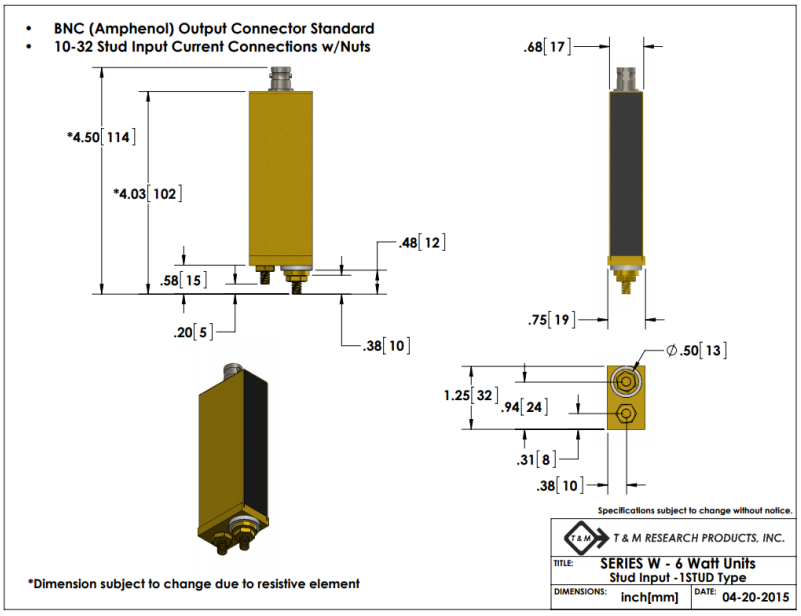

[48]

2) T&M shunt W-1-1-1STUD (S2)

6 Watt Units - 4 1/2 Inch Overall Height

Model	Resistance ohms	Bandpass MHz.	Risetime nsec.	Emax joules
W-1-1-1STUD	.1	400	1	200

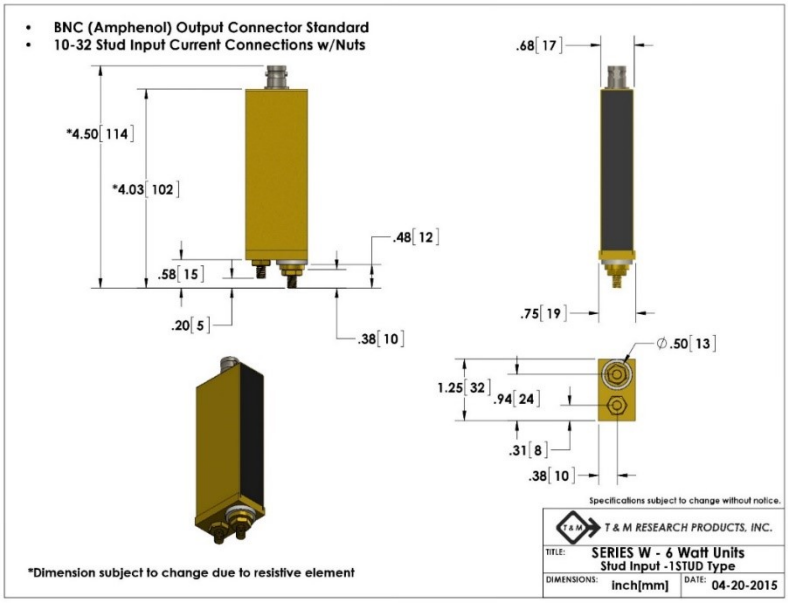

[48]

3) T&M shunt W-1-01C-2FC (S3)

7 1/2 Watt Units - 2 Inch Long Clamping Surface

Model	Resistance ohms	Bandpass MHz.	Risetime nsec.	Emax joules
W-1-01C-2FC	.01	800	0.45	80

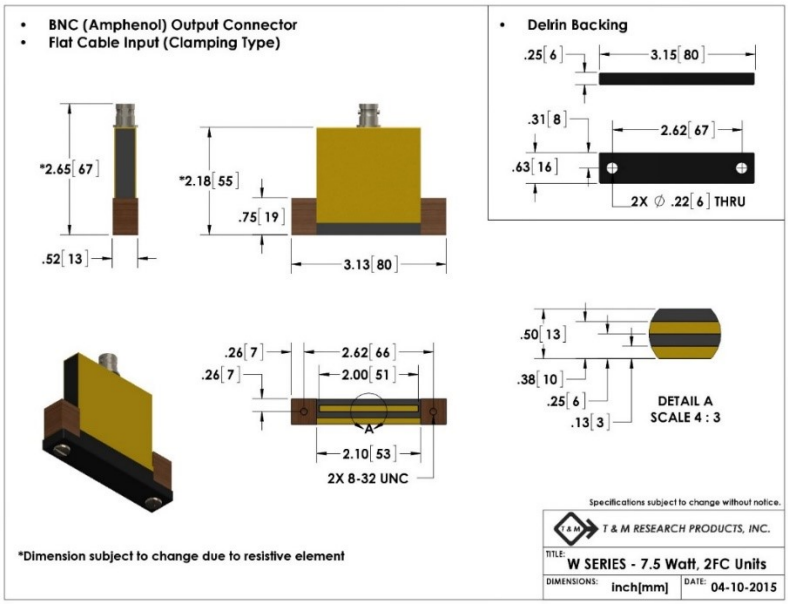

[48]

4) HILO-TEST shunt ISM 5P/50 (SH)

ISM CURRENT-VIEWING RESISTORS

Type	Current rating peak / rms		Nominal resistance	Power	Impulse-load integral	Rise-time	Band-width 1)	Size	Diameter/ Length	Weight
ISM 5P/50	5 kA	10 A	50 mΩ	5 W	1300 A^2s	1.8 ns	200 MHz	A	50/236 mm	1.5 kg

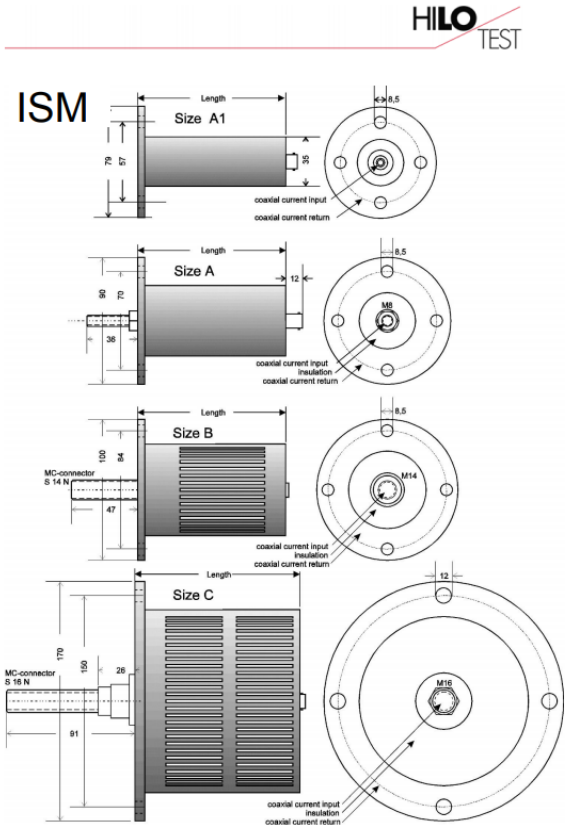

Technical specifications subject to change, ISME-DIM.docx, 05/17 Page 1 of 2
HILO-TEST GmbH, Am Hasenbiel 42, D-76297 Stutensee-Karlsruhe, Tel. 07244/20500-0, www.hilo-test.de

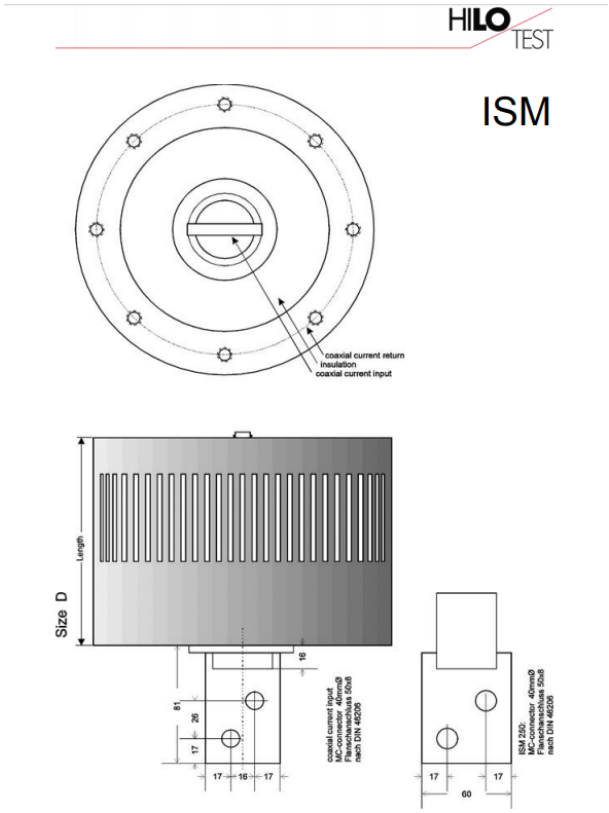

Technical specifications subject to change, ISME-DIM.docx, 05/17 Page 2 of 2
HILO-TEST GmbH, Am Hasenbiel 42, D-76297 Stutensee-Karlsruhe, Tel. 07244/20500-0, www.hilo-test.de

[49]

Details of Rogowski coils used

1) Pearson Electronics 110A (P1)

PEARSON ELECTRONICS, INC.

PEARSON™ CURRENT MONITOR MODEL 110A

Sensitivity	0.1 Volt/Ampere +1/-0%
Output resistance	50 Ohms
Maximum peak current	10000 Amperes
Maximum rms current	65 Amperes
Droop rate	0.8 %/millisecond
Useable rise time	20 nanoseconds
Current time product	0.5 Ampere-second maximum*
Low frequency 3dB cut-off	1 Hz (approximate)
High frequency 3dB cut-off	20 MHz (approximate)
I/f figure	1.5 peak Amperes/Hz
Output connector	Type N
Operating temperature	0 to 65 °C
Weight	22 ounces

* Maximum current-time product can be obtained by using core-reset bias as described in the *Application Notes*. 0.2 Ampere-second is typical without bias.

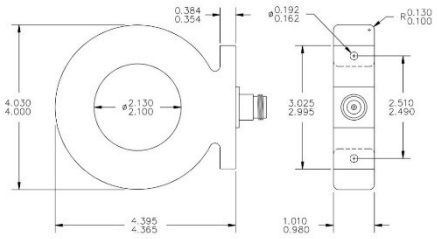

Pearson Electronics, Inc. • 4009 Transport Street • Palo Alto, CA 94303
Telephone 650-494-6444 • FAX 650-494-6716 • www.pearsonelectronics.com

2)Pearson Eletronics 2877 (P2)

PEARSON ELECTRONICS, INC.

PEARSON™ CURRENT MONITOR MODEL 2877

Sensitivity	1 Volt/Ampere +1/-0%
Output resistance	50 Ohms
Maximum peak current	100 Amperes
Maximum rms current	2.5 Amperes
Droop rate	0.2 %/microsecond
Useable rise time	2 nanoseconds
Current time product	0.4 milliamp-sec. maximum*
Low frequency 3dB point	300 Hz (approximate)
High frequency 3dB point	200 MHz (approximate)
I/f figure	0.0025 peak Amperes/Hz
Output connector	SMA
Operating temperature	0 to 65 °C
Weight	1.15 ounces

* Maximum current-time product can be obtained by using core-reset bias as described in the *Application Notes*. 0.14 milliAmpere-second is typical without bias.

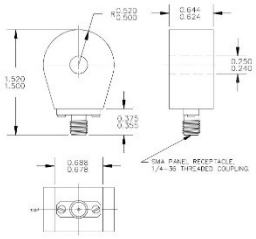

Pearson Electronics, Inc. • 4009 Transport Street • Palo Alto, CA 94303
Telephone 650-494-6444 • FAX 650-494-6716 • www.pearsonelectronics.com

[26]

Appendix B

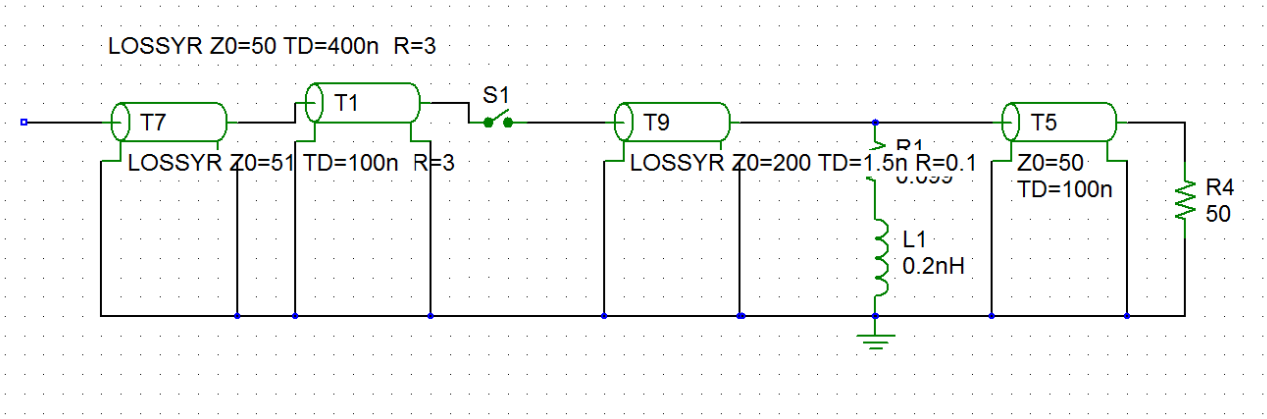

Figure 61 Simulation circuit used for the generation of current step with two coaxial cables having impedance difference.

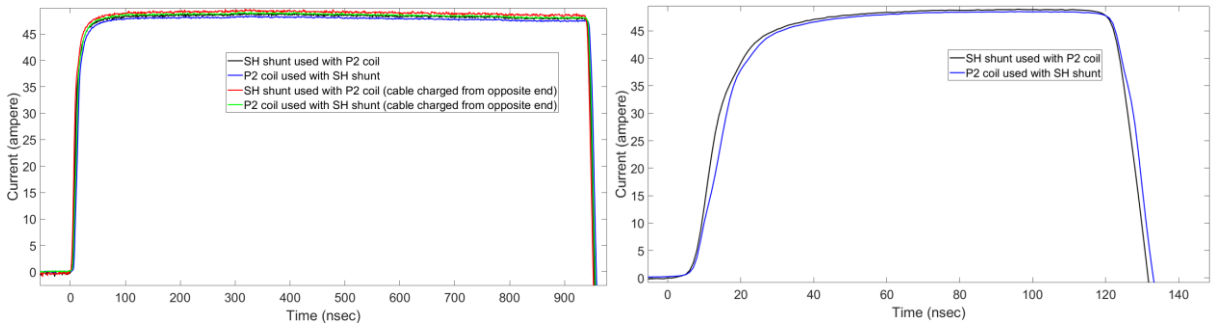

Figure 62 (a) current steps generated with coaxial cable charged from different ends, (b) *Ecoflex* coaxial cable with characteristic impedance of 50 Ω and length of approximately 15 m used for current step generation.

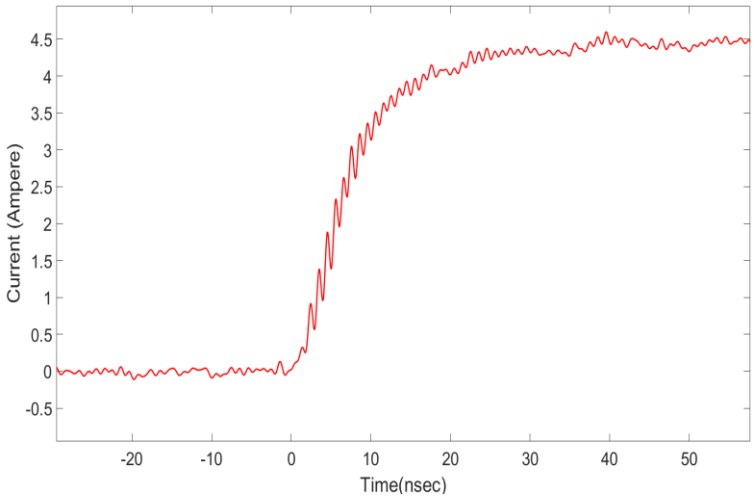

Figure 63 Rising edge of the current step measured with HILO-TEST (*SH*) shunt only, using Tektronix impulse generator.

Appendix C

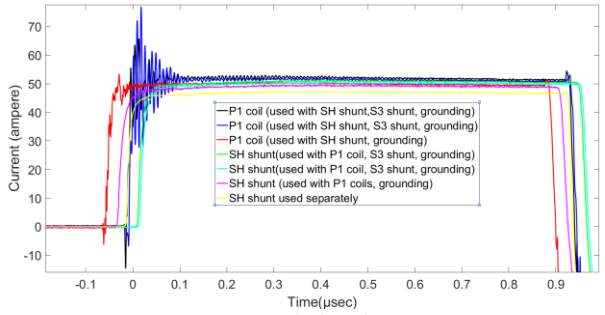

Figure 64 Current steps recorded with Test 1,3, 3A, 14,

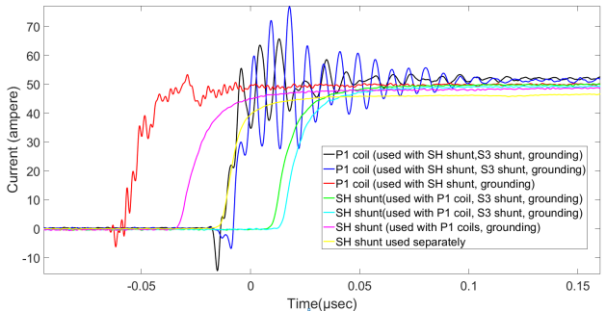

Figure 65 Rising edge for current steps recorded with Test 1,3, 3A, 14 (zero origin is displaced for clarity).

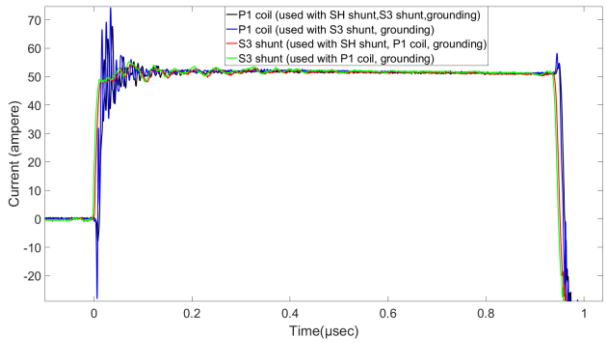

Figure 66 First current step recorded with Test 1A, 2.

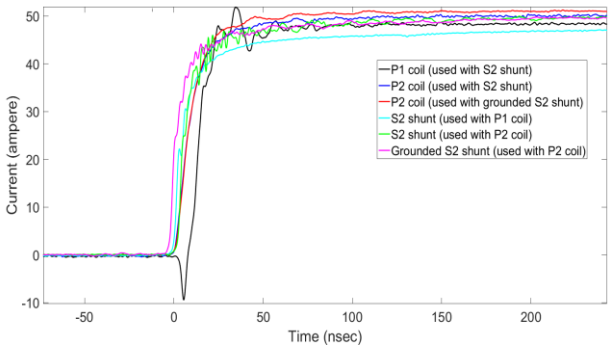

Figure 67 Detailed view of rising edge for current steps recorded with Test 4, 8 and Test 9.

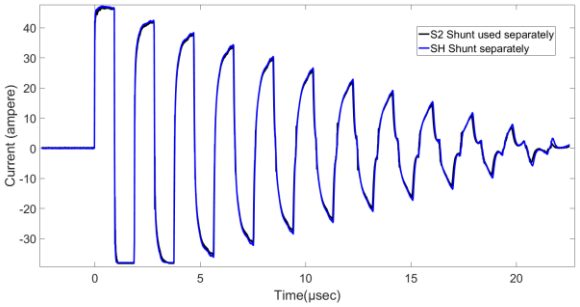

Figure 68 Current step recorded with Test 13 and test 14.

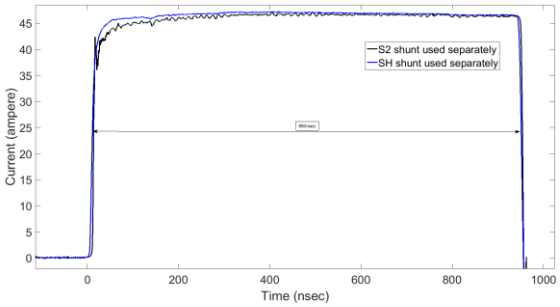

Figure 69 Current step recorded with Test 13 and test 14.

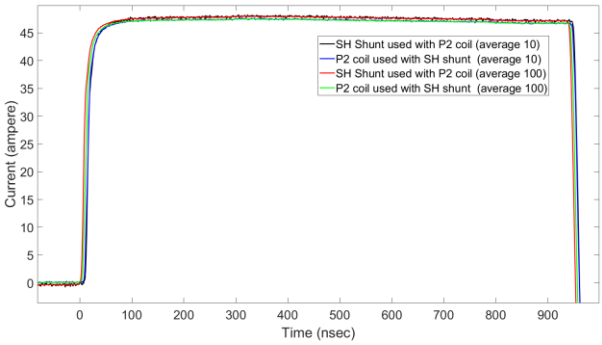

Figure 70 Improved current step measured with shunt *SH* and coil *P2* used together in the same measurement current.

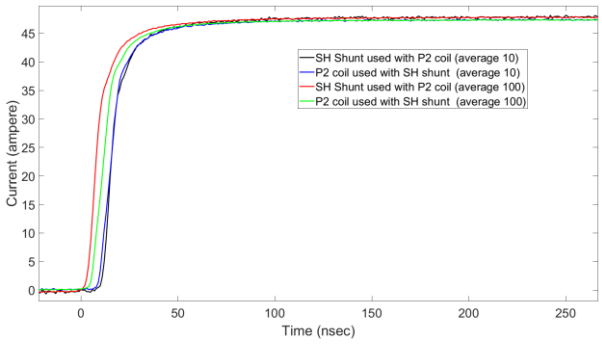

Figure 71 Rising edge of the improved current step measured with shunt *SH* and coil *P2* used together.

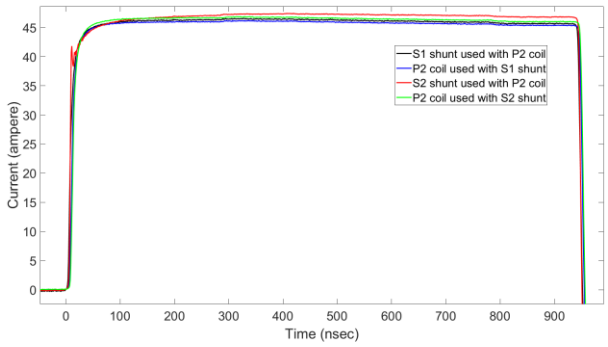

Figure 72 Current step measured with *S1* and *S2* shunts one at a time with the *P2* coil.

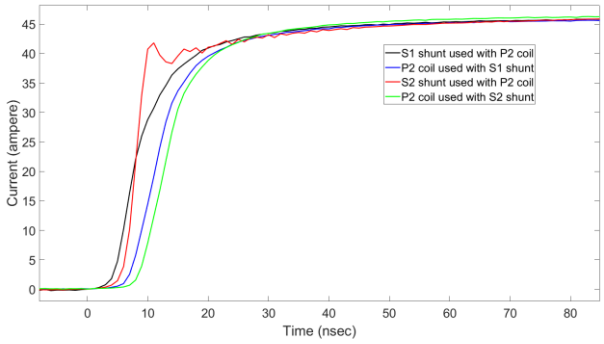

Figure 73 Rising edge of current step measured with *S1* and *S2* shunts one at a time with *P2* coil.

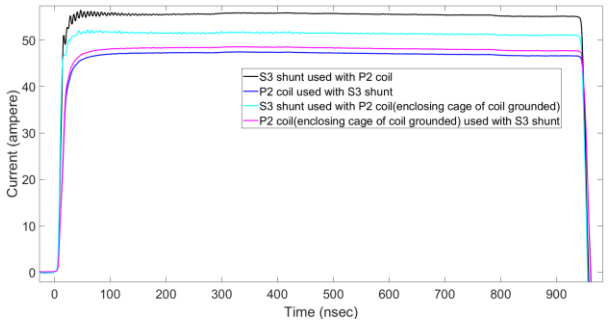

Figure 74 Current step measured with the *S3* shunt in combination with the *P2* coil with and without grounding.

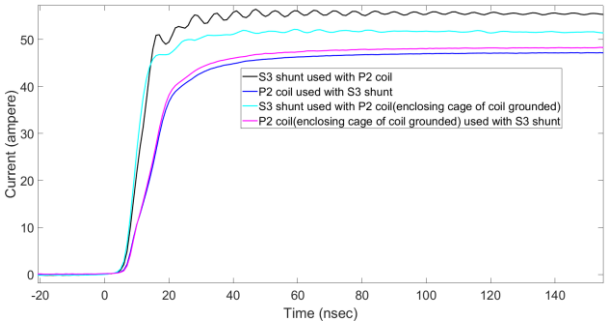

Figure 75 Rising edge of current step measured with the *S3* shunt in combination with the *P2* coil with and without grounding.

Results with digitizer of National Instruments

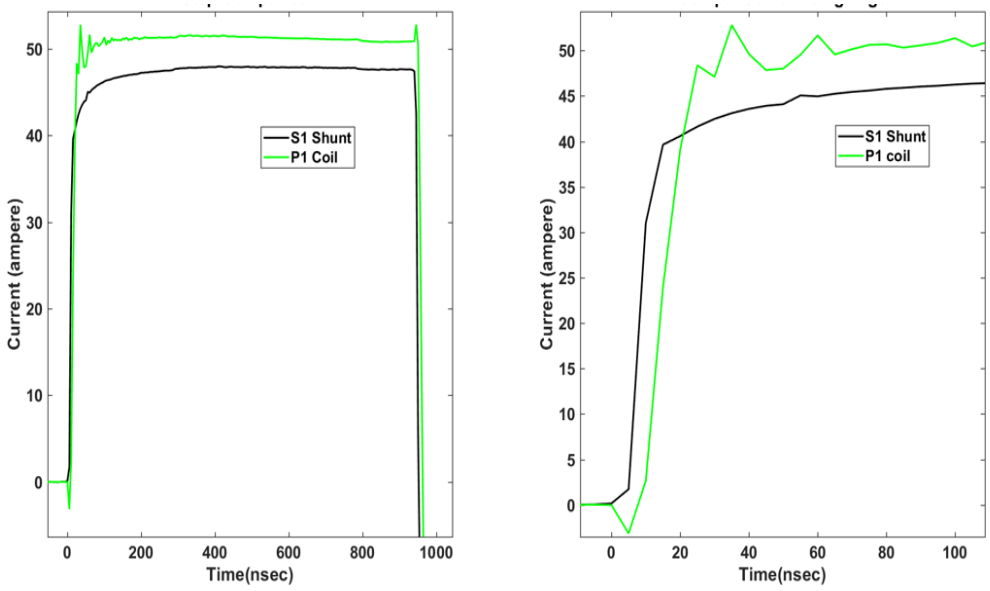

(a) (b)

Figure 76 (a) Current step for shunts *S1* and coil *P1* used separately for measurement purpose (b) rising edge.

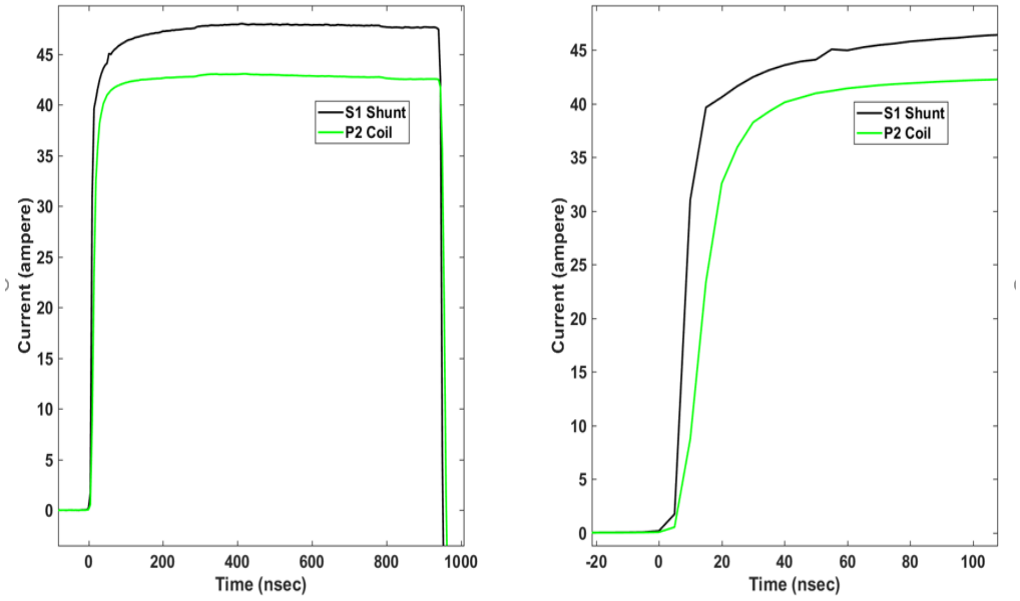

Figure 77 Current step for shunt *S1* and coil *P2* used separately for measurement purpose (b) rising edge of Figure 77 (a)

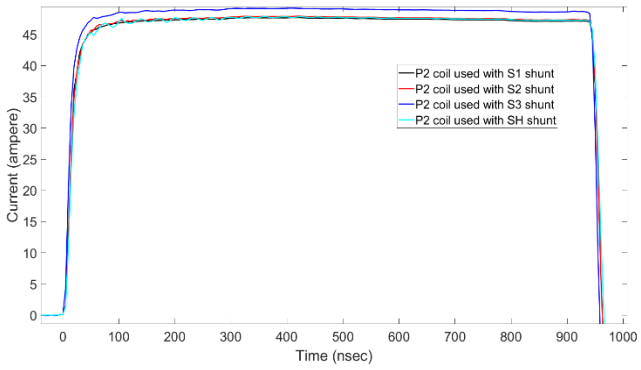

Figure 78 Current Step of the *P2* coil used with each shunt once at a time.

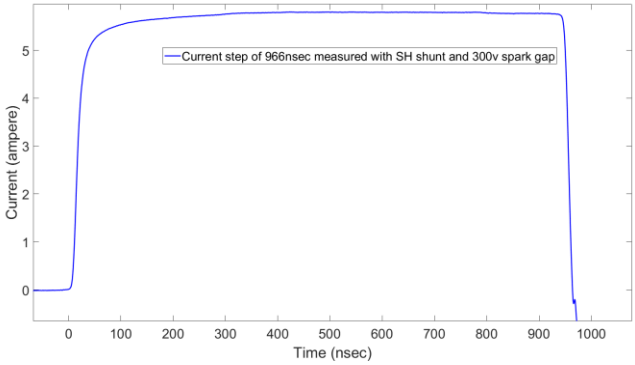

Figure 79 Current step measured with the *SH* shunt only, generated with 300 V spark gap.

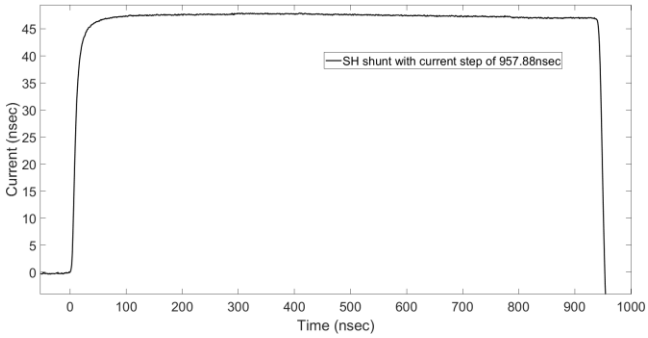

Figure 80 Current step measured with the *SH* shunt only.

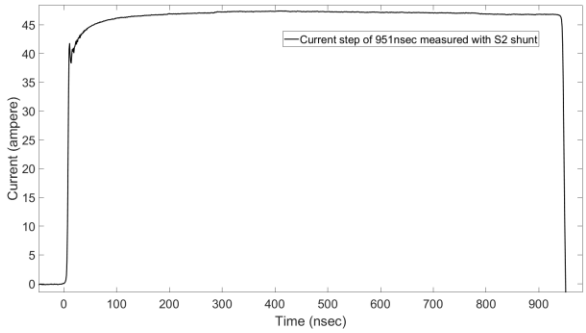

Figure 81 Current step measured with the *S2* shunt only.

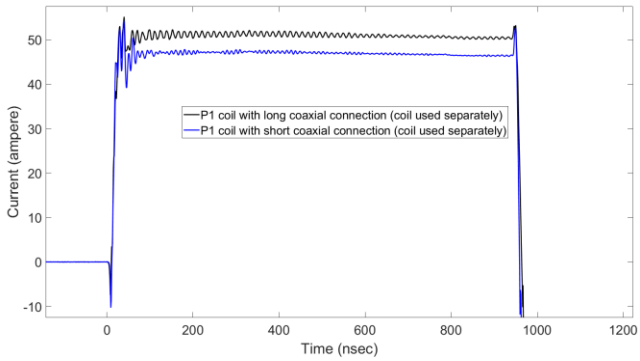

Figure 82 Current step measured with the *P1* coil by varying length of the coaxial structure.

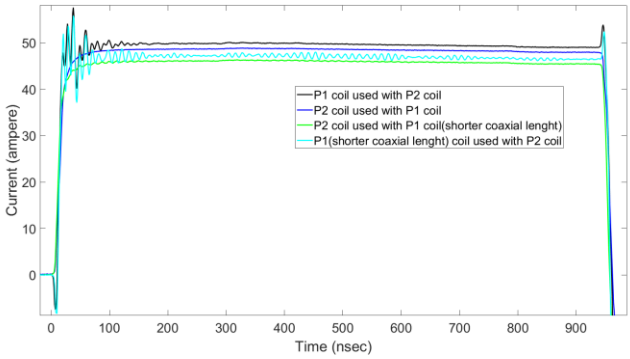

Figure 83 Current step measured with the *P1* and *P2* coil used together & by varying length of coaxial structure.

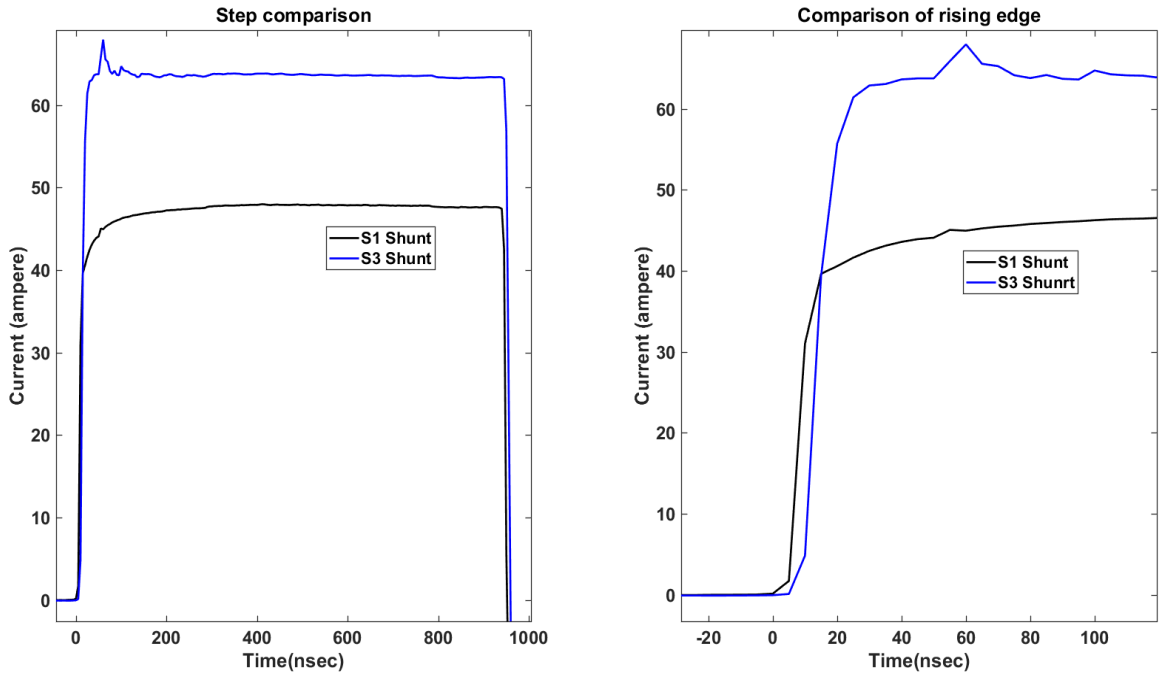

Figure 84 Current step and rising edge for shunts S1 and S3 used separately for measuring current step.